

IN-34-CR

73907

P-143

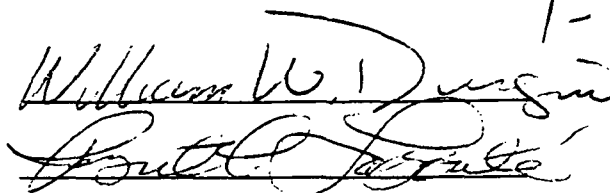
ROTATIONAL FLUID FLOW EXPERIMENT

Report submitted to:

Professor William B. Durgin

Robert C. Labonté

Professor Fred J. Looft



WPI/MITRE Advanced Space Design GASCAN II

By

Walter F. Daly, M.E.A.

Lee Harr, M.E.A.

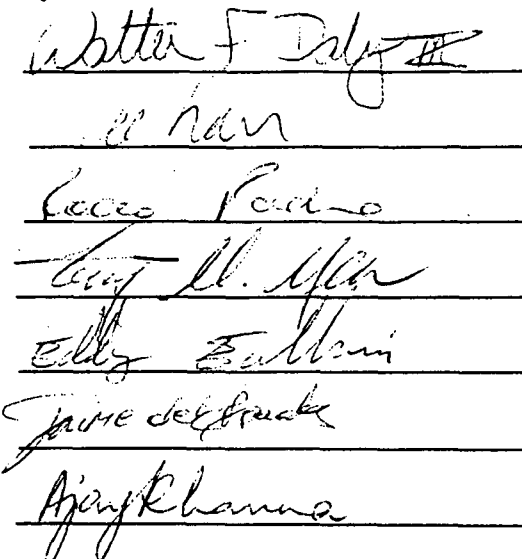
Rocco Paduano, M.E.A.

Tony Yee, M.E.A.

Eddy Eubbani, E.E.

Jaime Del Prado, E.E.

Ajay Khanna, E.E.



April 30, 1991

This project is submitted in partial fulfillment of the degree requirements of Worcester Polytechnic Institute. The views and opinions expressed herein are those of the authors and do not necessarily reflect the positions or opinions of Program Sponsors or Worcester Polytechnic Institute.

This report is the product of an educational program, and is intended to serve as partial documentation for the evaluation of academic achievement. The report should not be construed as a working document by the reader.

ABSTRACT

This project, begun in 1986 as a part of the WPI Advanced Space Design Program, focuses on the design and implementation of an electro-mechanical system for studying vortex behavior in a micro-gravity environment. Most of the existing equipment was revised and redesigned by this project team, as necessary. Emphasis was placed on the documentation and integration of the mechanical and electrical subsystems. Project results include the reconfiguration and thorough testing of all the hardware subsystems, the implementation of an infrared gas entrainment detector, new signal processing circuitry for the ultrasonic fluid circulation device, improved prototype interface circuits, and software for overall control of experiment operation.

ACKNOWLEDGEMENTS

As with any project, it could never have been possible without the help of many others. We would first like to thank the engineers of MITRE Corporation for their valuable input. Their knowledge and experience offered in order to improve our project was greatly appreciated. A special thanks goes to Mike Luparelli and Bob Taylor for their invaluable experience and expertise in building many of the components of the experiment, and Barbara Rodrique on finally getting the new pump delivered. We would also like to thank Elantec Corporation for their generosity in donating high-speed, temperature-resistant operational amplifiers to the project. Mr. Berrios and Mr. Elliot, respectively graduate assistants in the Electrical and Mechanical Engineering Departments at WPI, also deserve special mention for helping us overcome several technical aspects of the project. Most importantly, we would like to express our gratitude to our advisors, Professor William B. Durgin, and Robert C. Labonté for their continued support and guidance throughout the year.

EXECUTIVE SUMMARY

The following MQP details progress on the Rotational Fluid Flow Experiment for the WPI Advanced Space Design Program during the 1990-91 academic year. The overall goal for the project focuses on determining the effects of gravity on the development of a free-surface vortex. The experimental approach involves producing vortices in a test chamber mounted on a rotational platform. Altering the angular velocity of the platform provides a method for varying the effective acceleration applied to the chamber.

During the 1990-91 academic year the Rotational Fluid Flow Experiment MQP Team included two separate student groups. The Mechanical Systems Team consisted of four mechanical engineering students whose responsibilities centered around the testing, reconfiguration, and integration of the mechanical systems chosen in designs completed in previous years. The Electrical Systems Team consisted of three electrical engineering students each addressing a separate subgroup. These subgroups addressed the implementation of the infrared gas entrainment detector, new signal processing circuitry for the ultrasonic circulation device, improvements on prototype interface circuits, and software design for the overall control of experiment operation.

The Mechanical Systems Team addressed three separate subgroups, each requiring the attention of at least one mechanical engineering student. The tasks cited include thorough testing of the mechanical equipment, development of a step by step procedure for mounting the experiment on the GASCAN more efficiently, and taking test pictures of the vortex in simulated flight conditions in order to finalize the camera and flash configuration that will provide visual proof of successful experiment operation. The results of the mechanical

equipment testing led to the decision of buying a more powerful pump, since the pump bought by last year's MQP Team was not strong enough to form the vortex while the fluid within the chamber was experiencing coriolis acceleration. Several configurations were tested which revealed that the pump must be able to achieve a volumetric flowrate of at least 2060 ml/min in order to form the vortex while the platform rotates. The camera and flash configuration was explored in depth finding an acceptable arrangement for the positioning of the camera and the flash with respect to the vortex chamber, which will produce pictures showing clearly the outline of the vortex.

The tasks of the Electrical Systems Team for this academic year were divided into four major areas. These were the implementation of the infrared gas entrainment detector, the development of new process circuitry for the ultrasonic fluid circulation device, improved prototype circuits, and redesigning the software used for the overall control of the experiment to fit the changes that were made this year. All circuits were updated and changed accordingly, thus bringing them a step closer to flight readiness.

There is no appreciable change in the components that will get mounted on the plate, with the only difference that the weight lost by not including the flowmeter is compensated by the larger pump ordered during this academic year. Through the extensive analysis done by the 1989-90 MQP Team, the platform has a natural frequency of approximately 51 Hz, while the stresses that will be experienced by the platform are still within tolerance levels.

TABLE OF CONTENTS

Abstract	iii
Acknowledgements	v
Executive Summary	vii
 Chapter 1 Introduction	 1-1
 Chapter 2 Vortex Theory	 2-1
 Chapter 3 Experiment	 3-1
3.1 Mechanical Design.....	3-2
3.1.1 Pump, Piping, and Cylinder.....	3-2
3.2.1 Platform, Shaft, and Platform Motor Equipment.....	3-6
3.3.1 Camera and Flash.....	3-11
3.2 Electrical Design.....	3-14
3.2.1 Computer Hardware.....	3-14
3.2.2 Temperature Transducer.....	3-17
3.2.3 Motor and Pump Controllers.....	3-20
3.2.4 Accelerometers.....	3-23
3.2.5 Gas Entrainment Detector.....	3-25
3.2.6 Ultrasonic Circulation Measurement System.....	3-47
3.3 Computer Software and Control.....	3-66
 Chapter 4 Operations	 4-1
4.1 Mechanical Hardware Assembly.....	4-2
4.2 Flight Operation Sequence.....	4-6
 Chapter 5 Earth-Based Experiments	 5-1
5.1 On-Earth Experiment.....	5-2
5.1.1 Forces Involved.....	5-2
5.1.2 Equipment Used.....	5-3
5.1.3 Preliminary Design.....	5-4
5.1.4 Final Design.....	5-4
5.1.5 Running the Experiment.....	5-4
5.1.6 Problems Encountered.....	5-5
5.1.7 Results.....	5-5
5.2 Camera and Flash Testing.....	5-7
5.3 Electrical Equipment Testing.....	5-17
5.3.1 Computer Hardware.....	5-17
5.3.2 Hardware Proof-of-Concept Simulator.....	5-18
5.3.3 Gas Entrainment Detector.....	5-19
5.3.4 Ultrasonic Circulation Device.....	5-21
5.3.5 System Integration.....	5-22

Chapter 6 Conclusions	6-1
Appendix A	
Mechanical Equipment Data Specifications	A-1
Appendix B	
Electrical Equipment Data Specifications	B-1
ONSET C-44 BUS	
ONSET CPU 8088, 8085A, 6805A, 801	
ONSET MEM-64	
ONSET PAR-40	
ONSET RAM-512	
ONSET RAM-2M	
ONSET CPU 8088	
HARRIS 80C88 CMOS MICROPROCESSOR	
OKI MSM81C55 CMOS 256X8 Static RAM with I/O Ports and Timer	
OKI MM58274A MICROPROCESSOR Compatible Real Time Clock	
HARRIS 82C52 CMOS Serial Controller Interface	
ONSET MOR-800	
ONSET DS-64	
Other Components of Electrical Circuitry	
GENISCO Accelerometers	
Program Listings	
Appendix C	
Software Manual	C-1
Appendix D	
Free-Surface Vortex Calculations	D-1

CHAPTER 1

INTRODUCTION

The Micro-Gravity Vortex Formation Experiment is designed to study the effects of variable conditions on the strength of a rotational fluid flow in a non-terrestrial gravitational environment. To accomplish this, several devices have been designed and built to alter the gravitational level on a swirling fluid and to gather data on the effects of such variation.

The experiment is to be installed in a Get-Away-Special Canister (GASCAN) to be sent up on a future Space Shuttle mission. Artificial gravity is produced by rotating the experiment on a platform, whose angular velocity creates centripetal acceleration. In this project, the mechanical devices were thoroughly tested, the on-Earth experiment was conducted, the rotational flow sensor was designed and built, the gas entrainment detector was built, and the software was redesigned.

A vortex is a mass of fluid flowing in a circular motion, such as a whirlpool or a tornado, that causes a cavity or vacuum to form in its center. This effect can also be seen by draining water out of a sink.

There are many factors that must be taken into account, such as the fluid and the environment, to understand vortices. Gravity is a major factor in the formation of a vortex and is difficult to isolate or model while the experiment remains under Earth's gravitational acceleration. By eliminating the gravitational acceleration, one can easily simulate gravity by using centripetal acceleration. By performing this experiment in zero-G, it is possible to isolate gravity so that the vortex formation trials can be performed under different accelerations and flow rates. In such an environment, data can then be taken in order to understand the dependency of vortices on gravity.

Further understanding of the formation of vortices can improve the performance of

pumps and other machinery, for which entrainment can be detrimental to system performance.

MITRE Corporation donated GASCANs in order to provide WPI students with project opportunities such as this. The GASCAN is a small, self-contained payload used for Shuttle experiments in space. GASCAN-I was completed in 1985 and is scheduled to be launched in May 1991. GASCAN-II is to be used for the micro-gravity experiment described herein.

The micro-gravity experiment consists of a rotatable platform, to which all electronic equipment is attached, and a cylindrical vessel which contains the fluid. The fluid will be injected into the vessel, which will cause the fluid to swirl around in the vessel until it exits at the bottom. In addition to adjusting the flow rate of the fluid, the vessel is to be subjected to centripetal acceleration as a result of rotating the platform using a motor.

The process by which the effects of flow rate and acceleration have on vortex formation will be observed as follows: after verifying that both of these parameters are stable, the platform will be accelerated to a specific velocity and data will be recorded at a variety of flow rates. The centripetal acceleration will then be decreased and additional data recorded at the same flow rates as those that were used at the higher acceleration. Throughout the experiment, acceleration will be decreased seven times.

CHAPTER 2

VORTEX THEORY

In order to understand the relationship between a free vortex and gravity, it is necessary both to properly define a vortex and to highlight the parameters that govern its formation.

As it is theoretically defined, a vortex is a "whirling mass of water forming a vacuum at its center, into which anything caught in the motion is drawn." In nature, there are many examples of such fluid mechanics phenomena; such as: tornadoes, air swirls forming on airfoils, or just simply the swirling motion of water going down a drain. But what is really important about vortices is that they readily form in pipes and ducts, introducing air bubbles into the hydraulic systems and consequently, lowering the efficiency of pumps, motors, and other mechanical equipment which involves the transportation of water, or other fluids.

Although vortices appear as a common phenomenon to the naked eye, they are actually a complex combination of several fluid mechanics phenomena. Commonly, vortices are classified in two groups, free vortices and forced vortices. For free vortices the vorticity is zero ($\omega = 0$), meaning that a fluid element will not rotate about its own axis even though it rotates about the axis of the vortex. Consequently, for a forced vortex, the vorticity is not zero ($\omega \neq 0$), therefore, the fluid element is rotating about its own axis at the same time that it is rotating about the axis of the vortex.

The most common parameters used in determining vortex formation are: Reynolds Number, Froude Number, Weber Number, Bond Number, and Rossby Number. The relationships that govern calculation of these numbers are given by the following relationships:

$$\text{Reynolds Number } Re = \rho \frac{VL}{\mu} \quad \text{Eqn. 2-1}$$

$$\text{Froude Number } Fr = \frac{V^2}{gL} \quad \text{Eqn. 2-2}$$

$$\text{Weber Number } We = \rho V^2 \frac{L}{\sigma} \quad \text{Eqn. 2-3}$$

$$\text{Bond Number } Bo = \rho \frac{gL^2}{\sigma} \quad \text{Eqn. 2-4}$$

$$\text{Rossby Number } Ro = 4 \frac{Q}{VL^2} \quad \text{Eqn. 2-5}$$

where V=fluid velocity, L=characteristic length of the field to be measured, μ =viscosity, ρ =fluid density, g=gravitational acceleration, σ =surface tension, and Q=volumetric flowrate.

In many design projects, building a model to simulate the conditions of the full scale design is an accepted method of gathering valuable data prior to initiating any implementation process. In building these models, all the parameters -- with the exception of gravitational acceleration -- mentioned above can be manipulated easily (e.g.: either varying one

parameter while keeping the others constant or scaling down all the parameters according to the scale of the model being investigated). Since the purpose of a model is to simulate the final design, the inability to manipulate the acceleration of gravity introduces discontinuities between the model and the real size system. Consequently, the model can fail to predict accurately the functionality and behavior of the full-scale system.

To overcome this problem, it is necessary to conduct experiments that are able to assess the effects of partial gravity on the formation of vortices and, therefore, better define the physical and mathematical parameters that control and sustain vortex formation. This objective can be achieved only in the micro-gravity environment found in space.

CHAPTER 3

EXPERIMENT

The main purpose of this chapter is to give the reader a detailed description of the experiment's hardware and its function. In order to simplify this description, the chapter is divided into two major parts, one explaining the mechanical hardware (section 3.1), and the other explaining the electrical hardware and circuitry (section 3.2). After the introduction of all the mechanical and electrical equipment, section 3.3 explains the computer software and control, which comprises all the software which will control the operational sequence of all components on the platform.

3.1 MECHANICAL DESIGN

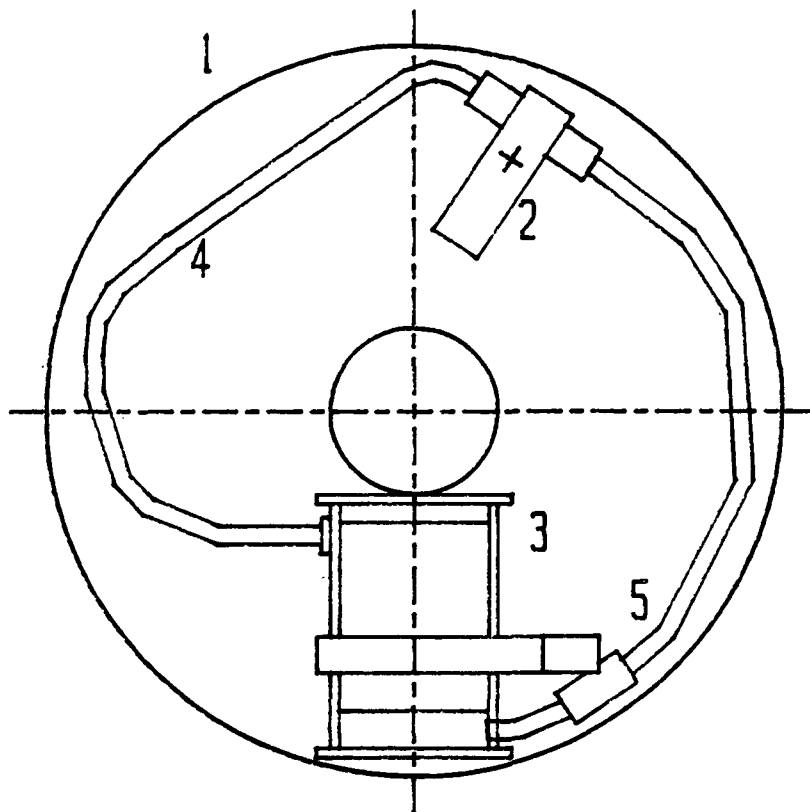
The rotating plate comprises a multitude of mechanical equipment, all of critical importance to the success of the experiment. Along with the major components; i.e. the pump and the vortex cylinder, there is the primary data collection equipment which is composed of the camera and flash. Although the equipment is not complex, it is natural to explain the various functions and purposes of the mechanical hardware by dividing the list of equipment into three major areas. The first area comprises all the equipment used to form the vortex: this includes the pump, the piping, and the vortex cylinder. Another area includes all of the equipment necessary for mounting the rotating plate to the central shaft, the slip rings, the ball bearings, and the motor used to rotate the plate. The third and last area includes all the equipment necessary to obtain visual proof that the experiment performed its function properly, the camera and flash arrangement.

3.1.1 Pump, Piping, and Cylinder

The major component of the experiment is the flow system. This system includes a positive displacement pump, the cylindrical chamber that will contain the vortex, aluminum tubing, and the bubble sensor.

The configuration of these components on the plate is shown in figure 3.1. The cylinder is placed horizontally with the cap at the center of the platform and the base at the edge.

Previous MQPs designed the vortex chamber, which is illustrated in figure 3.2. The vortex chamber is cylindrical in shape; it consists of an ultrasonic mount, two cylindrical



- 1 Platform
- 2 Pump
- 3 Cylinder
- 4 Aluminum Tubing
- 5 Bubble Sensor

			WPI Advanced Space Design Center MITRE/WPI NASA - USRA		
ITEM	# Req.	Material	<input checked="" type="checkbox"/> Flight <input type="checkbox"/> Prototype <input type="checkbox"/> Other		
Used On:			Signatures	Date	Part Name:
Next Higher Assy:			Drawn By: RP	3/31/91	ROTATIONAL FLUID FLOW
Number Required:			Checked:		Scale: Units:
Unless otherwise specified:			Shop:		1" = 4" <input checked="" type="checkbox"/> in <input type="checkbox"/> mm
Machine Dim ±			ICWG:		A
Angular Dim ±			Advisor:		
			Approved:		Drawing Number: Rev:
					GS-II-5.0

Figure 3.1 Fluid Flow System

pieces of lucite (4 in. ID X 1/4 in. thick), a cap, and a base. The ultrasonic mount (or ultrasound mount, as referred to in figure 3.2, part 5.4b) is specifically designed to hold the transducers for the ultrasonic circulation meter. The mount does not have to be located in any particular place, since the circulation of the vortex, once it has reached a steady state, is constant along the height of the cylinder. Presently, the transducer mount is located in the lower 1/3 segment of the cylinder so as not to obstruct the camera view of the vortex mass. The base and cap are also illustrated in figure 3.2 as parts 5.4a, and 5.4c. Although the design of the base resembles that of the cap, the base has an 0.20-in. diameter exit hole. To secure the cylinder from leaking any fluid, O-ring seals are situated at all connections (the exact location of the O-ring seals are shown in the exploded view of the vortex chamber).

Another critical component of the flow system is the bubble sensor. On occasional experimental runs, it was observed that the vortex can gain such high vorticity that air bubbles begin to exit the cylinder, and enter the pump. Since no air should be allowed to enter the pump, a bubble sensor is set up to detect the passage of bubbles. The bubble sensor is installed in the aluminum piping at the exit of the cylinder. There, if bubbles are detected, a feedback signal to stop the experimental run is generated. Since the bubble sensor design is part of the electrical engineering design, a more detailed description of the hardware and circuitry used can be found in section 3.2.

Referring back to figure 3.1, the pump is placed along the aluminum tubing, recycling the fluid exiting the vortex chamber back into the top of the chamber. This, in nature, creates a swirling mass of fluid which becomes a vortex. Previous MQP groups selected two Micropumps from Cole-Palmer, but through on-earth experimentation (for more details

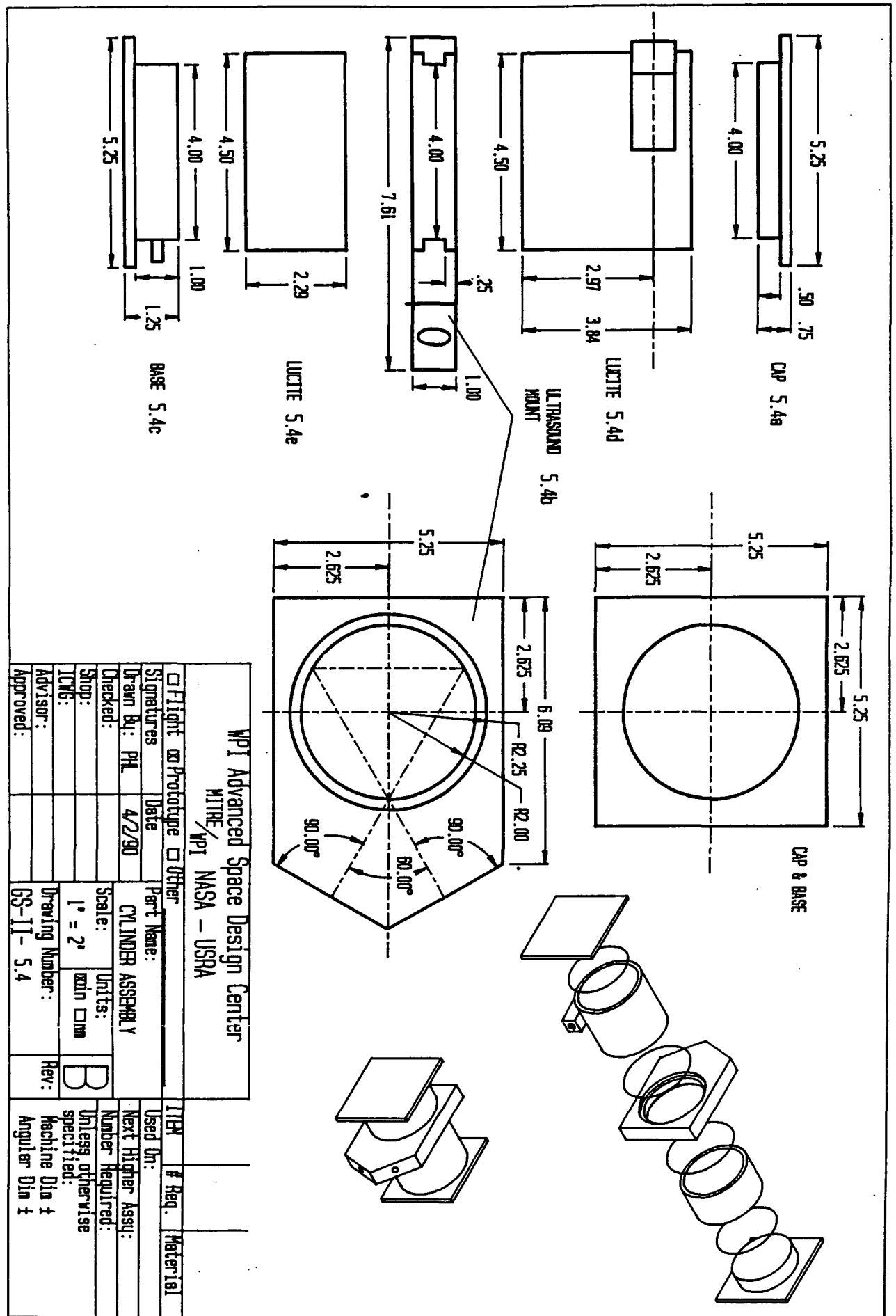


Figure 3.2 Vortex Chamber.

concerning the On-Earth Experiment, refer to chapter 5, section 5.1) it was observed that the pumps chosen have insufficient power to form the vortex while the plate spins.

Consequently, a new pump was selected, based on the results of the experiments conducted with the On-Earth Experiment. Complete specifications on the new pump can be found in Appendix A.

3.1.2 Platform, Shaft, and Platform Motor Equipment

Platform, Shaft, and Slip Rings - All the equipment, both mechanical and electrical, is mounted on the platform. This rotating platform is made from aluminum and consists of a hollow cylinder with two large, circular mounting plates, one at either end. The cylinder portion of the platform is the mechanism by which the experiment is connected to the GASCAN mounting shaft. The cylinder also houses the slip rings which carry electrical power to the experiment. The circular plates on the ends of the cylinder provide the means to mount the experiment and insure stability (see figure 3.3).

All of the experiments in the GASCAN are mounted to the "mounting shaft". This shaft is made of aluminum and is 2-in. in diameter. The mounting shaft must be hollow in order to allow the power cables to be run from the battery box to the other experiments. Since the Vortex Formation in Microgravity Experiment is the bottom experiment in the GASCAN, its mounting is facilitated. The bottom of the shaft is connected to the bottom plate of the cannister. Thus the Vortex Formation Experiment does not need an independent bottom mount, since the bottom plate of the cannister can be utilized for that purpose.

The platform bearings are those which allow the platform to rotate smoothly. There

are two sets of bearings, one on each end of the platform. The bearings are seated in mounts which are connected to the top and bottom of the platform.

The slip rings are that part of the power supply delivery system which are attached to the mounting shaft. The brushes are connected to the cylindrical portion of the platform. As the platform rotates, the brushes keep in constant contact with the slip rings, thus providing electrical power to the experiment. The input side of the slip rings are connected to the battery supply and the output side to any equipment in the experiment needing electrical power.

Rotational Drive Equipment - An electric motor is used to rotate the experiment package. It is mounted to the top mounting plate of the rotating platform. The shaft of the motor protrudes far enough through the plate to allow for a small gear to be attached to it. The gear is essential to insure that the motor shaft and drive belt do not slip over each other. The gear also has top and bottom edges to insure the drive belt does not slide off the shaft.

The drive gear is mounted onto the shaft just above the platform. The gear serves a twofold purpose. First, it's stationary mount to the shaft is what enables the platform to rotate. The drive belt connects the gear and the motor. Secondly, the collar used to attach the gear to the shaft also serves as the top mounting bracket for the platform. The cannister plate underneath and the gear above both prevent the platform from moving up and down on the shaft. The collar of the gear is made of aluminum and the gear itself of plastic. The gear mounts to the shaft by means of set screws.

The drive belt is a reinforced rubber belt. It is smooth on the outer side; the inner

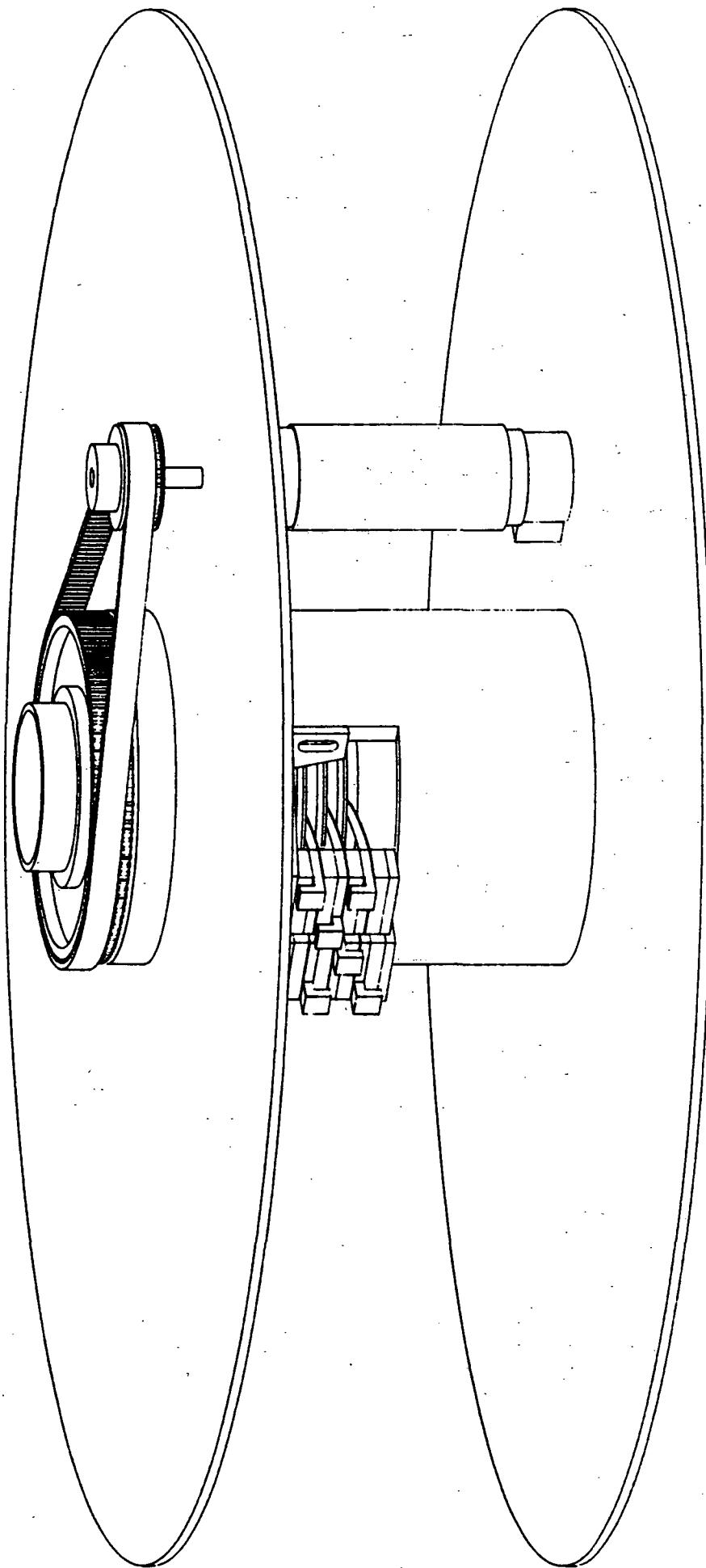


Figure 3.3 Platform

WPI CAD LABORATORY

TITLE: ASSEMBLED PLATFORM

NO: 1

SCALE: 5 DATE: 3/26/90

DRAWN BY: ELLIOTT-BARRY

SHEET: 1

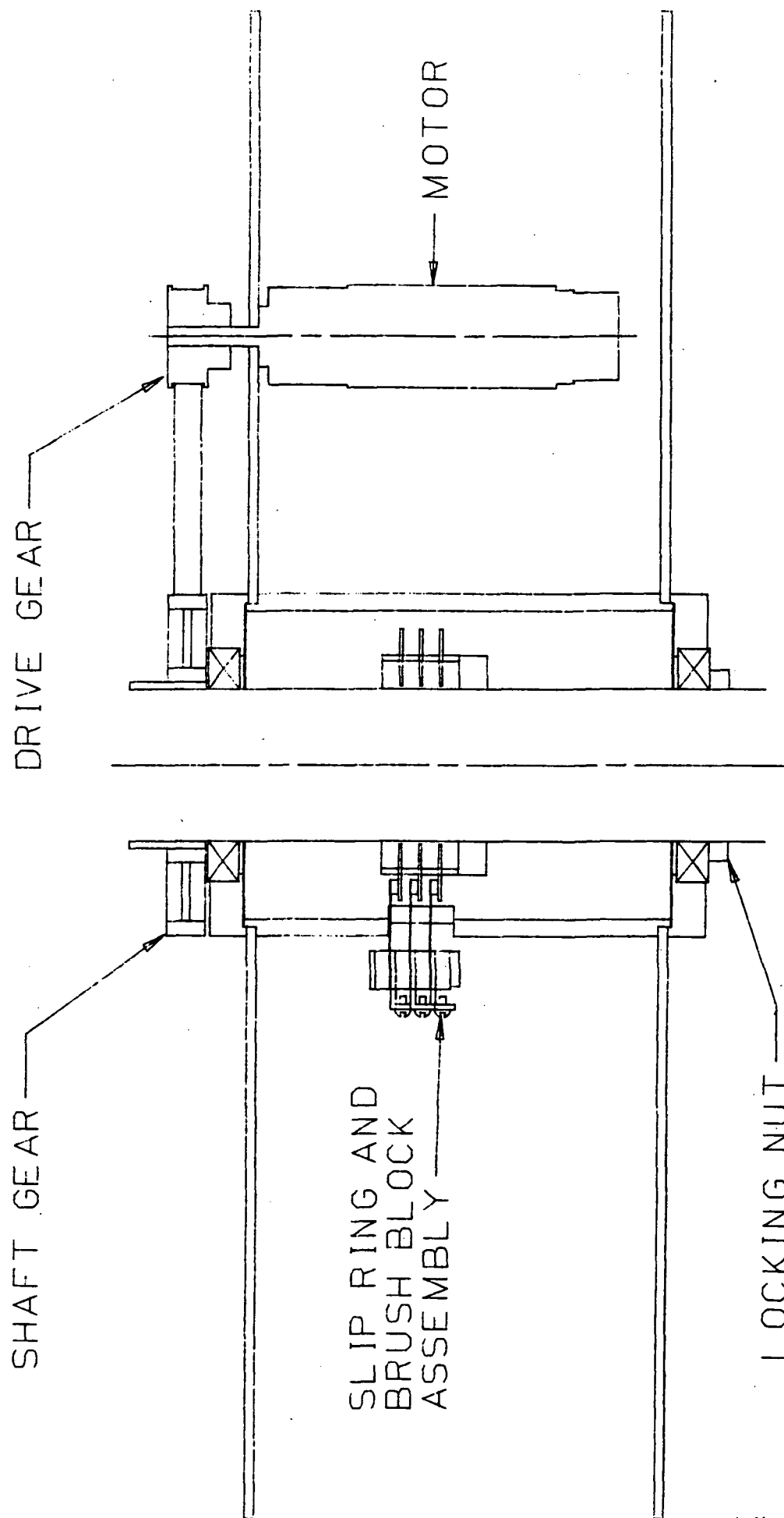


Figure 3.4 Slip Rings, Brushes, and Motor

WPI CAD LABORATORY

TITLE: CROSS SECTIONAL VIEW

NO: 1

SCALE: 5 DATE: 3/25/90

DRAWN BY: ELLIOTT-BARRY

SHEET: 1

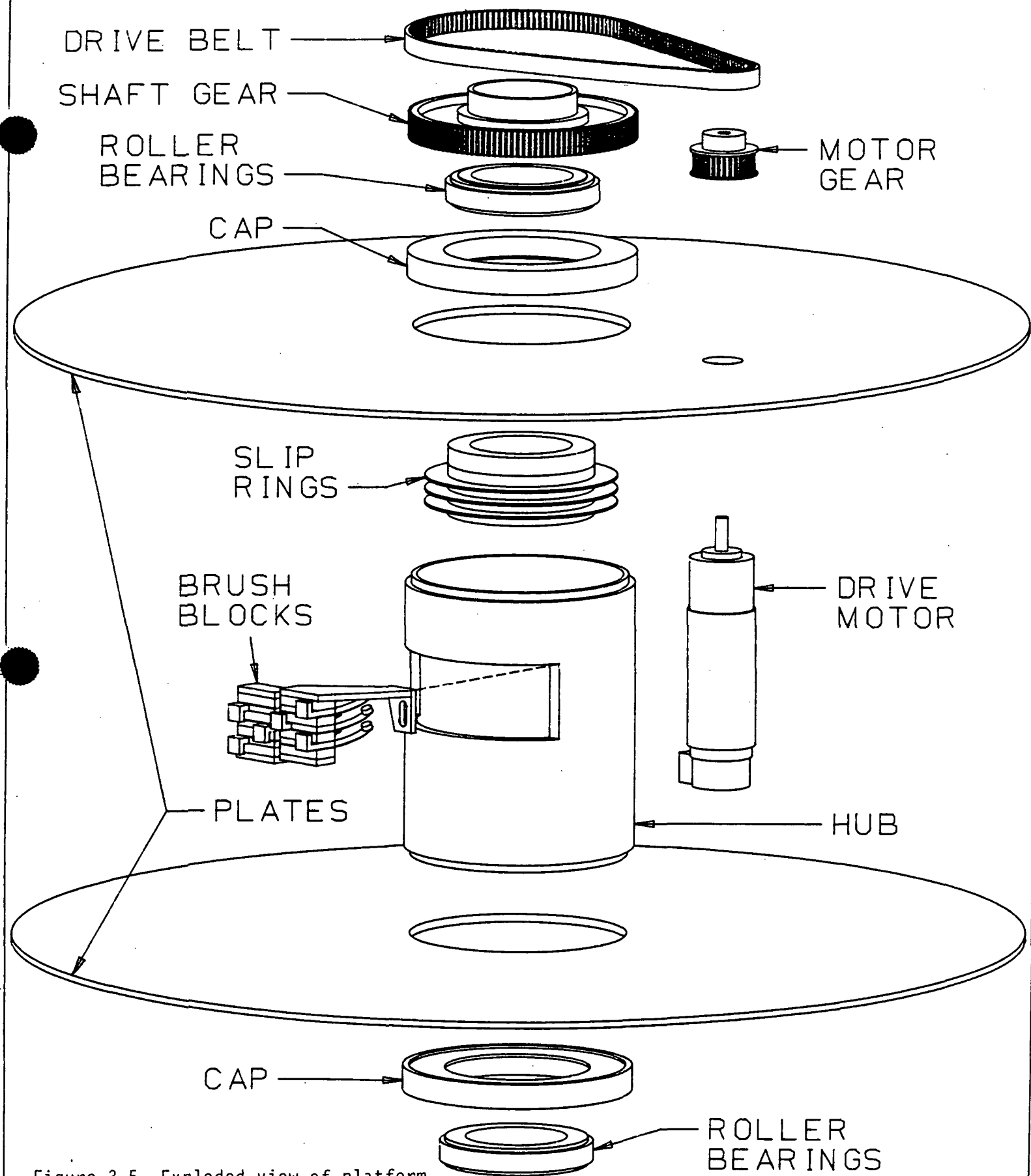


Figure 3.5 Exploded view of platform

WPI CAD LAB	TITLE:	ASSEMBLY VIEW
DATE: 11/19/89	DRAWN BY:	ELLIOTT-BARRY
SCALE: 0.4	NO: 4	SHEET: 1

surface is notched to simulate teeth of a gear. The belt is used to connect the motor and the gear. Since the notched surface of the belt exactly matches the teeth of the drive gear, slipping of the belt is avoided.

3.1.3 Camera and Flash

Unlike the other electronic feedback and data acquisition systems prepared for the experiment, the camera and flash represent the only means used to provide visual proof that the experiment has worked correctly. Through observation of the pictures obtained from the camera/flash arrangement, it will be possible to get a clear indication of vortex shape as a function of the G-levels which are being experienced.

The camera chosen to be used on during the experiment is a commercial unit that was modified by a previous MQP project group. It should be emphasized that the camera selected had requirements not only for operation in "hostile" conditions, but for such other important features as: autowind, short focusing distance, flash capability, and the ability to be triggered by an electrical impulse. Among the "hostile" operating conditions expected to be encountered, that of greatest concern is the low temperature which the camera and film will be exposed to when operating. The Thermal Design Group examined a worst-case scenario in which the Space Shuttle bay would be facing space for long periods of time. Under such conditions, the temperature experienced could reach as low as -30°C . The camera must be able to operate at that temperature without experiencing mechanical and/or electrical failures in any of its components.

Although there are specially designed cameras built to work in such "hostile"

environments, they are typically large and heavy, as well as extremely costly. In choosing the camera, the problem of space is also a consideration. While the selected camera was not built for "hostile" environments, its dimensions are small as compared to other choices.

In order to evaluate the effects of the expected thermal environment, the Thermal Analysis group conducted low temperature experiments on various types of films and observed the reaction of film exposed to low temperatures. The film tested was a 400 ASA black & white. Pictures were taken immediately after the film was taken out of the freezer, and then developed after refreezing the film. The tests showed that the film was virtually unaffected by the low temperature environment and that the pictures developed well. The only residual concern is that the film tends to become brittle at these low temperatures, raising concern that breakage might occur while the camera is winding to the next frame. The risk has been judged to be acceptable.

As mentioned above, two other very important features that the camera must possess are an autowind system, and a means for electrical triggering. These two features are important since the GASCAN will be completely sealed off. The camera that was chosen is a 35mm Pentax A4000 model (refer to Appendix A for full camera specifications and data sheets), which can not only be electrically triggered, but has an autowind system directly built in the body. Another requirement is that the camera must be capable of using alkaline batteries, since the use of lithium batteries is prohibited by NASA safety regulations.

Providing electrical power to the camera required another critical design decision. The camera must be placed within the GASCAN with its power switch in the ON position, since it will be completely sealed when the GASCAN will be ready for flight. By placing

regular batteries within the body of the camera with the power switch in the ON position results in a battery life of approximately 24 hrs. One design option is to power the camera using the payload battery supply. This requires an appropriate connection within the body of the camera. Somewhere along this power circuit, a switch controlled by the CPU would be installed. As soon as the CPU sends the signal for the pump to start pumping fluid, it would also send a signal to supply power to the camera just before it gets electrically triggered to take a picture. After the picture is taken, the CPU sends another signal to disconnect the camera from the power source. This process would be repeated everytime the CPU sends a signal to the pump at the start of a new experimental run.

Although there was not enough time to explore this design option further, it seems to be one possible way to overcome the camera's powering problem. This design decision is one that future project groups will have to evaluate carefully.

3.2 ELECTRICAL DESIGN

This section presents the design and function of the electrical hardware and related software used in the Rotational Fluid Flow Experiment. This equipment consists mainly of sensors, transducers, and controllers, and is built around a central 8088 microprocessor-based controller system. Its purpose is to supervise the operation of the mechanical equipment and to record data of interest for postflight analysis.

The variables monitored by the system are: the circulation and temperature of the fluid, the acceleration exerted on the containment vessel (and so the fluid) because of the platform's rotation, and the depth of the dimple of the vortex. For this purpose the system uses an ultrasonic circulation instrument, a temperature transducer, two accelerometers, and a camera equipped with a macro lens. Besides these components, two identical Pulse Width Amplifier controllers adjust the operation of the platform drive motor and of the fluid pumping system. Finally, a gas entrainment detector is used to signal the entrainment of air in the pumping system. The following pages provide an in-depth description of these components.

3.2.1 Computer Hardware

An Onset C-44 Bus computer system was chosen by previous groups as the core hardware used for the Rotational Fluid Flow experiment. Onset hardware was chosen due to its low power consumption and small size. Onset hardware has successfully been used by NASA and the Air Force in the past.

The configuration chosen for the system consists of an 8088-based CPU board (CPU-

8088), a four-channel analog-to-digital converter card with scratch-pad RAM (MOR-800), and a 64K-byte EPROM-burner card for data storage (DS-64). These three cards are interconnected using an Onset C-44 Bus/Card cage.

This section describes the basic features offered by these devices. For detailed information on system integration and programming, refer to appendix B.

The CPU-8088 board comes supplied with a HARRIS minimum mode 80C88 microprocessor, an 81C55 Parallel Interface Adapter, an 82C52 Serial Controller Interface, an MM58274 Real Time Clock, and an 27C64 EPROM. This EPROM contains a monitor program that can be used as an operating system for software development. It can be replaced with either an 27C64, 27C128, or 27C256 EPROM containing a full-length program that executes upon system power-up. On-board devices are mapped to the upper half of the one megabyte address space available to the 80C88 microprocessor. A 34-pin connector at the top of the card carries the I/O connections from the 81C55 and the 82C52.

The 80C88 microprocessor provides hardware multiply (16×16) and hardware divide (32×16) both signed and unsigned. All 20 address lines are available off board allowing 512K of external memory without resorting to bank switching. External memory is mapped to the lower half of the address space. A switchable RC oscillator drives the CPU's clock input at about 4 MHz. For compatibility with other C-44 cards, the clock frequency is divided down to 2 MHz before being placed on the bus. The 80C88 allows for six hardware interrupts. Under software control, the CPU can enter two different low power idle modes: WAIT and HYBERNATE. Both modes stop the oscillator input to the CPU, accounting for its low power drain in these modes ($200 - 500 \mu\text{A}$ and $80 - 200 \mu\text{A}$, respectively), and can be

entered and exited in one clock cycle.

The 81C55 port chip provides the 80C88-board with 22 programmable I/O lines, 256 bytes of static RAM, and a 14-bit timer. The 22 I/O lines come as two banks of eight and one bank of six and can be programmed by bank as either inputs or outputs. The two eight-bit ports may also be configured for strobed I/O, taking their control from the six-bit port.

The 82C52 Serial Controller Interface allows rates from 50 to 38,400 baud, 5 to 8 data bits, 1, 1.5, or 2 stop bits, and a variety of parity signals. The UART can be made to cause interrupts on a received character, so that an incoming signal can be used to awaken the board.

The MM58274 Real Time Clock has two 4-bit control and status registers, and fourteen 4-bit read-write time registers which contain time information ranging from tenths of seconds to tens of years. The clock can be programmed to provide repeated or single interrupts at 0.1, 0.5, 1, 5, 10, 30, and 60-second intervals.

The MOR-800 10-bit analog to digital converter card has a four-channel, single-ended converter that accepts inputs covering the range of 0 to 2.5 volts. An LM236 is used as the voltage reference. The card uses an NEC 7002 4-channel converter. The chip has an on-board multiplexer and can be programmed to make 8-bit or 10-bit conversions of any of the four input channels by writing the appropriate command word to the control port. The card also provides 4K of additional system RAM and a 6818 Real Time Clock.

The DS-64 EPROM-burner card burns EPROMs under program control over a wide temperature range, is vibration insensitive, and has totally random access and complete read-after-write capability. The CPU can program the data into NMOS EPROMs at an average

rate of 200 bytes/second. CMOS EPROMs can be used instead of the NMOS variety if the power switching circuitry that controls the Vcc supply to each of the EPROMs is defeated. The board has four sockets for EPROMs which give it a data storage capacity of 32K bytes when 2764's are installed in these sockets, or of 64K bytes when 27128 EPROMs are used.

3.2.2 Temperature Transducer

The temperature transducer interface is based on the Analog Devices AD590 temperature transducer. The AD590 has a wide temperature range covering -55° through 150° Celsius. Basically, the transducer is a current regulator whose output is proportional to absolute temperature. Thus, when powered, the device's current output is proportional to temperature with a scale factor of 1 μ A per degree Kelvin. The interface design is shown in figure 3.6.

Since we desire to have the transducer connected to the MOR-800's analog-to-digital converter (ADC), the temperature-to-current relationship must be translated to a temperature-to-voltage relation. To accomplish this, a 1K Ω resistor is connected between the AD590's negative terminal and ground. If the voltage is tapped at the AD590's negative terminal, the voltage drop there is now proportional to the observed temperature:

$$1m \frac{V}{K^{\circ}} = (1\mu \frac{A}{K^{\circ}})(1K\Omega) \quad \text{Eqn. 3-1}$$

For example, ambient temperature of 300°K generates a 300 μ A current. Thus, there will be

a 300mV drop across the 1K Ω resistor.

Now, the signal must be conditioned and its gain adjusted to meet the input requirements of the MOR-800's ADC. The ADC allows input signals in the range of 0 to 2.5 volts. To scale the transducer signal appropriately, a temperature range must first be selected. In this case, rather than optimize the resolution at a given temperature range, the signal was scaled to accommodate the full operating range of the transducer; 218°K through 423°K. Assuming full scale input:

$$(150^{\circ}\text{C}) \ 423^{\circ}\text{C} \Rightarrow 423\text{mV} \text{ (upper limit of transducer)}$$

$$\text{(full scale ADC input)} \ \frac{2.5\text{V}}{423}\text{mV} = 5.9 \text{ (required gain)}$$

By using a non-inverting op amp configuration, again with the high input impedance TL084, the gain adjustment can be performed. Choosing 10K Ω and 2K Ω resistors yields a gain of:

$$\text{GAIN} = \frac{10\text{K}\Omega}{2\text{K}\Omega} + 1 = 6$$

With a gain of 6, a problem occurs only at the upper limit of the transducer. A temperature of 150°C will produce a 423mV drop across the 1K Ω resistor. A gain of 6 amplifies this drop to 2.54V. This exceeds the maximum input for the MOR-800's ADC (2.5V). However, at 150°C (302°F) the complete GASCan system would fail! Since operation at this temperature is not anticipated, it can be disregarded.

The temperature transducer interface is connected to the flight computer through the MOR-800's analog-to-digital converter; Channel 0.

3.2.3 Motor and Pump Controllers

The platform motor controller and the pump controller are identical pulse-width modulated amplifier (PWMA) based feedback circuits that govern the rotational speed of the platform and the flow rate of the pump, respectively. These controllers receive their directives for speed and flow rate control from the flight computer. These controllers were developed during the 1989-90 project year; refer to the MQP report for further design details.

The motor and pump controllers are designed to take a 0 to 5-volt analog input and effect a corresponding rotational speed or flow rate. From the computer point of view, the requirement is the conversion of an 8-bit digital word into the 0 to 5-volt signal. Refer to figure 3.6 to follow discussion on circuit design.

To provide the two simultaneous 8-bit words to the pump and motor controllers, the two 8-bit ports, PA and PB, from the CPU-8088's 8155 are used. In addition, two bits from port C are used to serve as strobes for latching the 8-bit words to the digital to analog

converter (DAC). These strobe bits are PC0 and PC1.

An Analog Devices AD7524 digital to analog converter is used for the conversion. A negative voltage reference is required by the AD7524. Since the full-scale analog output is 5 volts, a -5 volt reference is required. In this case, a single National Semiconductor LM320T was used as the voltage reference.

The next consideration is whether the DAC will operate in unipolar or bipolar mode. The bipolar mode is used when both positive and negative output signals are required. In the bipolar mode, the resolution is limited to 128 levels in the negative and positive domains. The unipolar mode is used for strictly positive output signals. This is the mode used on the experiment. The following equation governs the digital to analog conversion process:

$$\text{An. Out. Volt.} = \frac{\text{Digital Value}}{256}(-V_{ref}) \quad \text{Eqn. 3-2}$$

$$\text{Resolution is 1 Bit} \Rightarrow \frac{1}{265}(-V_{ref}) \quad \text{Eqn. 3-3}$$

With a -5 volt reference, the resolution is approximately 20 mV. See figure 3.7 for comparison of both modes.

The output signals from the DAC are fed through a high input impedance operational amplifier, a TL084, which serves as a buffer. Notice that the gain for the op amp is not

UNIPOLAR OPERATION

DIGITAL INPUT		ANALOG OUTPUT
MSB	LSB	
11111111		$-V_{ref} \times (255/256)$
10000001		$-V_{ref} \times (129/256)$
10000000		$-V_{ref} \times (128/256)$
01111111		$-V_{ref} \times (127/256)$
00000001		$-V_{ref} \times (1/256)$
00000000		$-V_{ref} \times (0/256)$

BIPOLAR OPERATION

DIGITAL INPUT		ANALOG OUTPUT
MSB	LSB	
11111111		$+V_{ref} \times (127/128)$
10000001		$+V_{ref} \times (1/128)$
10000000		0
01111111		$-V_{ref} \times (1/128)$
00000001		$-V_{ref} \times (127/128)$
00000000		$-V_{ref} \times (128/128)$

Figure 3.7 DAC Operation Modes.

adjusted (i.e., it equals one). The DAC feedback line, R_{FB} , is connected directly to the output of the op amp.

DAC control is possible via chip select (CS) and write (WR) lines; both active low. In this case, the two control lines are tied together and connected to the PC0 and PC1 strobes. PC0 strobes data to the motor controller DAC, while PC1 strobes data to the pump controller DAC.

To provide the user with visual feedback of the current state of each DAC, hexadecimal displays have been added. The TIL311 device has on-chip decoding and driving capabilities. Four lines provide the data path and an active low line (STR) strobes the data in. Two independent supplies are used for display power (V_a) and logic power (V_{cc}). The strobe lines are connected to the same strobes that latch data into the DACs.

3.2.4 Accelerometers

Two Genisco 3001-03 DC accelerometers are used to monitor the centripetal acceleration exerted on the containment vessel (and consequently the fluid) as the result of the platform's rotation. By placing two diametrically opposed accelerometers on the platform, the flight computer can obtain accurate acceleration readings. Although the platform motor control circuitry has its own feedback mechanism for assuring accurate speed-up of the platform, the availability of accelerometer data provides the flight computer with the ability to adjust platform speed if necessary. However, rather than using accelerometers to provide feedback, accelerometer readings are stored for postflight correlation with other data and analysis.

The 3001-03 accelerometer uses strain gages bonded to a cantilever beam and is connected to a four-active arm Wheatstone bridge. A mass is attached to one end of the beam causing it to deflect proportional to acceleration. Although rated at $\pm 2\text{Gs}$, the 3001-03 will survive shock accelerations of up to $\pm 20\text{Gs}$. Refer to figure 3.6 to follow discussion on accelerometer interface design.

The Genisco 3001-03 is a four-terminal device. Two terminals are used for excitation. In this case, a 12-volt excitation is used. Given this excitation, at full scale the accelerometer will output a value of 1.5 mV per excitation volt. Thus, at 12 V excitation and 2Gs, the accelerometer will output 18mV. The acceptance data (see appendix B) supplied by the manufacturer provides more details on the linearity of the accelerometers.

The accelerometers are interfaced to the MOR-800's analog to digital converter. For this reason, their output signal must be conditioned and scaled to work with the ADC's 0 to 2.5-volt constraint. Assuming full-scale output from an accelerometer:

$$2\text{ G Acceleration} = 18\text{mV output}$$

The value obtained should correspond to 2.5V input to the ADC; thus:

$$\frac{2.5\text{V}}{18\text{mV}} = 138.88 \text{ (required gain adjustment)}$$

By using a 33K Ω resistor and two 510 Ω resistors in parallel, the gain can be adjusted such that:

$$GAIN = \frac{33K\Omega}{510\Omega \parallel 510\Omega} = 129.41$$

Thus, the operating range of the accelerometer circuit is 0 to 18mV (0 to 2Gs) and this translates into an ADC input range of 0 to 2.333 volts.

An Analog Devices AD521 instrumentation amplifier was used for each of the accelerometers. Instrumentation amplifiers are precision differential voltage gain devices. They are characterized by high input impedance, balanced differential input, low bias currents and high common mode rejection ratio. Unlike most op amps, the inputs are protected against overvoltages of up to $\pm 15V$ beyond the amplifiers supply voltages. Instrumentation amplifiers are ideal when small signals, such as accelerometer signals, need to be acquired.

To complete the functional description, the AD521's TRIM pin is connected to the output. TRIM is used as an additional feedback line to adjust the AD521's output further. In this case, no additional adjustment is needed; TRIM is directly connected to the output.

The two accelerometer interfaces are connected to the flight computer through the MOR-800's analog to digital converter; Channels 1 and 2.

3.2.5 Gas Entrainment Detector

As described earlier, a vortex is a swirling mass of fluid having a low pressure column in its center. This low pressure column is called the dimple of the vortex. The

stronger the vortex, the greater the dimple depth will be. However, the dimple depth is limited to the dimensions of the containment vessel. If the dimple reaches the bottom of the vessel, air is ingested into the pump and plumbing system. This event adversely affects pump performance. Air ingestion reduces the pressure in the pump, which results in a decrease on the amount of fluid pumped. It also strains the operation of the pump motor, considerably reducing its life. In extreme cases, motor overheating can lead to pump breakdown. For these reasons, a gas entrainment (or ingestion) detector is needed for the Rotational Fluid Flow experiment. If air is being ingested, the current vortex formation trial must be terminated.

So as not to impede the fluid flow in the outlet tube, an early design decision was to use a non-intrusive method of detecting air presence. This detection method mandated the passing of a signal through the outlet tube in a direction perpendicular to that of the fluid flow and observing differences between the transmitted and received signals as evidence of the passage of bubbles through the signal path. Two prospective signal frequencies were examined: ultrasonic and infrared (IR). The ultrasonic approach was discarded because a detection method utilizing optoelectronics was a simpler and less expensive approach. Therefore, it was decided by previous groups to implement infrared optoelectronic devices for the purpose of bubble detection.

The infrared devices chosen are the TIL 31b infrared emitter and the TIL 81 phototransistor. These devices were chosen because they are mechanically and spectrally matched (see figures 3.8-3.11), consume little power, and are readily available.

The TIL 31b is a P-N Gallium Arsenide infrared emitting diode. This device has

electrical characteristics similar to those of a normal diode (i.e., it passes current in one direction and blocks it in the other), but emits infrared light when biased in the forward direction. It requires typical forward operating voltages of about 2V. A forward current of 25 mA or greater is required because currents lower than this are near the non-linear portion of the forward conduction graph for the device. The device radiates light at a wavelength of 940nm.

The TIL 81 is an N-P-N planar silicon phototransistor device. A phototransistor can be regarded as a conventional transistor housed in a case that enables its semiconductor

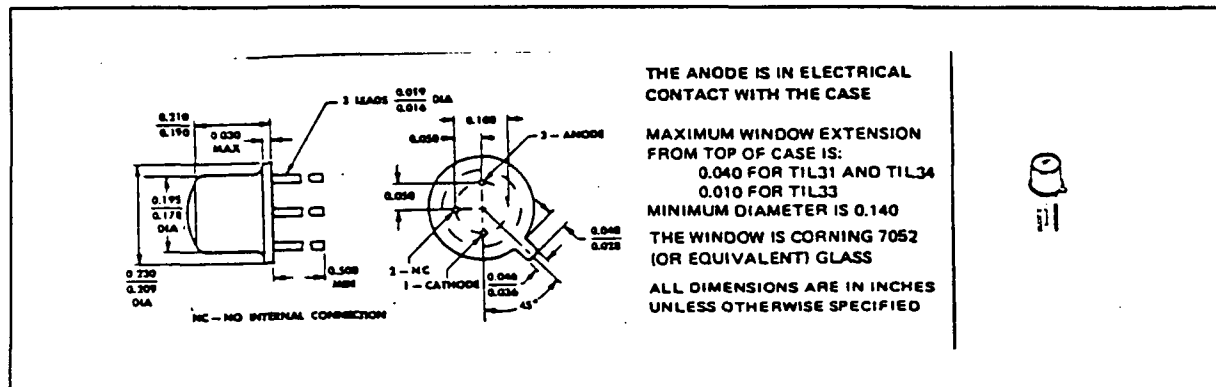


Figure 3.8 TIL 31b Mechanical Specifications.

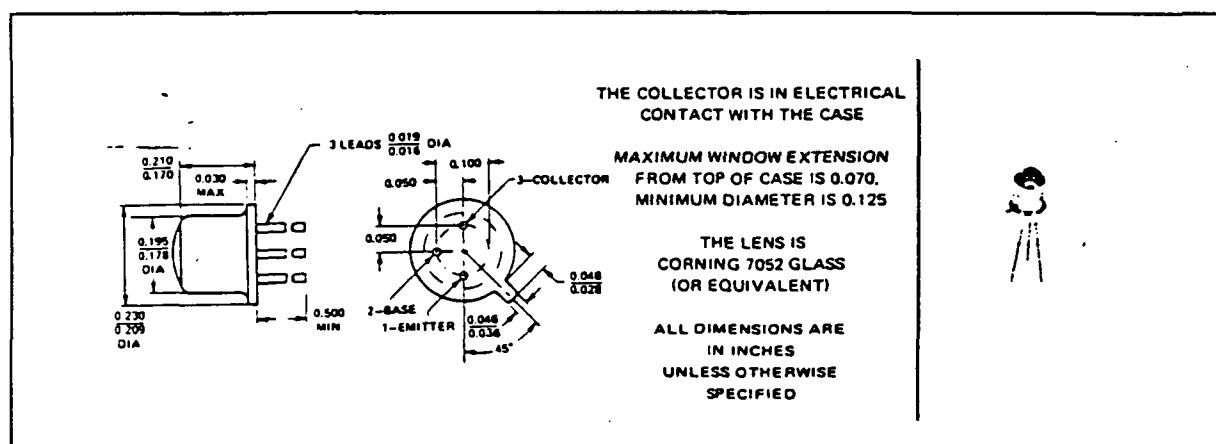


Figure 3.9 TIL 81 Mechanical Specifications.

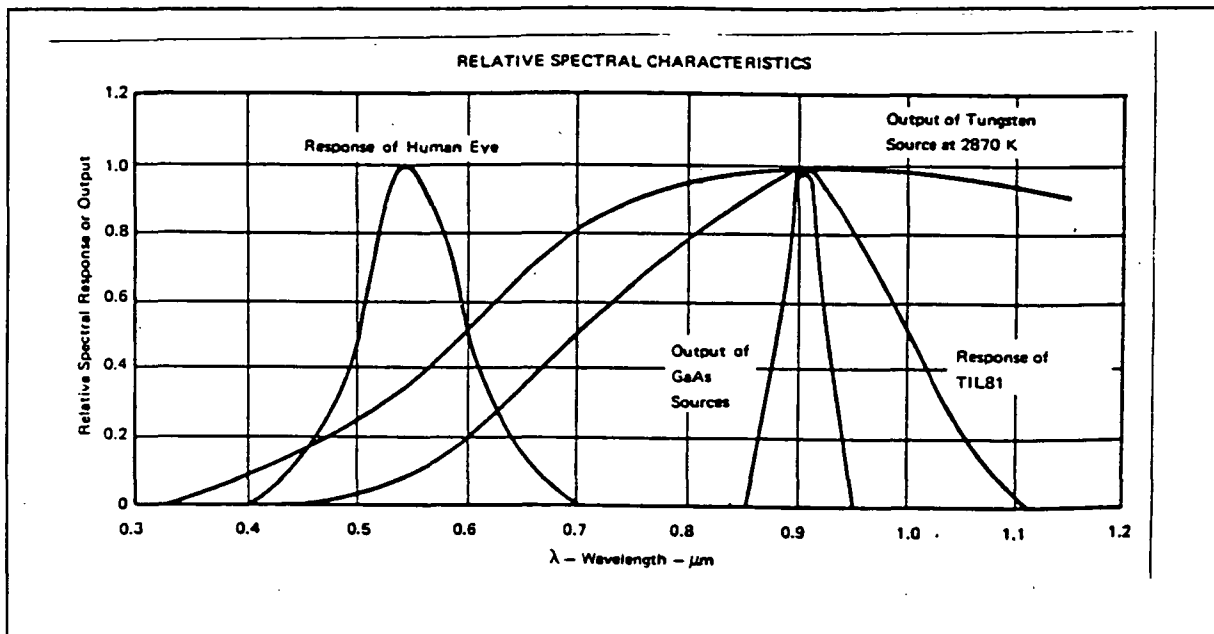


Figure 3.10 TIL 81 Spectral Characteristics.

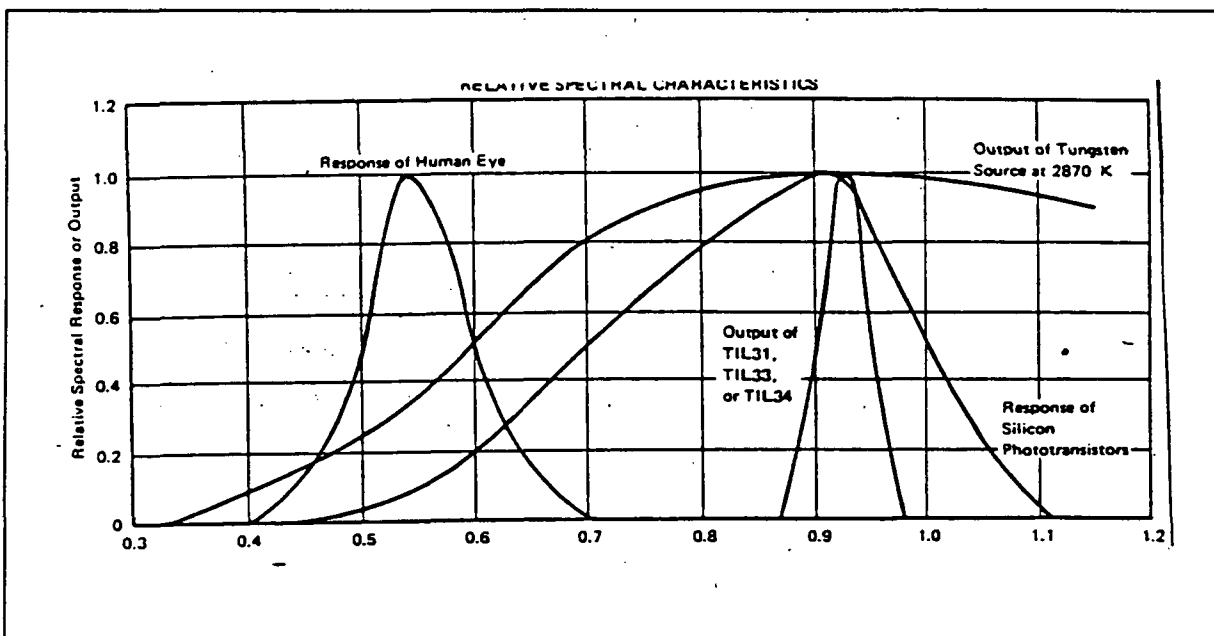


Figure 3.11 TIL 31b Spectral Characteristics.

junctions to be exposed to external light. Refer to figure 3.12 for an explanation of phototransistor operation.

As seen in figure 3.12, the base-collector junction of the transistor is reversed biased and acts as a photodiode, a light sensitive device which generates current when irradiated with light. The photo-generated currents of the base-collector junction feed directly into the base of the device, and the normal current-amplifying transistor action causes the output current to appear (in greatly amplified form) as

collector current. The resistor causes this current to generate an output voltage as shown in figure 3.12.

To ensure that the infrared devices are mounted collinearly, a mounting structure was designed and built. This structure is shown in figure 3.13. It consists of a Plexiglass block machined to have a channel through it with a cross sectional area equaling that of the outlet tube so as not to impede the fluid flow. A hole was drilled through two opposite sides of the Plexiglass structure to accommodate the optoelectronic devices. The IR components are epoxied into place and fittings are attached to the Plexiglass to accommodate the outlet tube.

A Plexiglass structure identical to the one just described was used to experimentally determine the proper biasing current for the TIL 81 phototransistor. Using this structure and a syringe, a "bubble generator" was constructed. This assembly is shown in figure 3.14.

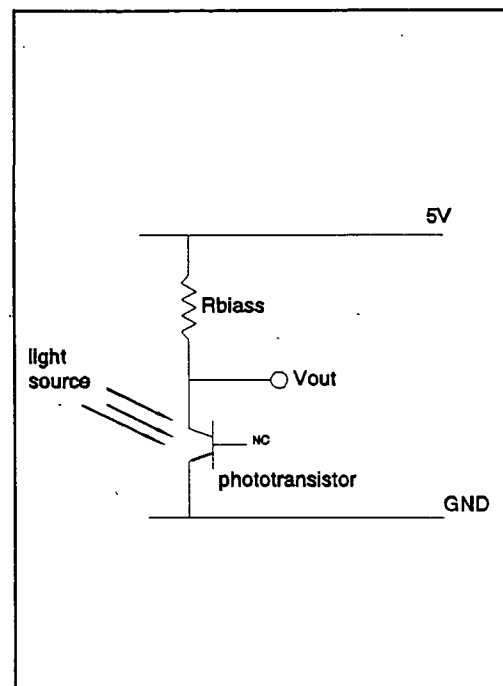


Figure 3.12
Phototransistor
Operation.

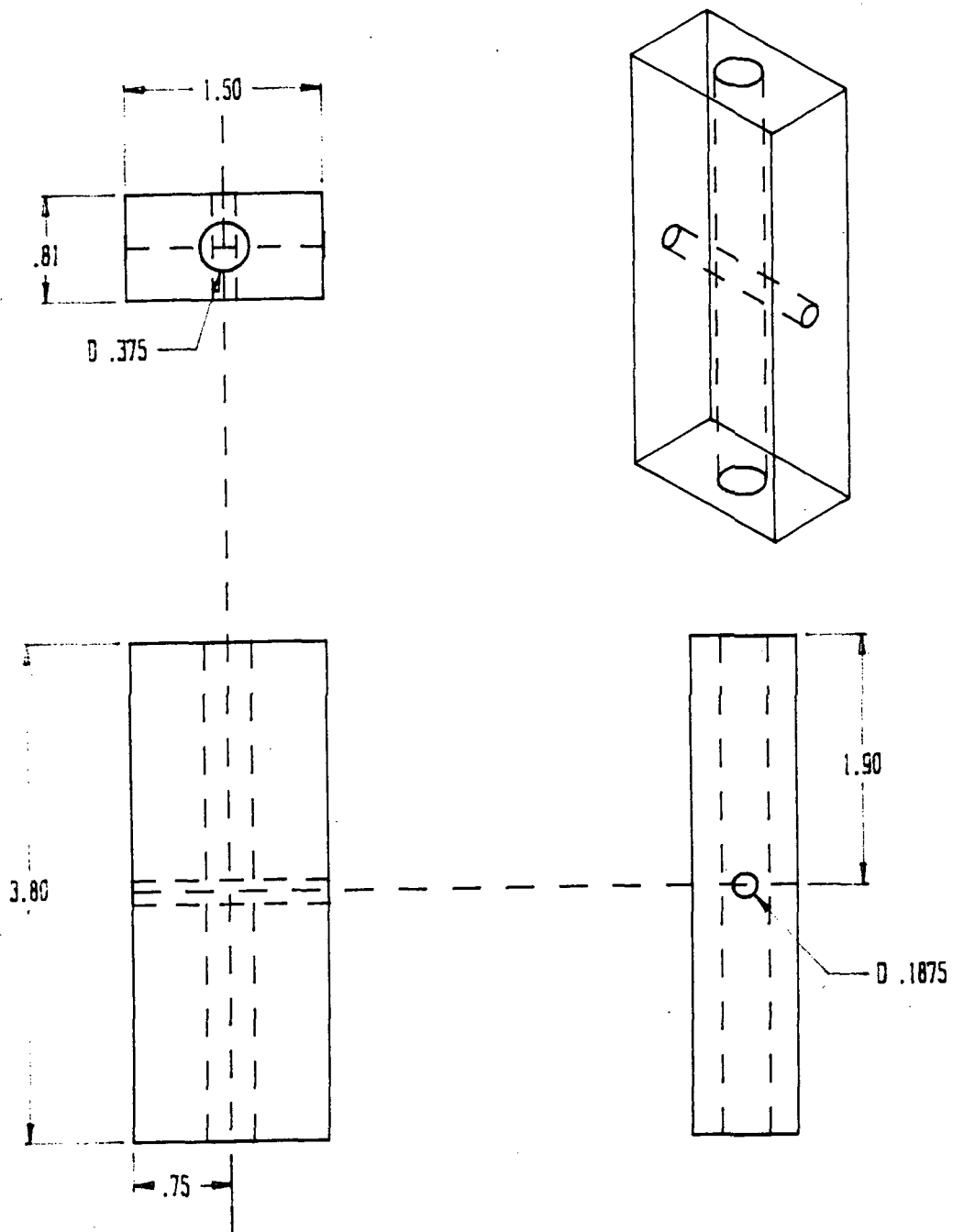


Figure 3.13 Plexiglass Mount.

The biasing current was determined by constructing the circuit shown in figure 3.12 and recording the smallest variation in the collector voltage for different resistor values. The results of this experiment are shown in table 3.1.

The final layout of the emitter-receiver IR circuit is shown in figure 3.15. An MC78L00C 5 V, 0.1 A voltage regulator is used to provide a stable voltage from the 12 V power supply. On the emitter side, a 150 Ω resistor is placed in series with the 5 V source and the TIL 31b diode. This provides a forward bias current of 25.75 mA to the diode at the measured voltage drop of 1.23 V. The resistor dissipates 97 mW and the diode dissipates 31 mW. On the receiver side, a 3 K Ω resistor was used to bias the phototransistor because it produced the greatest ΔV_o at the lowest current (see table 3.1). This current, without a bubble present, is approximately 0.7 mA. The resistor dissipates 1.5 mW and the phototransistor dissipates 2 mW, approximately.

The bubble detector sub-assembly described above functions as follows: small gas bubbles scatter the IR beam and drive the TIL 81's collector voltage higher while

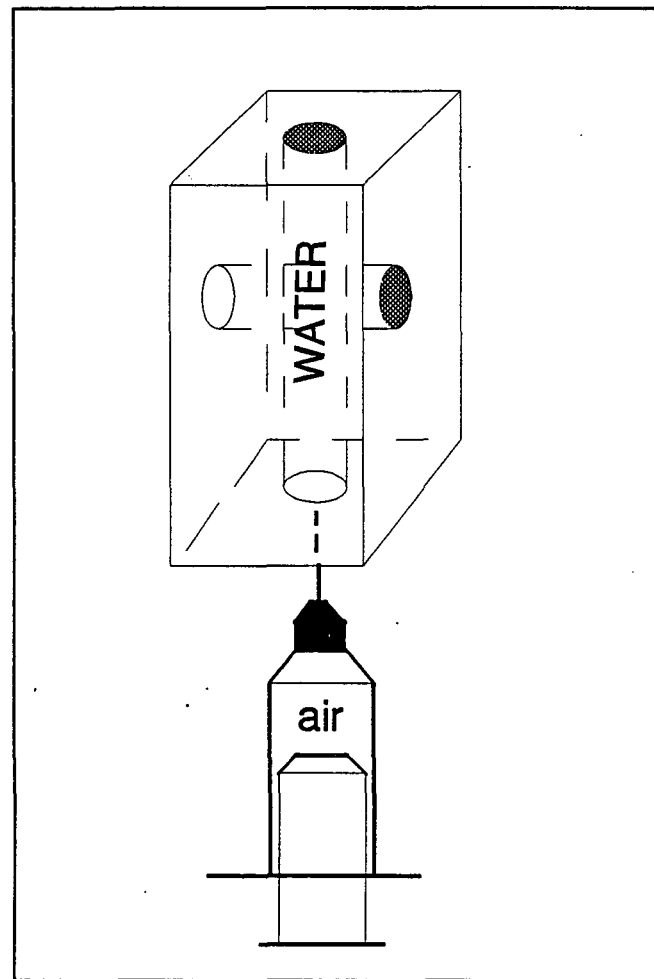


Figure 3.14 "Bubble Maker" Assembly.

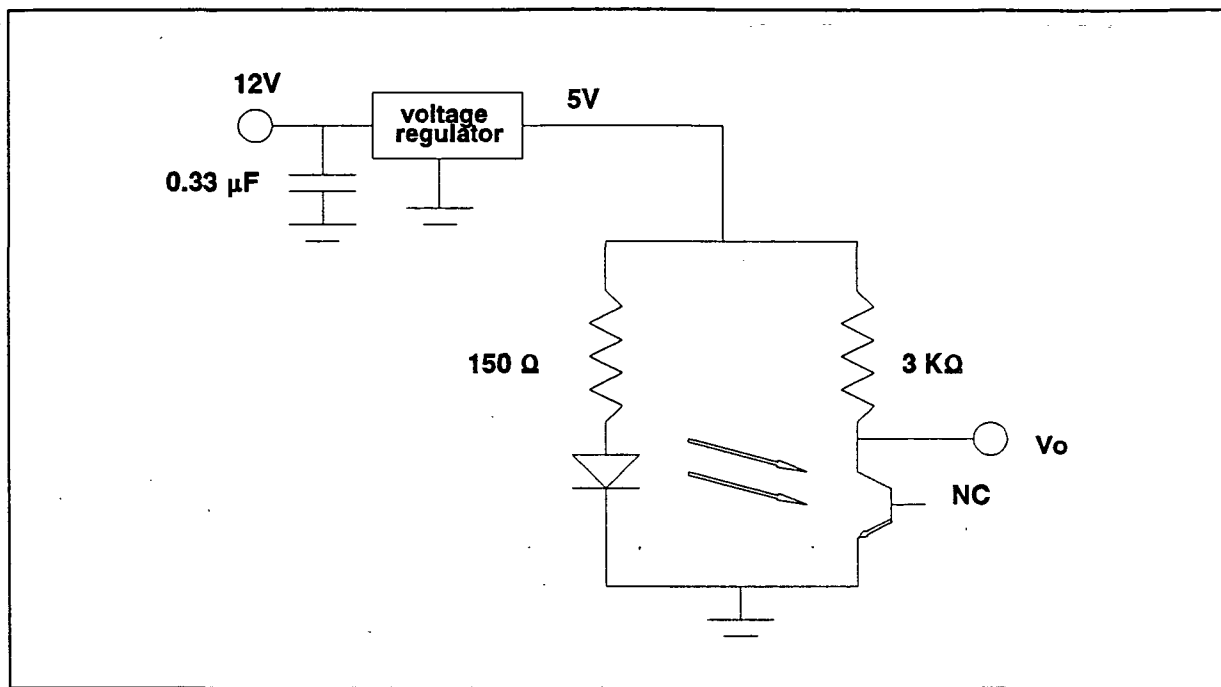


Figure 3.15 IR Emitter-Receiver Setup.

large bubbles allow more of the beam to reach the TIL 81 and drive the collector voltage lower. The effect of small gas bubbles is illustrated in figure 3.16, and the effect of large bubbles in figure 3.17.

A signal conditioning circuit was needed to interface the bubble detector to the central microprocessor-based controller. Previous MQP teams designed an interface that featured user-selectable sensitivity. Refer to figure 3.18 for a discussion of circuit function. For an in-depth description of this design, refer to the 1990 Rotational Fluid Flow Experiment MQP report.

The first stage in the diagram is a bubble detector similar to the one previously described. The detector is followed by a non-inverting amplifier with gain of 2 that is used to amplify the voltage peaks resulting from bubbles passing through the detector. Next, an active differentiator is used that functions as a temperature compensator. This differentiator

Table 3.1

R (Ohms)	V_o (DC Volts)	Smallest ΔV_o (V)
1 K	4.13 V	0.07 V
2 K	3.36 V	0.07 V
3 K	2.89 V	0.1 V
4 k	1.59 V	0.1 V

generates the differential of the input signal, minus any DC component present. The Schmitt Trigger detects the passage of a bubble through the outlet tube as peaks on the differentiator output signal. A four-bit counter monitors the number of times the Schmitt Trigger provides an output. This counter, in turn, is reset by an astable multivibrator which produces a waveform at a chosen frequency and duty-cycle. Finally, a four-bit comparator compares the output from the counter with the settings of four DIP switches. If the counter output is greater than the number defined by the DIP switches, an "entrainment detected" signal interrupts the CPU. Therefore, by changing the position of the DIP switches and the frequency of the multivibrator, the rate of gas bubble flow which causes the "entrainment detected" signal can be varied.

The above circuit was built and tested during the present project year. The circuit performed as expected. However, it was found that it would not serve its purpose when integrated to the Rotational Fluid Flow system. There is no certainty about how gas entrainment will occur in a microgravity environment. Entrainment could occur suddenly, or it could be preceded by a shower of small gas bubbles. If the dimple reached the bubble detector before the count dictated by the DIP switches was finalized, the "entrainment detected" signal would never be generated.

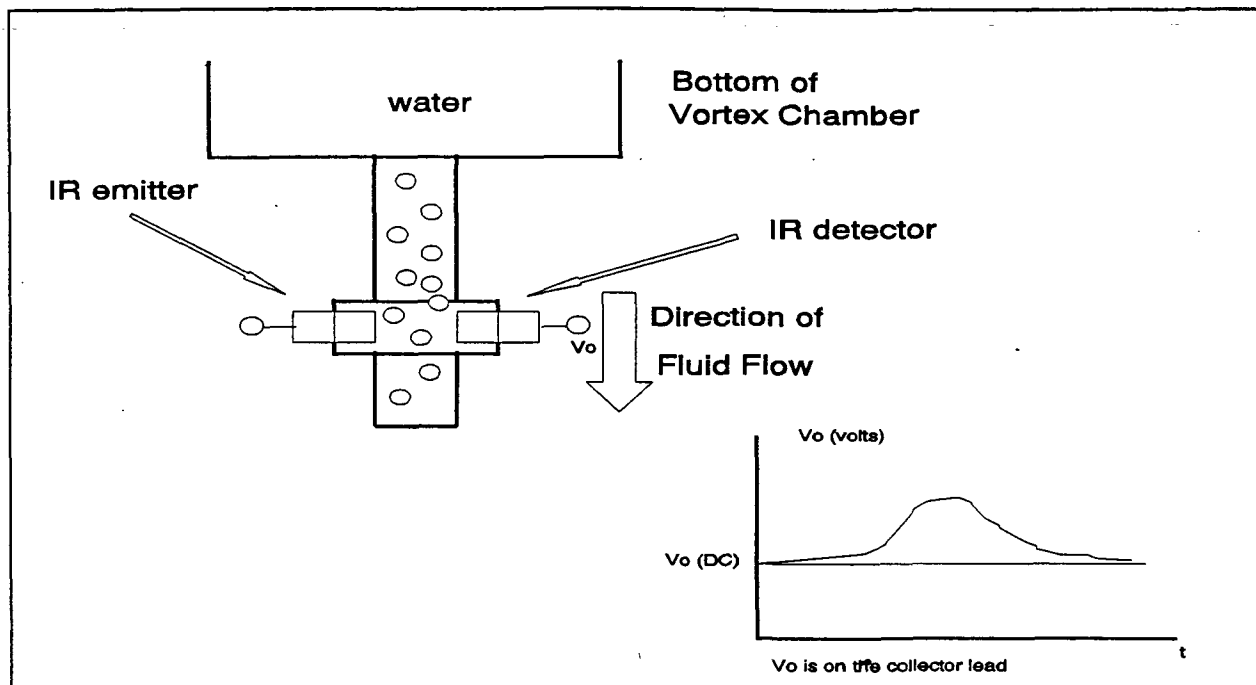


Figure 3.16 Effect of small gas bubbles.

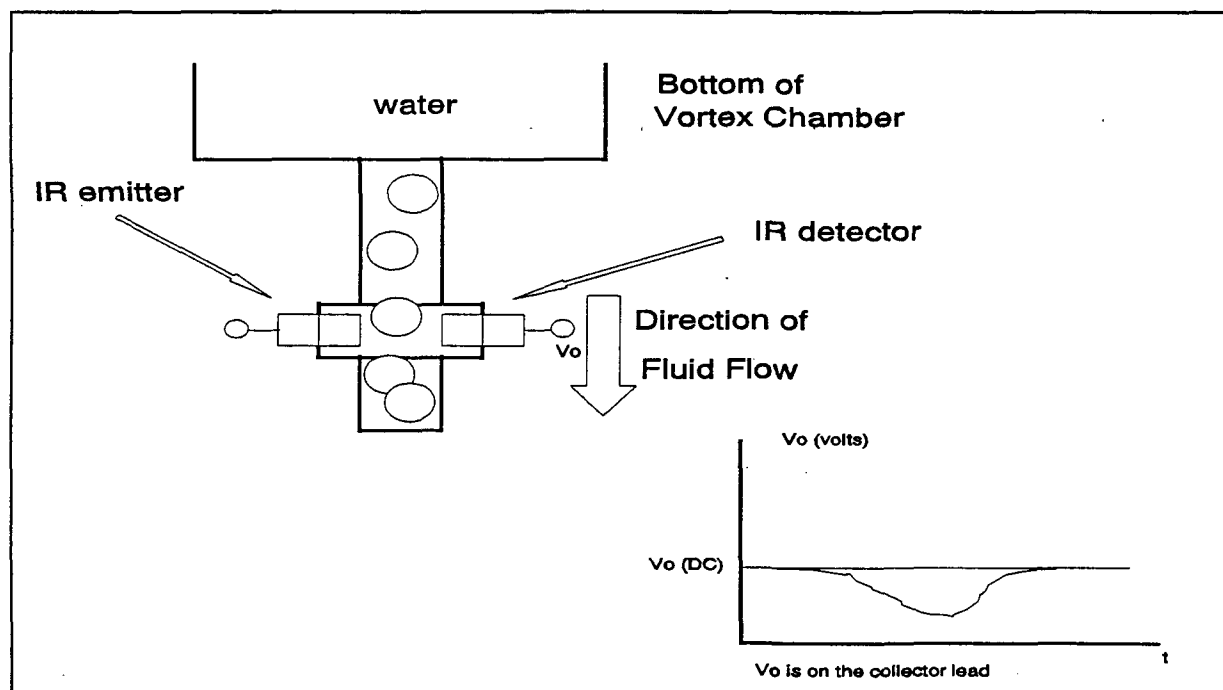


Figure 3.17 Effect of large gas bubbles.

A first solution to the problem was to set the DIP switches for a count of one. This measure would generate the "entrainment detected" signal whenever a single bubble went

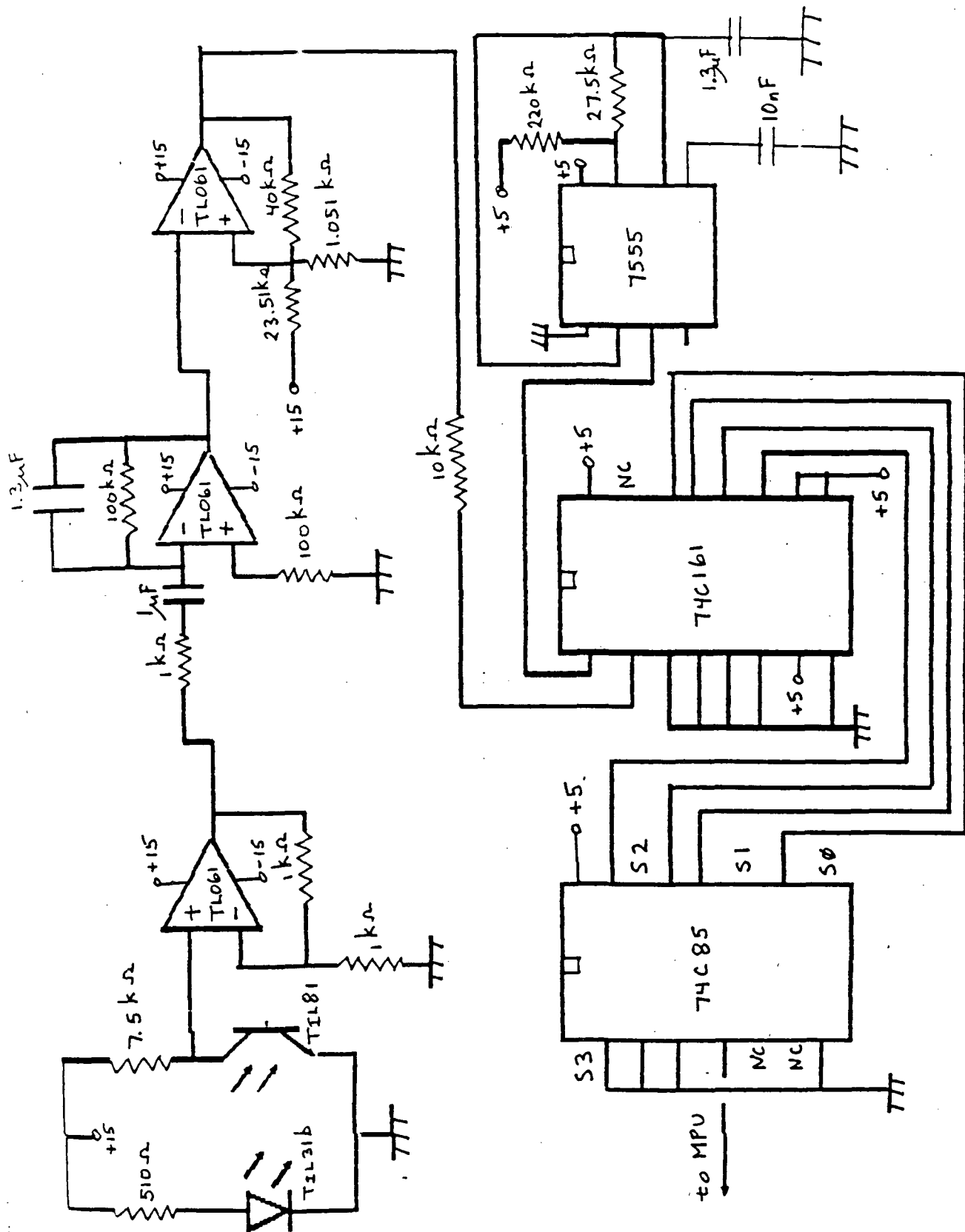


Figure 3.18 1990's gas entrainment detector circuit diagram

through the bubble detector. However, when vortex formation trials were run, a bubble was originated in the fluid about 60% of the time. This bubble was enough to trigger the gas entrainment detector, even though the vortex formation trial was evolving positively.

A second approach used logic circuitry to gate the pulses generated by the Schmitt Trigger. This solution relied on the ability of a differentiator to generate voltage peaks both at the beginning and the ending of each bubble. Each voltage peak causes the Schmitt Trigger to generate a pulse. This pulse is then used to clock a toggle flip-flop, which was cleared at the beginning of each trial. Since bubble with no ending, final entrainment, would leave the flip-flop permanently set, this information is used to signal the microprocessor controller that final entrainment has occurred. When this circuit was tested, it was found that small bubbles caused the differentiator to generate only a single voltage peak. Consequently, while this circuit detects final entrainment, it possessed the undesirable feature that it allows a continuous stream of small bubbles to be passed undetected.

The final solution for the gas entrainment detector relies both on hardware and software. It detects and distinguishes between single bubbles and final entrainment. Since it can detect single bubbles, the user can control the number allowed to pass through the detection chamber before aborting the on-going vortex formation trial. Final entrainment automatically ends the current trial. A block diagram of the circuit is shown in figure 3.29, and discussion of the design and function of the circuit.

The circuit in figure 3.29a is based on the gas entrainment detector designed during the 1990 project year. Its purpose is to detect bubbles in the fluid. The first block in the diagram corresponds to the emitter-receiver IR circuit discussed previously and shown in

figure 3.15. This is followed by a non-inverting amplifier with a gain of two that is used to buffer the signal from the emitter-receiver circuit to the differentiator. The non-inverting amplifier circuit is illustrated in figure 3.19.

The purpose of the differentiator is to function as a temperature compensator. This is needed since the infrared devices are quite susceptible to temperature changes (see figure 3.20). Because variations in the radiant intensity of the IR diode produce differing DC offsets at the collector of the phototransistor, only the phototransistor is temperature stabilized by the circuit. The differentiator generates

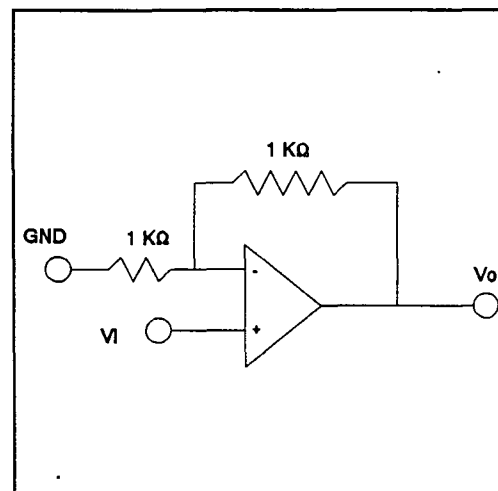


Figure 3.19 Non-inverting amplifier.

the differential of the input signals, minus any DC component present. Figure 3.21 shows the differentiator circuit and figure 3.22 illustrates the differentiator basic operation. The differentiation region extends from $f_D = 1.6$ Hz to $f_{ID} = 160$ Hz, as determined by the relations shown in figure 3.22.

In order to avoid operational amplifier stability problems at high frequencies, an integrator stabilizer was added to the circuit. The integration region extends from $f_{ID} = 160$ Hz to $f_I = 16$ KHz (see figure 3.22).

The transfer function of the active differentiator is:

$$\frac{V_o}{V_i} = -(j\omega R_D C_D) \frac{1}{(1 + j\omega R_D C_D)^2}$$

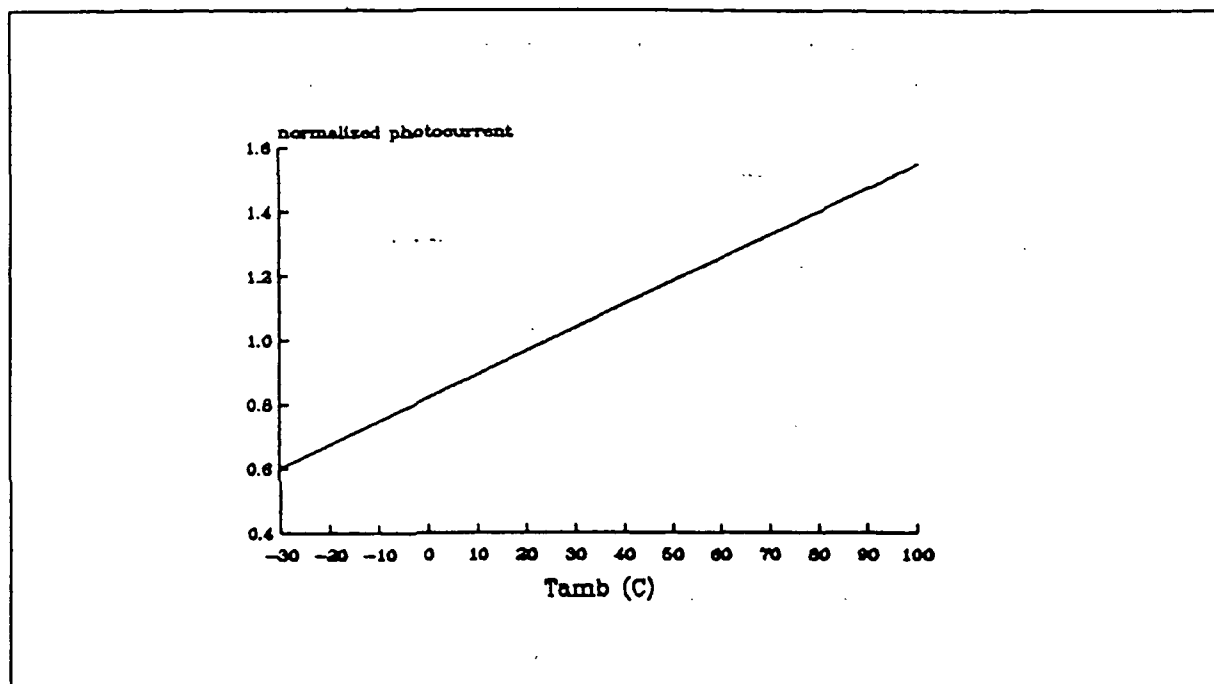


Figure 3.20a Photocurrent of TIL 81 vs Ambient Temperature.

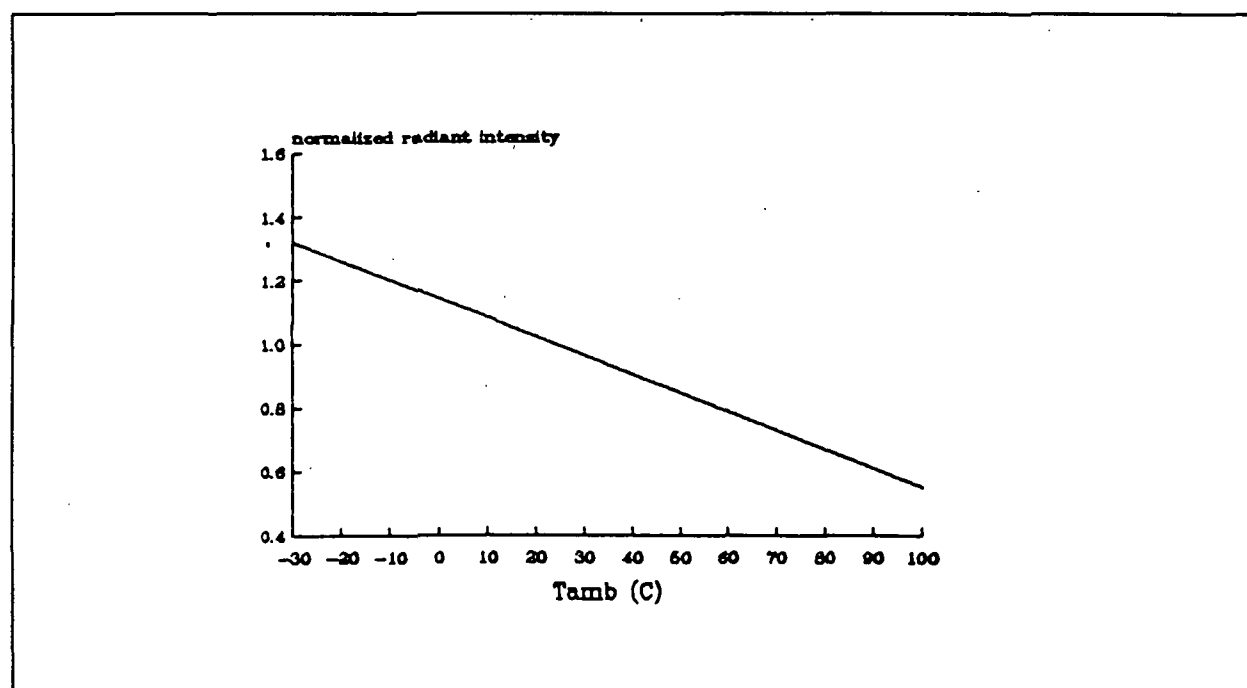


Figure 3.20b Radiant Intensity of TIL 31b vs Ambient Temperature.

Thus, the active differentiator has a transfer function of $V_o = -sR_D C_D (V_i)$ at input frequencies ranging from approximately 1.6 Hz to 160 Hz, an adequate range for detecting gas

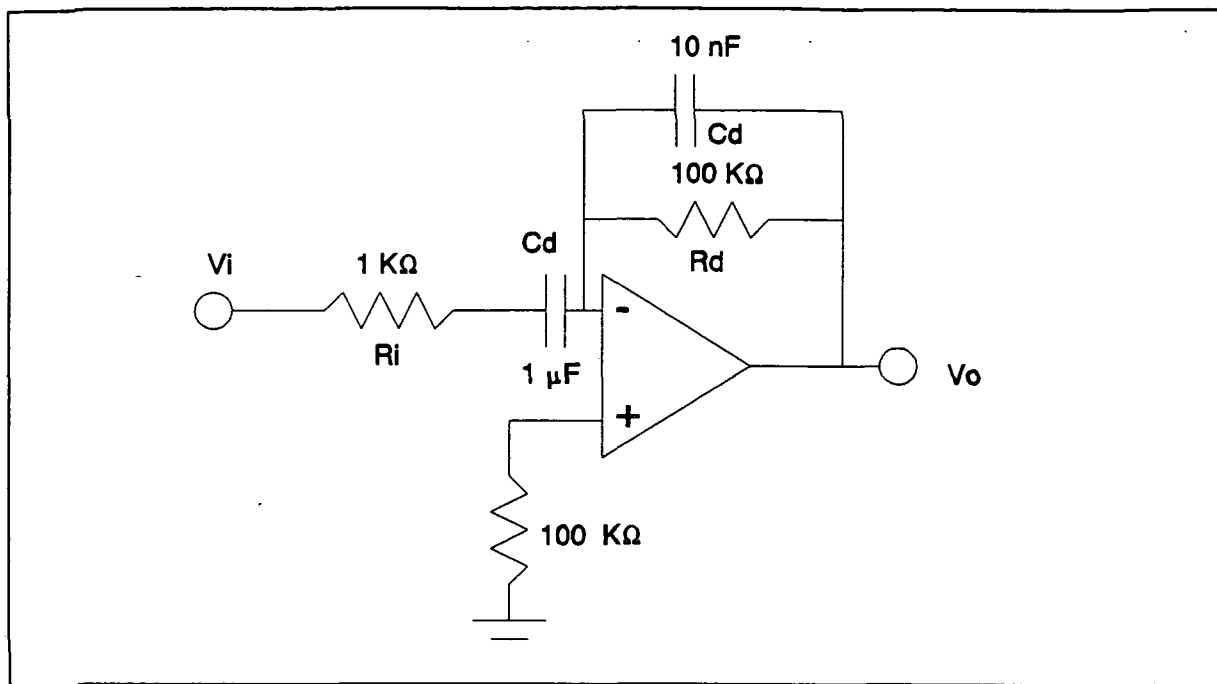


Figure 3.21 Active Differentiator.

entrainment.

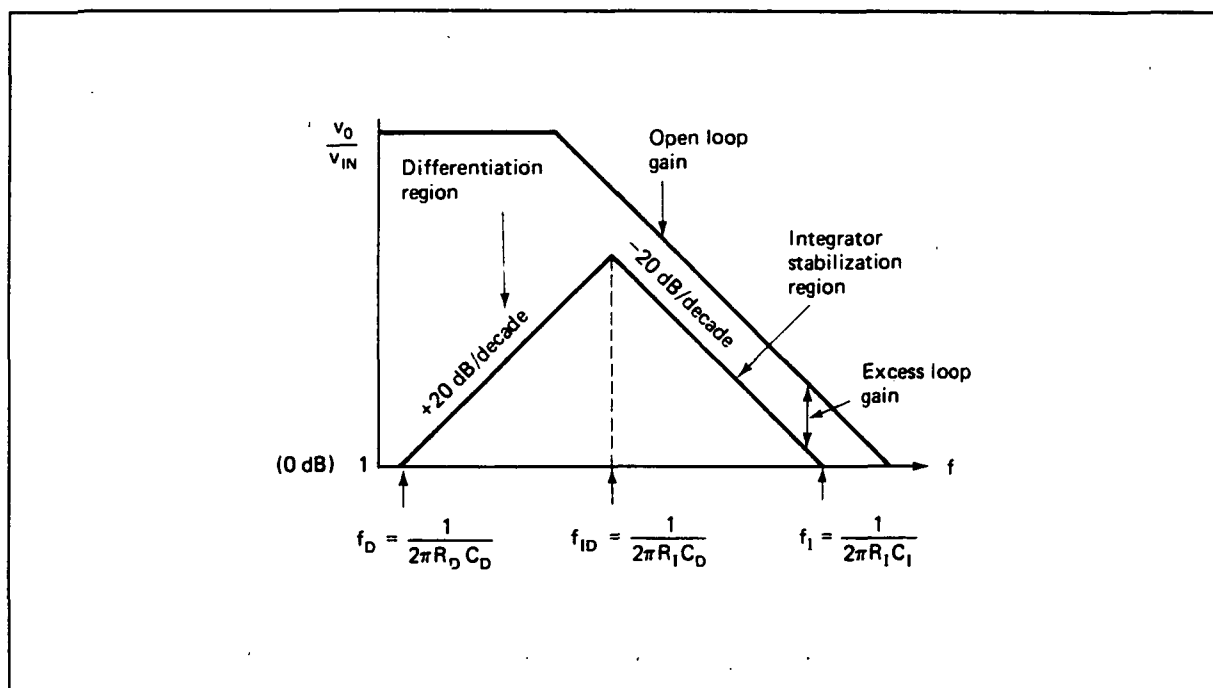


Figure 3.22 Active Differentiator Operation.

The magnitude and phase response of the active differentiator are illustrated in figure 3.23.

The Schmitt Trigger detects the passage of a bubble through the outlet tube as peaks on the differentiator output signal. As described earlier, an input (to the differentiator) signal with a peak of 100 mV was experimentally determined to be the smallest signal to occur when a gas bubble flows past the detector, providing (after the 4X amplifier) a minimum voltage of 1 V to be detected. Therefore, the Schmitt Trigger is designed for a trigger-high voltage (V_{TH}) of 1 Volt and a trigger-low voltage (V_{TL}) of 0.2 Volts, this was found to provide a sufficient amount of hysteresis to avoid "chattering" problems. The resistor ratios and reference voltage are given by the following relations:

$$|V_{TH} - V_{TL}| = 2\left(\frac{R_I}{R_F + R_I}\right)|V_S|$$

$$V_R = \left(\frac{V_{TH} + V_{TL}}{2}\right)\left(\frac{R_F + R_I}{R_F}\right)$$

$$V_R = \frac{R_2}{R_1 + R_2}(\pm V_S)$$

The Schmitt Trigger circuit is illustrated in figure 3.24.

A half-wave precision rectifier with gain lowers the ± 12 V output from the Schmitt Trigger to a 0 - 5 logic level. The resistor ratio is found using the relation:

$$V_o = -\frac{R_F}{R_I} V_i$$

This circuit is depicted in figure 3.25.

The output of the rectifier clocks a D-type flip-flop that has its D-input tied to 5 V and its Q-output connected to an input port of the central microprocessor-based control system. This port is decoded at address 0301. A "1" in the least significant bit of this input port informs the controller of bubble occurrence. This circuit is depicted in figure 3.26.

The circuit shown in figure 3.29b allows the controller to determine whether a single bubble or final entrainment has occurred. This circuit relies on the voltage output developed by the emitter-receiver circuit shown in figure 3.15. At room temperature, this voltage is 2.8 V when water is present between the infrared devices and 0.28 V when no water is present. At -12° C, the voltage drops to 2.5 V and 0.17 V respectively. By comparing this voltage with a fixed voltage of 1 V, the controller can determine whether there is water or air between the infrared devices.

The first stage in the circuit consists of a device that compares the output from the emitter-receiver circuit with a constant 1 V source. This circuit is depicted in figure 3.27. The signal is then transferred to a half-wave precision rectifier with gain, identical to that shown in figure 3.25. The output of the rectifier is transferred to an input port where it is available for processing by the central controller. This port is identical to that shown in figure 3.26 and is decoded at address 0302. A "1" in the least significant bit of this port is interpreted by the controller to be an entrainment event. The decoding logic for the input

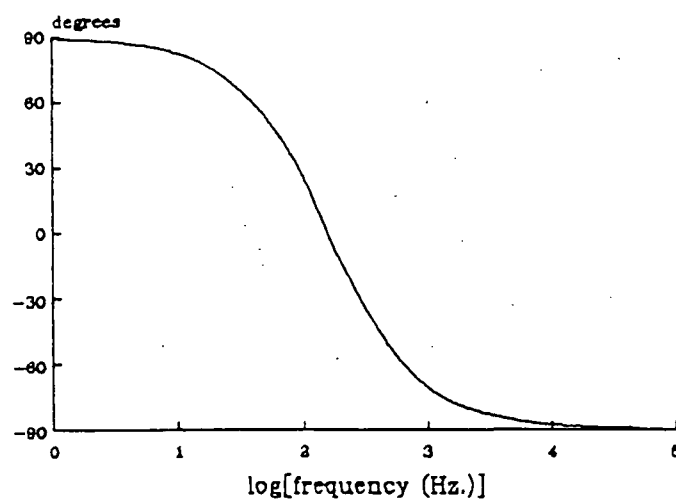
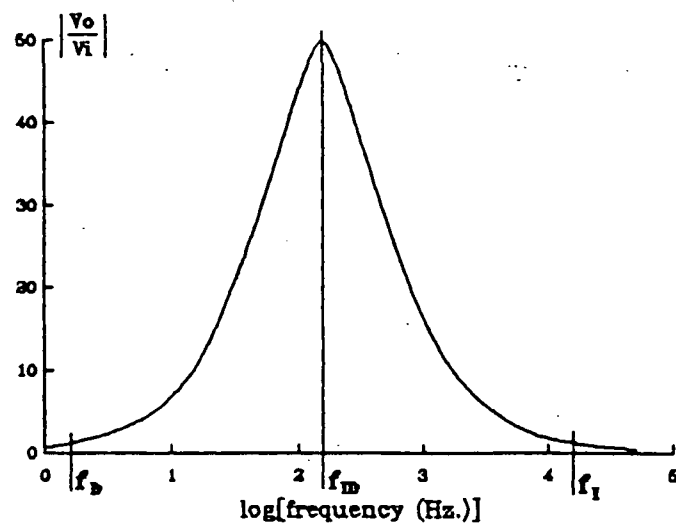


Figure 3.23 Amplitude and phase response

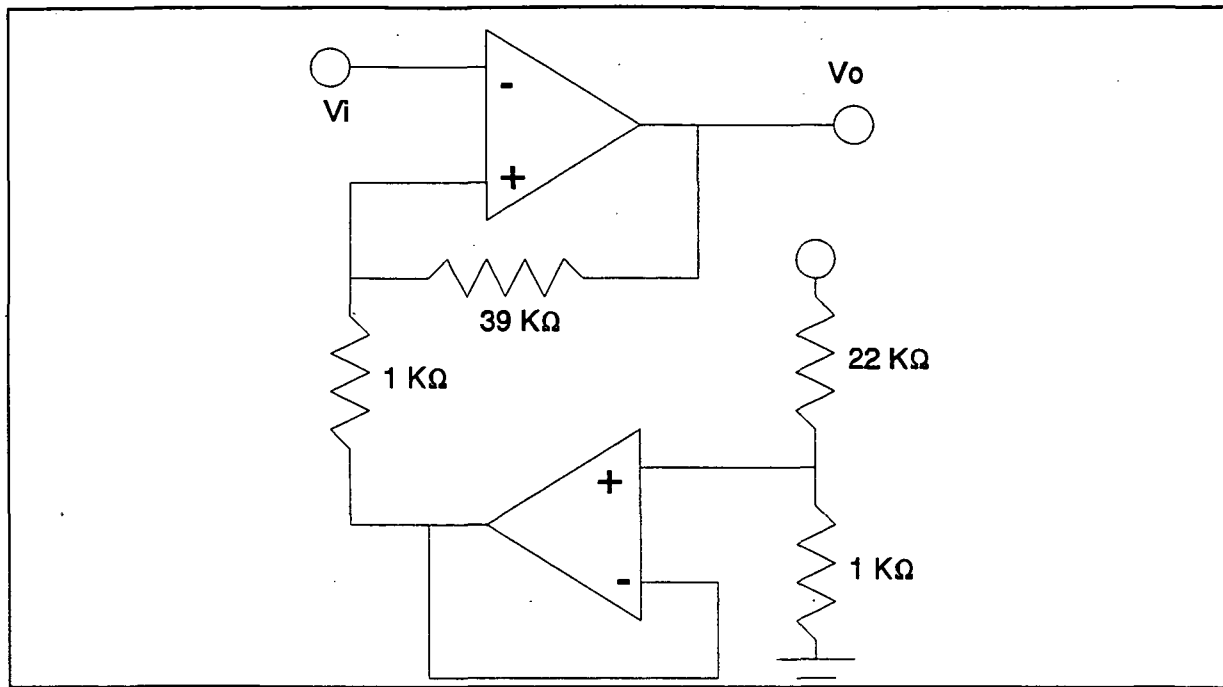


Figure 3.24 Schmitt Trigger.

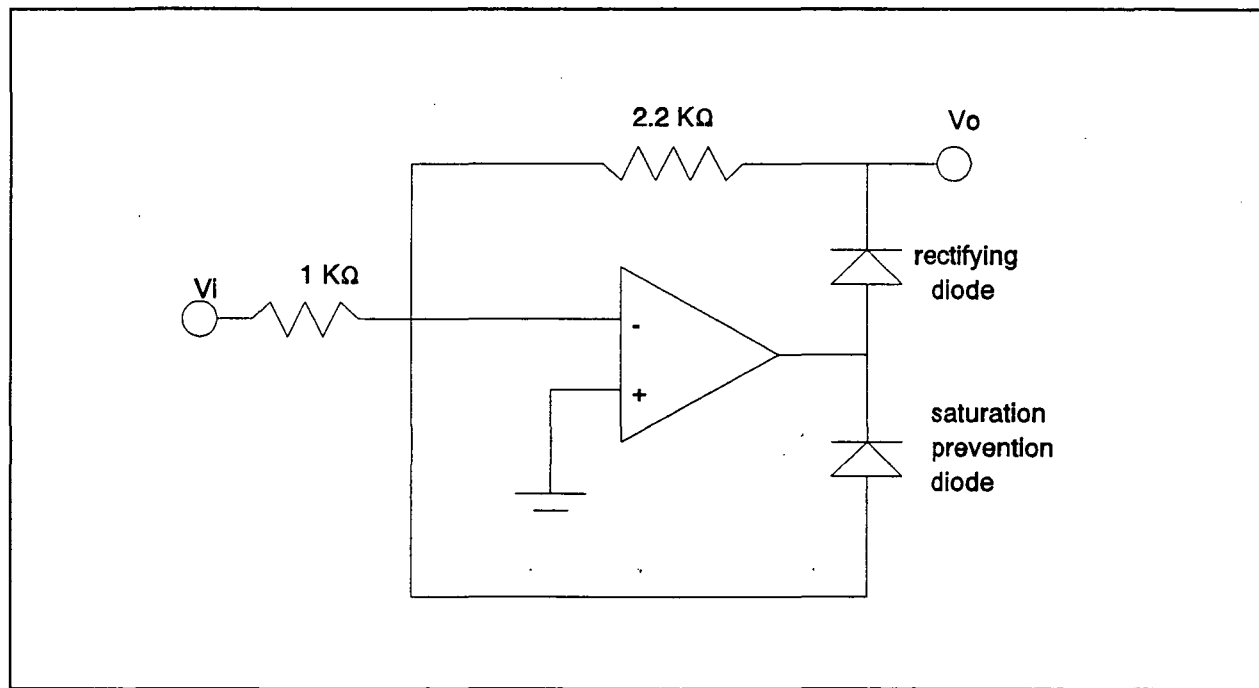


Figure 3.25 Half-wave Rectifier.

ports is shown in figure 3.28.

Under software control, the central controller repeatedly reads port 0301. Whenever

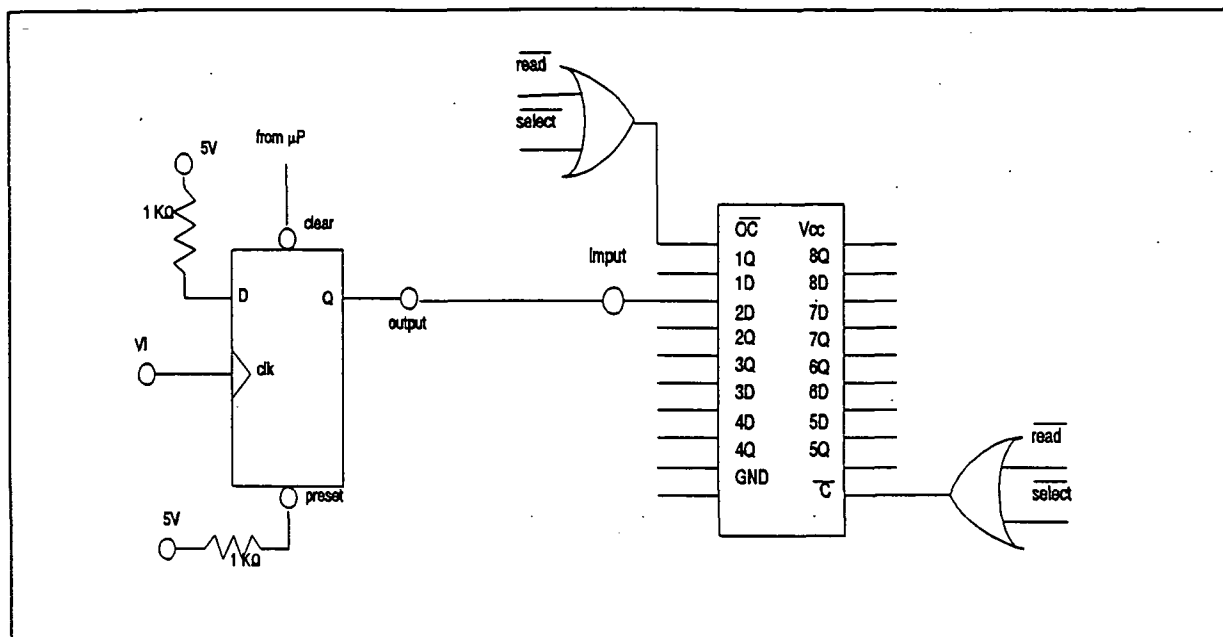


Figure 3.26 Input Port.

a "1" is present in the LSB, the controller immediately reads port 0302. If a "0" is present in the LSB, then a bubble has gone through the detector; the controller decrements the "maximum bubbles allowed" count and tests for zero. Once this count becomes zero the trial is terminated. Otherwise, the process is repeated. A "1" in the LSB of port 0302 informs the controller of final entrainment. The controller then automatically terminates the current vortex formation trial.

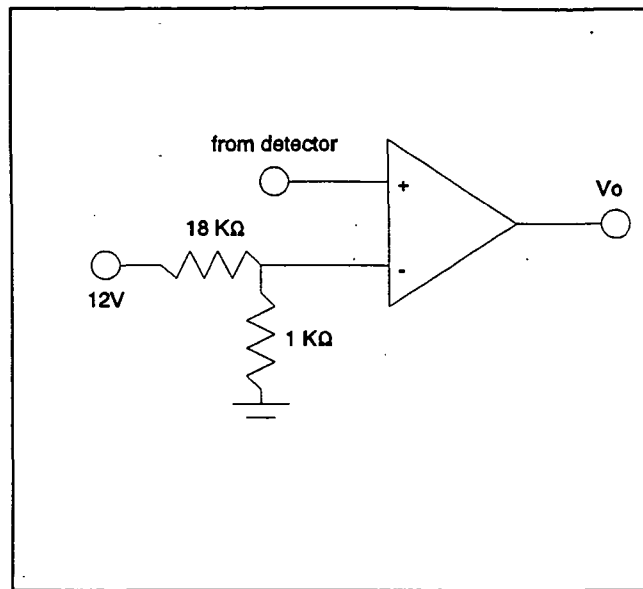


Figure 3.27 Comparator.

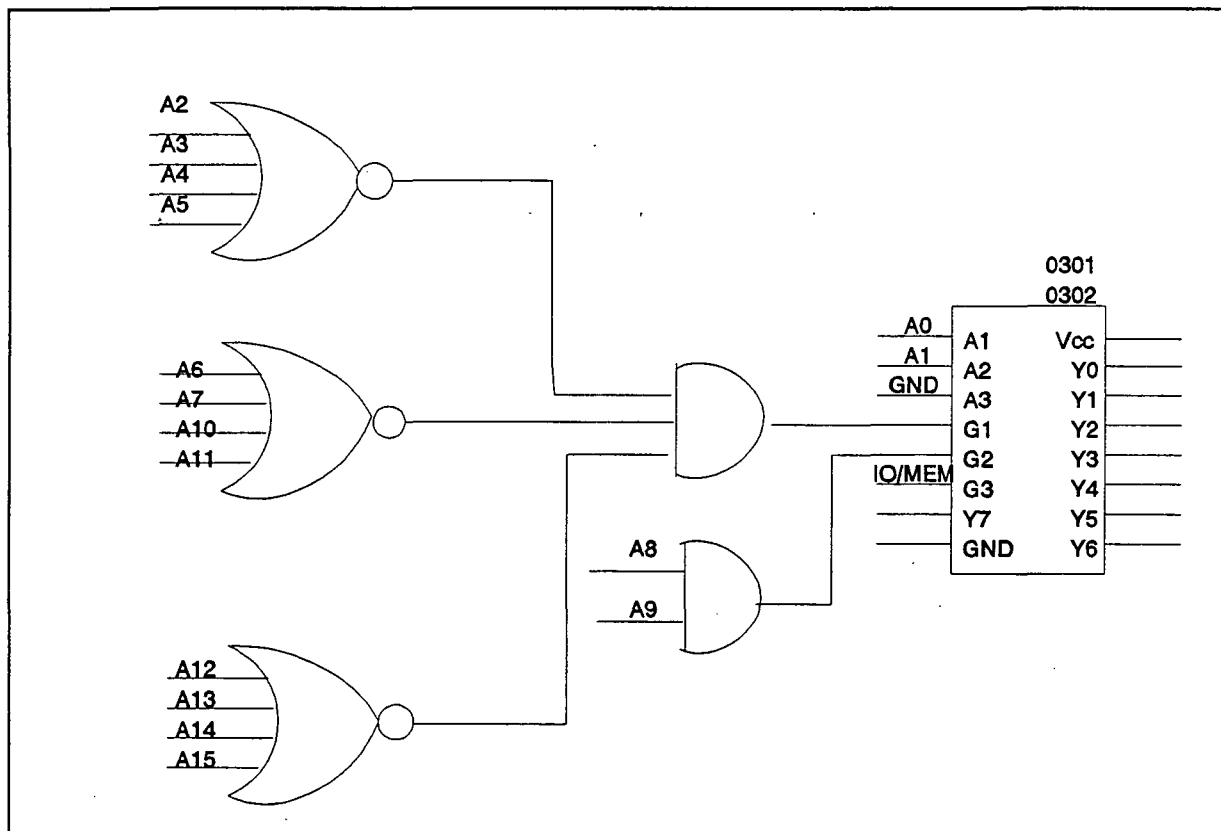


Figure 3.28 Decoding Logic.

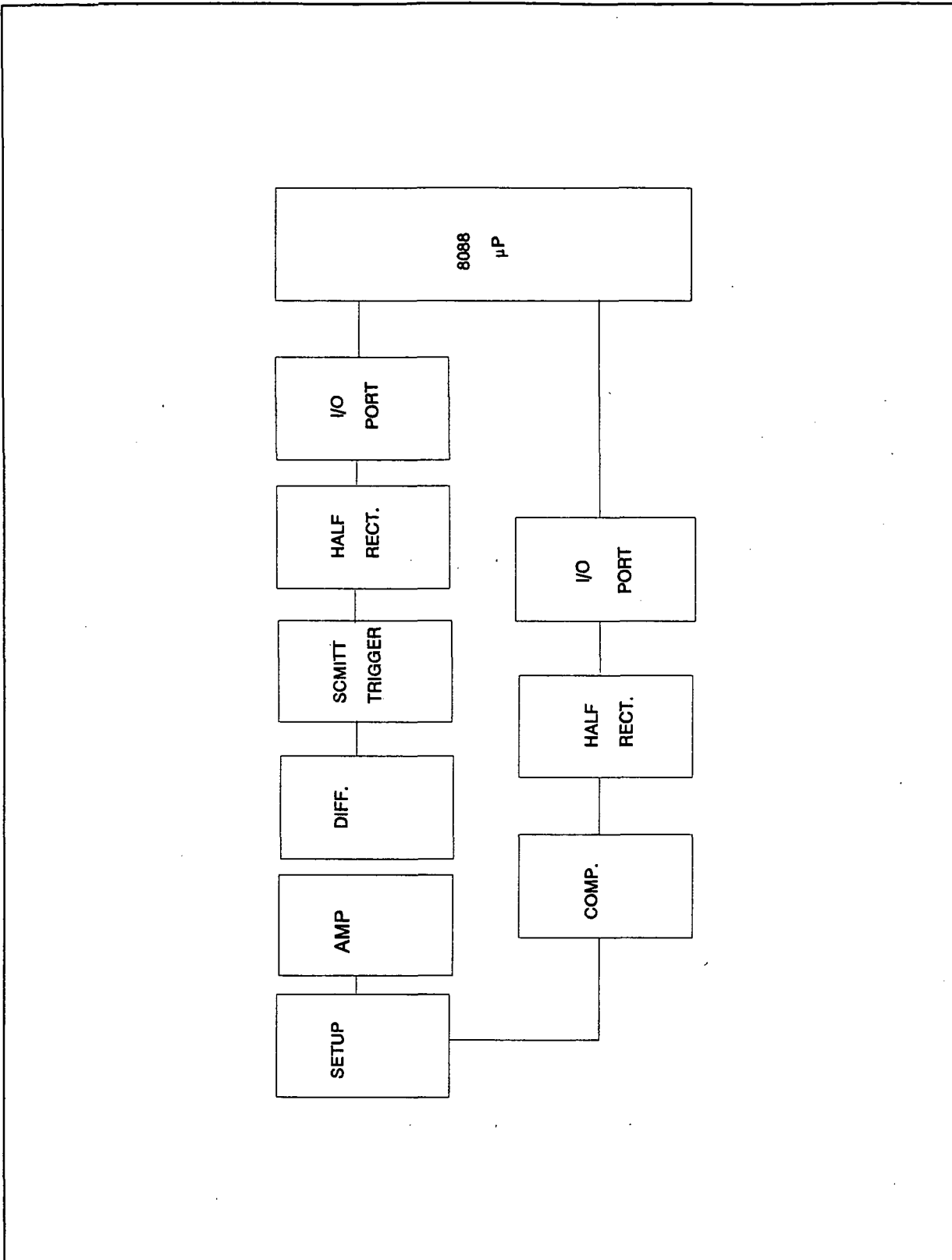


Figure 3.29 Gas Entrainment Detector Block Diagram.

3.2.6 Ultrasonic Circulation Measurement System

It was found by previous ME MQP's that it was essential to measure the vortex circulation in order to compute the intensity. In order to determine the circulation velocity, it is necessary to find V_{avg} , which is the average velocity of the fluid particles, and L , which is the length of the chosen path that the fluid particles travel. The circulation, Γ , is defined as:

$$\Gamma = \int V dL = V_{avg} L \quad \text{Eqn. 3-4}$$

There are three methods to determine Γ . These include ionic detection, hotfilm/wire anemometry, and ultrasonic methods. All will be described below.

Ionic detection consists of measuring the changes in conductivity of an ionic solution caused by changes in the circulation rate of a substance. This method is appropriate for measuring velocity when the substance is a gas. However, it was reported by a previous MQP teams that this solution is not feasible if the substance is a fluid.

Another method uses a hot-wire anemometer which is a small electrically heated sensor that is placed in the midst of the fluid motion. It measures the circulation rate by sensing the changes in heat transfer from the sensor. Since fluid temperature, pressure, and composition are constant values, the only parameter that changes is the fluid velocity and thus is the only variable that affects the heat transfer. A hot-film anemometer works on the same principle, but its construction differs.

There are several reasons why this method can not be used. These are: 1) The shape and size of the sensors impeded fluid flow, 2) continued usage causes bubbles to arise, and 3) the sensors consume approximately 20 watts, far too high for a battery powered system.

The ultrasonic circulation method uses high frequency sound waves that pass through the fluid to measure the velocity of the fluid particles along the assigned path that the sound wave travels. In order to produce the sound wave that passes through the fluid, an ultrasonic transducer is needed to convert an electrical signal to the sound wave.

One type of ultrasonic transducer is a piezoelectric crystal. The crystal expands or compresses depending on whether a positive or negative voltage is applied to the crystal. If the signal is an AC signal the crystal will vibrate in proportion to the AC signal. If the frequency of the signal (sinusoid) is equal to the resonant frequency of the crystal, the amplitude of the signal will greatly increase. The transducers used in the system can be used both as the transmitter and the receiver since they can convert energy bi-directionally. For more information about the transducers used in the design, data sheets are provided in appendix B.

A major concern in this project is the time available for measuring the velocity of the fluid in the container. As a result, it is important to know exactly how the travel time is affected.

The travel velocity of the sound wave in this experiment is made up of two parts. One is the velocity of the sound wave itself, (C) and the other is the average velocity of the fluid particles along the closed path, (V_2). If C is traveling in the same direction as V_2 , the total velocity of travel will be $C + V_2$. If C is traveling in the opposite direction of V_2 , the

total travel velocity will be $C - V_2$.

The time of travel of the wave when the fluid is not in motion is:

$$T_c = \frac{L}{C} \quad (L = \text{closed path length}) \quad \text{Eqn. 3-5}$$

When the fluid is in motion and is traveling in the same direction as the sound wave, the total time is:

$$T_t = \frac{L}{C + V_2} \quad \text{Eqn. 3-6}$$

If the fluid is traveling in the opposite direction as the sound wave, the total time is:

$$T_t = \frac{L}{C - V_2} \quad \text{Eqn. 3-7}$$

Since, in this experiment, the sound wave is traveling in the same direction as the fluid motion, eqn. 3-6 is the only one that is applicable.

The phase delay to be detected is $T_t - T_c$; this delay equals:

$$T_t - T_c = \frac{L}{C + V_2} - \frac{L}{C} \quad \text{Eqn. 3-8}$$

This equation can only be used if there fluid motion. If there is no fluid motion, one can see

that the answer would be zero and that would be incorrect.

However, once the phase delay has been determined, the velocity of the liquid is obtained by solving for V_2 as below:

$$V_2 = \frac{L}{T_t - T_c + \frac{L}{C}} - C \quad \text{Eqn. 3-9}$$

Substituting this equation into the formula for circulation given in eqn. 3-4, the only parameter needed to find the circulation velocity is to obtain the phase delay, $T_t - T_c$; this is the purpose of the Ultrasonic Circulation device. L is already known and C is the velocity of the sound wave in the medium.

Choosing the path length is very important to determining the minimum to maximum amount of phase delay that it is possible to experience. If the path length is too short the phase delay will be too small to detect; and, if the path length is too long, the signal frequency that would be needed would exceed the capabilities of available devices (OP AMPS, Logic devices).

The original path length that was chosen was 5-cm. (straight across the container) between the transmitter and the receiver. Assuming that the minimum fluid velocity would be 1 cm/s and using eqn. 3-8, the phase delay that would be observed would be 0.22 nanoseconds. This delay is much too small to be determined with reasonable accuracy. Consequently a longer path, 26-cm. was used. This path length is obtained by reflecting the wave across multiple chords in the cylinder (see figure 3.30).

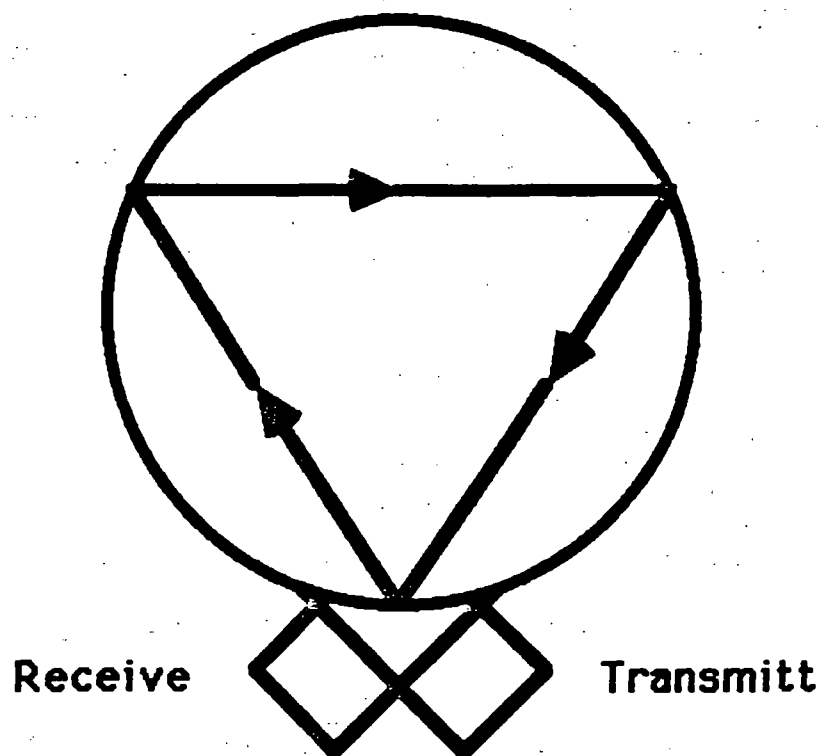
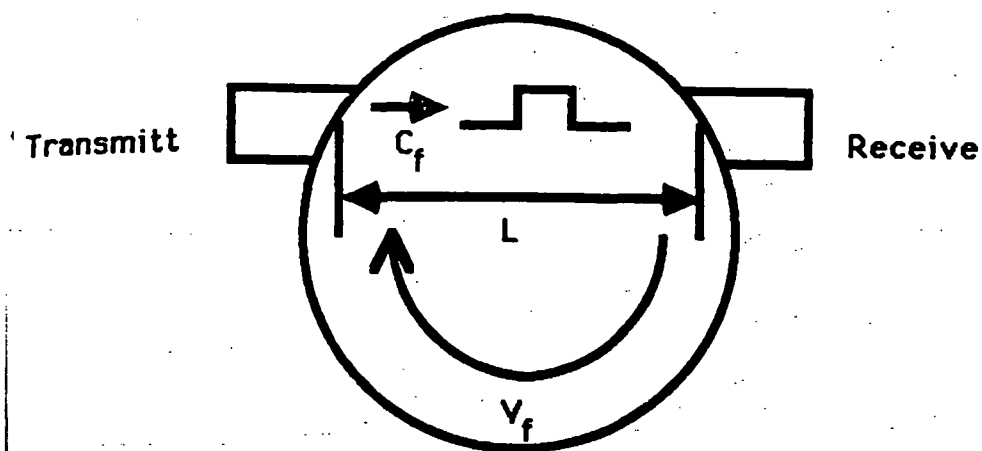


Figure 3.30 Circulation Path.

The frequency that was chosen for this experiment was 10 Mhz. This choice was a result of extensive research by a previous MQP group. Through experimentation with a vortex chamber with a diameter of 8 cm, it was determined that it was possible to get a resolution of 1 cm /s with a triple chord beam path, a frequency of no less than 10 Mhz was needed. Also as the wave is being reflected, it is necessary to keep refraction to a minimum so that interference with the closed path of the soundwave does not occur.

Rotational Flow Sensor Measurement - The method that is used is the ultrasonic circulation measurement system with unidirectional travel. The information derived from this system is fed into an intel 8088 after passing through a phase delay detector circuit. This phase delay circuit has to be able to detect time delays in the order of magnitude of 100 ps, or phase angle delays of 3.6° . There are several alternate ways of determining the phase delay; a description of the more appropriate is provided below.

Nonlinear Method - A method that was studied by a previous MQP¹ team required multiplication the transmitted signal and the received signal.

$$\begin{aligned}\text{Transmit} &= A\cos(2\pi f) \\ \text{Received} &= B\cos(2\pi f + \theta)\end{aligned}$$

$$(\text{Transmit})(\text{Received}) = \frac{1}{2}AB [\cos(4\pi f + \theta) + \cos(\theta)]$$

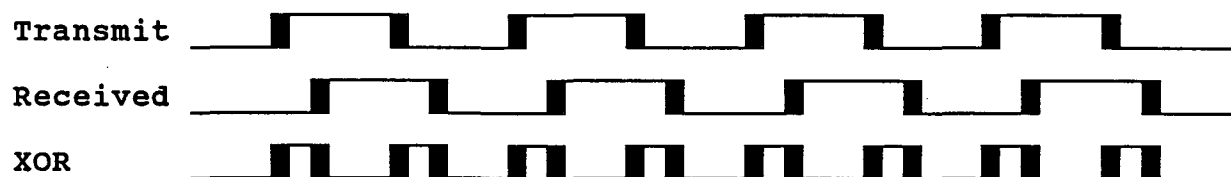
After the multiplication, the resultant signal would be passed through a low pass filter so that the resulting voltage would be proportional to the \cos^{-1} of the phase. There are two reasons why this method is not appropriate.

¹. 1986 MQP report, chapter 7.2

The phase difference that is expected is very close to zero. Consequently, the sensitivity of the device will be close to zero. This means that a small change in the input will result in an even smaller change in the resulting solution; a result that would be unmeasurable in a practical sense.

The second reason that this would be infeasible is that the output voltage is non-linear. Consequently, transforming the voltage to a phase difference on the 8088 using the \cos^{-1} function would take too long. On the other hand it is possible to just store the voltage values obtained in space and make the calculations on earth upon return. However, this does not overcome the measurability problem previously discussed.

XOR Method - Another MQP² studied an XOR phase detection method. In such an approach the transmitted signal and the received signal are provided to an XOR logic gate. This process requires preprocessing to convert the sine wave to a square wave and to produce a TTL output.



The time that the pulse remains high for the XOR signal is the phase delay. The phase delay can be found if the Fourier analysis of the XOR signal is taken. The result of the Fourier analysis is proportional to the duty cycle. The duty cycle is the percentage of time that the XOR gate remains high.

The output of an appropriate low pass filter will output a voltage proportional to the

². 1987 MQP group, Chapter 2.2.5.2

$$DutyCycle = \frac{d}{p}$$

d = phase delay
p = period of
signal

phase. This voltage can then be transferred to the 8088 by an (A/D) converter. So that there is no error in measurement, it would be necessary to filter the ripple voltage one level lower than the (A/D) converter can handle.

One problem with this approach is that the transmitted phase and the received phase differ by about 0.0013% at the minimum average flow. Accordingly, better than 20-bit binary precision would be required to determine the phase difference with a 1% accuracy. This kind of (A/D) converter is currently beyond the state-of-the-art for such devices. Another problem is that it can only detect phase differences less than 180°.

Gated-Counter Method - The gated-counter method has gone through extensive study and changes, to obtain a practical fluid velocity measurement system. Once again, the sine waves from the transmitted and the received side will have to be converted to square waves. A method that was studied by a previous MQP³ was to send both signals into a counter. The rising edge of the transmitted signal will start the counter and the rising edge of the received signal will stop the counter. Once the counter stopped, the 8088 would read the count and then reset the counter before the next rising edge of the transmitted signal occurs. Once the 8088 has received the signal it calculates the time delay:

$$d = \frac{C}{F}$$

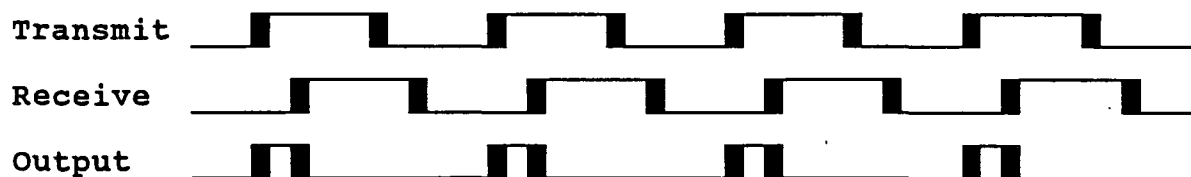
³. 1987 MQP group, Chapter 2.2.5.1

Where d is the time delay, F is the clock frequency of counter, and C is the counts of the counter.

The error associated with this method is $\pm 1/F$. From this, we can see that the faster the clock frequency of the counter, the better the resolution. This method can give a very high resolution depending on the choice of the clock frequency and of a counter that can function at the operating frequency.

There is a problem with this method. Since we are limited to the choice of counters and clock oscillators by the present upper bound of device technology, a counter and clock oscillator of appropriate performance are not presently available. Since the minimum delay is approximately 1 ns, a clock frequency around the 10's of GHzertz would be required along with a counter that could operate at that speed. Presently, the best counters are only able to operate at around 100's of MHzertz.

To solve for problem a basic change was made to the circuit. The two signals are provided through an A/B gate.



The output is transferred to a frequency divider (timer) which stretches the pulse by a predetermined amount. The amount stretched is made sufficient for the counter to perform with accuracy. One setback that was encountered, however, was that the pulse would be too small for the logic gates to handle. This was resolved by adding a 10 ns delay to the received signal before it is transferred to the logic gates. As a result, the signals are able to be processed properly by the logic gates.

The one remaining difficulty was associated with the frequency dividers used. While these readily handle the pulse size expected, they operate on even numbered pulses. This required the use of a timer to overcome. However, the use of a timer at higher frequencies, although possible, produces a higher degree of inaccuracy. Consequently, while this method can be used, a more accurate method is preferred.

Heterodyne Method - A preliminary research into the Heterodyne method by a previous MQP group⁴ and was continued by another MQP⁵. This method combines the non-linear method with that of the gated-counter method.

Heterodyning can be defined as frequency shifting. Multiplying a time-domain signal by a sinusoid causes the spectral components to be shifted both up and down in relation to the frequency of the sinusoid. When any signal is multiplied with a sinusoid of a certain frequency, it is said to be heterodyned with that frequency. The principle is explained below in terms of a trigonometric identity

$$A\cos(a) B\cos(b) = \frac{1}{2}AB[\cos(a+b) + \cos(a-b)]$$
$$a = 2\pi f_1 t$$
$$b = 2\pi f_2 t$$

Suppose f_2 is 10.000 MHz and f_1 is 10.001 MHz. When both frequencies have been multiplied using high frequency mixers, the output of the mixer will contain two spectral components, one at 20.001 Mhz and the other at 1 khz.

In this experiment, both the transmitted signal and the received signal, 10.000 Mhz are mixed with a local oscillator which is 10.001 Mhz. Frequency shifting these signals does

⁴. 1987 MQP report, Chapter 2

⁵. 1990 MQP report chap 2.2.3.2

not change their phase relationship. As the waves are now at a much lower frequency, phase detection methods for low frequencies can now be used.⁶ For a variety of reasons, this approach was also rejected for use in the flight system.

Integrator Method - The integrator method involves the use of logic gates, integrators, and peak detectors. It is the method chosen by this MQP. The theory behind this method is that after the transmitter and a received signal is passed through a sine wave to square wave converter, a 10 ns delay line of the received signal is obtained. The two signals are then transferred to an A/B Gate and a pulse similar to the one shown for the gated counter method is produced. This signal is integrated and an output obtained as predictable by:

$$V_{\max} = \frac{1}{RC} \int_a^b v dt \quad \text{Eqn. 3-10}$$

b-a = phase delay
v = max voltage at input (5v)
R = Resistor value in integrator
C = Capacitor value in integrator

The output of the integrator is then processed by a peak detector whose output is a dc value equal to maximum voltage produced by the integrator. This signal is transferred to an A/D converter which produces a digital representation of V_{\max} that is sent to the 8088. The phase delay is calculated directly from eqn. 3-10. A block diagram of the whole circuit in figure 3.31.

⁶. For more information on the heterodyne method see Mike Haley "Ultrasonic Circulation Measurement System" Jan 10 1990.

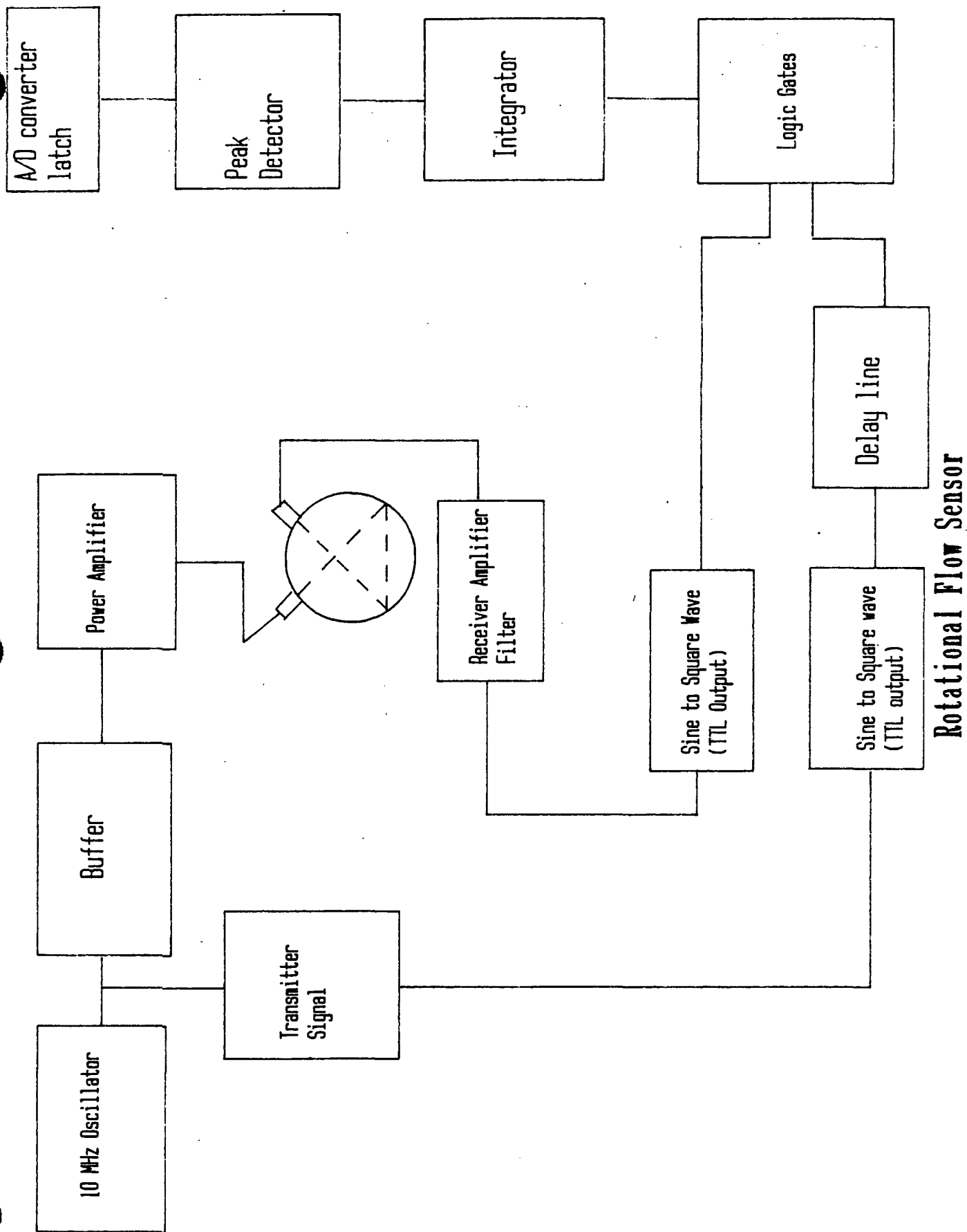


Figure 3.31 Block Diagram of Circuit.

Ultrasonic Circulation Device Design - This report, gives background information describing the operation of the rotational flow sensor in terms of signals and the system as a whole. In this section the implementation of these ideas and the complete description of the circuit is given. The electrical schematics of the ultrasonic circulation device is shown in figure 3.32.

To generate the 10 MHz signal, a 10 MHz oscillator has been developed. The design for this oscillator was obtained from the ARRL handbook of radio design. The design is basically a Pierce crystal oscillator that uses a 10 MHz crystal.

To create positive feedback, the crystal feeds the output back into an FET. This creates a gain in the output that depends on the ratio of C3 and C4 or C7 and C6. To increase the amplitude, or gain, C4 is held constant and the capacitance of C3 is increased. A 1mh choke is used to reduce the load on the FET, allowing the voltage to vary freely. One drawback to this design is that it produces a high impedance at the output which must be reduced before the signal is transmitted.

The output of the oscillators is buffered and amplified. The output of the oscillator buffer is the transmitted signal that will be compared to the received signal. The main purpose of the oscillator buffer is to provide adequate drive for the device circuitry.

The buffer consists of two amplifier stages. The first stage is a variable-gain stage and the second stage is a slightly-smaller-than-unity-gain buffer which loads the first stage with about 30kOhms.

The transmitter amplifier serves two purposes. The first is to increase the amplitude as much as possible and the second is to decrease the impedance as much as possible. The

design that is being used involves four stages. These stages are the variable-gain stage, the voltage-follower buffer stage, the current drive stage, and the high power output stage. Three of these are buffer stages used to match the impedance to that of the transducer.

The variable gain stage uses a voltage follower to decrease the impedance of the oscillator to about 10kOhms. It also increases the gain of the output of the oscillator by a factor of 10. The next two stages maintain signal voltage, but increase its current. The last stage is used to increase the power to as high a level as possible before the signal is provided to the transducer.

After the signal is transmitted, it is received by the receiver transducer. The output of the receiver is approximately a 20mv signal and is virtually distinguishable from the noise. The receiver amplifier amplifies the signal to the same amplitude that provided to the transmitter and filters the result using a low-pass filter. This signal is then compared to the transmitter signal.

After the received signal has been amplified and filtered, both the transmitted signal and the received signal are transferred to a zero-crossing detector. The received signal is delayed by six nanoseconds before it arrives at the zero-crossing detector. The delay is sufficient to allow the Op-Amps in the circuit enough time to operate properly. The zero-crossing detector contains two EL400C, 200MHz current feedback amplifiers. The transmitter signal will pass through one of the amplifiers, which produces a squarewave synchronous to the timing with which the transmitter signal transitions through a value of 5mv. The other amplifier inverts the received signal and produces a squarewave synchronous to the timing with which the inverted received signal transitions through a value

of 5mv. Both squarewaves are then transferred to two 2n2222a transistors which act as a gate to combine the signals and output a signal whose amplitude varies between 0 and 5v depending on the delay between the input signals.

The output of the zero-crossing detector is then transferred to a noninverting integrator (refer to eqn. 3-10). The values of R and C in this circuit are calculated so that the value of V_{\max} is maintained at values less than 5v when the phase delay is between 6 ns and 12 ns; otherwise, clipping of the signal occurs. The values of R and C that satisfy this requirement are $R = 22 \text{ Ohms}$ and $C = 1 \text{ nanofarad}$.

The accuracy achieved for the phase measurement is better than 200 picoseconds. Table 3.2 lists values of phase delay between 6 ns and 12 ns, in steps of 100 picoseconds, and the corresponding experimentally observed values for V_{\max} .

As it is possible that the capacitor in the integrator fails to fully discharge prior to arrival of the next pulse, full discharge is assured by external means. This external discharge can occur at any time after the falling edge of the pulse has occurred, between 20 ns and 90 ns. The discharge is accomplished by sending output of the zero-crossing detector through a 30ns delay line and then to a tmp102 FET. Thus, the capacitor is discharged 14-20 ns after each pulse is processed by the integrator and 60 ns before the next pulse arrives.

The signal output of the integrator is then provided to a peak detector whose output is the DC value of V_{\max} . As this value ranges from 3-4 volts and the A/D converter that is used requires an input of 0 - 2.5 volts, the output of the peak detector is processed by a difference amplifier. This amplifier subtracts the DC output of the peak detector from 5 volts and produces an output that varies from 1-2 volts. Once processed by an A/D

converter, the value of V_{\max} is transferred to a latch which stores it until read by the system-control processor.

Table 3.2 Phase delay vs. V_{\max}

<u>Phase Delay(nanoseconds)</u>	<u>V_{\max} theoretical(volts)</u>
6.0	3.636
6.1	3.614
6.2	3.591
6.3	3.568
6.4	3.545
6.5	3.523
6.6	3.500
6.7	3.477
6.8	3.455
6.9	3.431
7.0	3.409
7.1	3.386
7.2	3.364
7.3	3.341
7.4	3.318
7.5	3.295
7.6	3.272
7.7	3.250
7.8	3.227
7.9	3.205
8.0	3.182
8.1	3.159
8.2	3.136
8.3	3.114
8.4	3.091
8.5	3.068
8.6	3.045
8.7	3.023
8.8	3.000
8.9	2.977
9.0	2.955
9.1	2.932
9.2	2.909
9.3	2.886
9.4	2.863
9.5	2.841
9.6	2.818
9.7	2.795
9.8	2.773
9.9	2.750
10.0	2.727
10.1	2.705
10.2	2.682
10.3	2.659
10.4	2.636
10.5	2.614
10.6	2.591
10.7	2.568

Phase delay (nanoseconds)V_{max} theoretical (volts)

10.8	2.545
10.9	2.523
10.0	2.500
11.1	2.477
11.2	2.455
11.3	2.432
11.4	2.409
11.5	2.386
11.6	2.364
11.7	2.341
11.8	2.318
11.9	2.295
12.0	2.273

3.3 Computer Software and Control

A computer and software are needed to control the vortex experiment, send data to various devices, take measurements, and record data. These components include an 8088 computer, a DS-64 EPROM data bank, two accelerometers, a temperature transducer, an ultrasonic fluid circulation rate measurement instrument, a gas entrainment detector, a motor controller, a pump controller, and a 35mm camera. All these devices are described in section 3.2.

The computer's tasks during the execution of the experiment include running through the predetermined list of trials, monitoring gas entrainment, periodically sending data to the motor and pump controllers, keeping track of the centripetal acceleration, the fluid flow rate, and the temperature, taking pictures, and recording all activity on the EPROMs.

By the end of the 1989-90 project year, three primary packages had been developed to drive the vortex experiment simulator and effect data recovery. They are described below, along with all modifications made this year. FLIGHT.C is the flight simulation software. It implements the operational scenario described in chapter 4. READ.C is a generic data extraction program that dumps the entire contents of the DS-64 EPROM bank to a text file as hexadecimal characters. DATEX.C performs a more sophisticated frame data recovery from the text file generated by READ.C.

FLIGHT, READ, and DATEX are written in MANX Aztec C. All source code listings are provided in appendix B. All software can also be found in the enclosed disk.

Flight Software: FLIGHT.C

FLIGHT.C is intended to implement the operational scenario outlined above.

FLIGHT is an EPROM resident program. It replaces Onset's Monitor on the CPU-8088 and executes upon system power-up.

During the year, the flight software was enhanced to include more error checking and recovery, since it was determined that it should be as fault-tolerant as possible. The software was modified to time out on ports after 100 milliseconds. The data saved to EPROM was also changed to include all the devices, record activity, and maintain a checksum. See figure 3.33a for a description of the EPROM data storage format. The program was extended to read data from the rotational flow sensor, and the code for platform locking and unlocking was removed, since the locking mechanism might fail. The gas entrainment value is now read from a port instead of from an interrupt, because the speed of the response does not warrant the overhead of an interrupt. The program periodically checks the gas entrainment port for bubbles, and the ultrasonic instrument port for a steady fluid flow rate. The code was optimized to minimize repetitive tasks to keep power consumption down.

The operational scenario proposed by the mechanical engineers aims at examining vortex formation at various acceleration and flow rates. Figure 3.34 shows the 8088 microprocessor interfaces for the vortex experiment. A detailed description of the flight operation follows. See section 4-2 for a brief explanation and the flow chart.

The first item in the listing is the interrupt handler, which handles interrupts from the CPU-8088's real time clock (MM58274). The handler operates on the external global variables COUNTER and TIMER. Every second, when an interrupt is caused by the real

time clock, they are incremented. They are initialized in the main module of the program.

The #ASM and #ENDASM assembler directives delimit the block of code that handles the interrupt caused by the real time clock. First, all registers are saved. Then the segment register is made to point to the location in high memory where the flight software resides in EPROM. The data segment is also initialized. The instruction to read address F6000H clears the interrupt flap. The necessary variables are incremented. Finally, the routine to check for gas entrainment is called. Upon return, registers are restored.

The declaration of the MAIN code module follows. The 8155 device is initialized such that ports A, B, and C are outputs. All three ports are initialized to zero. Then the assembly block delimited by the #ASM and the #ENDASM assembler directives sets up the interrupt vector table. The code segment and instruction pointer for the real time clock are 01F2h and 01F0h respectively.

To stabilize the MOR-800's analog to digital converter (ADC) and insure proper conversions, a dummy conversion is performed. The ADC is first powered-up, followed by enabling conversions. The next channel is selected. The DO-WHILE loop implements the best procedure for reading the ADC reliably by waiting until an end-of-conversion flag signifies a conversion, and timing out after approximately 100 milliseconds, if the device does not respond, rather than blindly reading the ADC channel. The dummy conversion value is stored into ACCEL1.

Now, the flight operation is ready to begin. First, real time clock (RTC) interrupts set at 1 millisecond intervals are used to provide the necessary timing. The computer waits a few minutes for the microgravity experiment to complete before initiating the vortex

EPROM DATA STORAGE FORMAT

Byte #1	Start-of-frame marker.
Byte #2	Low byte of time (Time is taken in seconds)
Byte #3	High byte of time (from beginning of trial)
Byte #4	Data from the first accelerometer.
Byte #5	Data from the second accelerometer.
Byte #6	Value from the temperature transducer.
Byte #7	Circulation rate from the rotational flow sensor.
Byte #8	Gravity level sent to the motor controller.
Byte #9	Flow rate sent to the pump controller.
Byte #10	Status byte to indicate problems.
Byte #11	Checksum byte to verify data on EPROMs.

Figure 3.33a EPROM Data Storage Format.

EPROM STATUS BYTE FORMAT

Bit #0	Accelerometer #1 bad?
Bit #1	Accelerometer #2 bad?
Bit #2	Temperature transducer bad?
Bit #3	Ultrasonic device bad?
Bit #4	Gas entrainment detected?
Bit #5	Photograph taken?
Bit #6	Not used.
Bit #7	Odd parity bit.

Figure 3.33b EPROM Status Byte Format.

8088 Microprocessor Interfaces

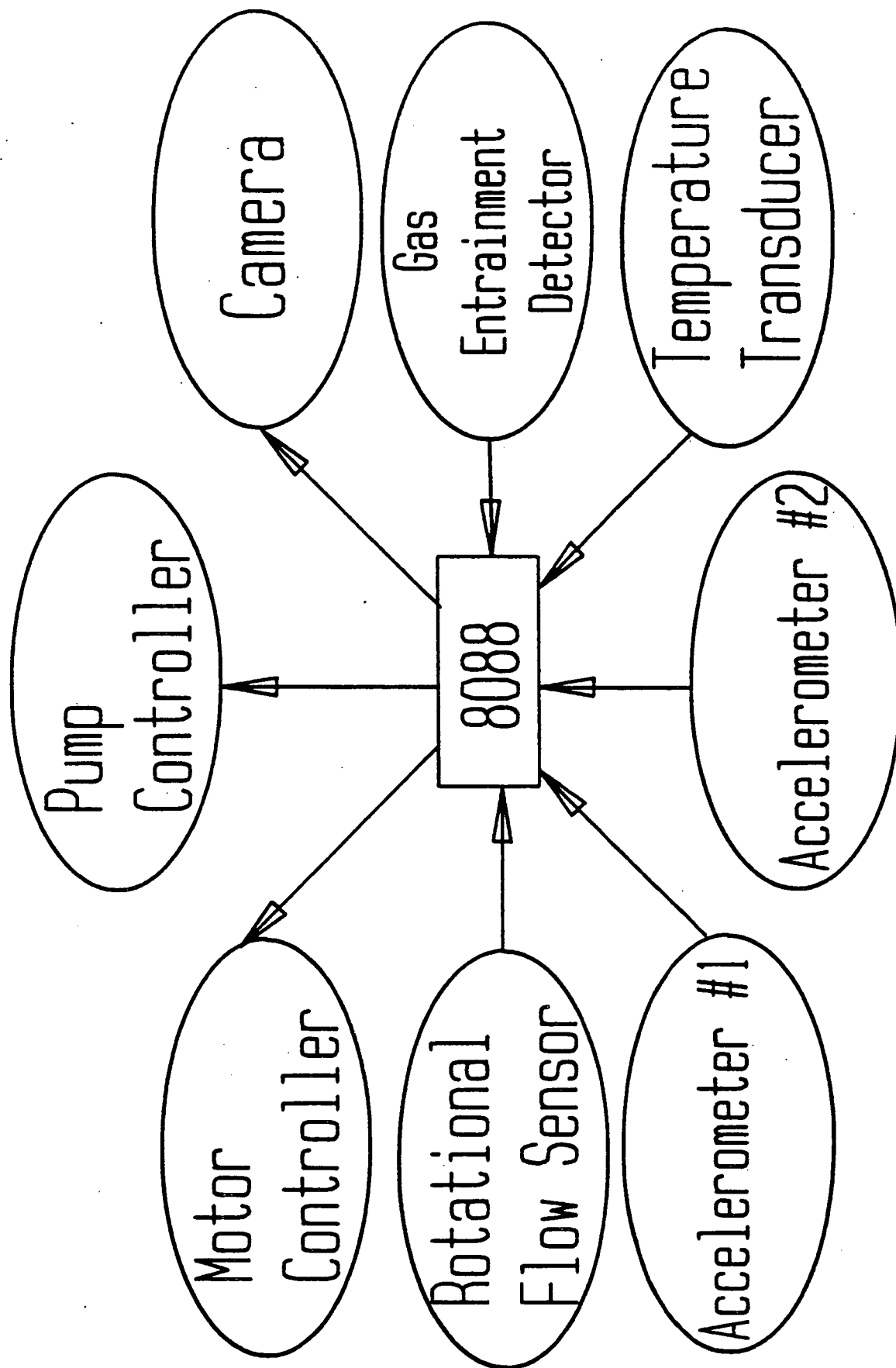


Figure 3.34 8088 Microprocessor Interfaces.

formation trials. As mentioned earlier, eight acceleration levels, with three flow rates each, are used for the trials. The eight acceleration levels are evenly spaced and are: 255 (FFh), 224 (E0h), 193 (C1h), 162 (A2h), 131 (83h), 100 (64h), 69 (45h), and 38 (26h). The three flow rates used for each acceleration level are: 225 (FFh), 170 (AAh), and 85 (55h). Two nested DO-WHILE loops are used to conduct the trials. There is an external loop, whose control variable is GLEVEL (the acceleration level), and an inner loop with control variable FLOWRATE.

The first task in the outer loop is to reset the clock, and begin keeping time. After this, the acceleration level is established by sending the proper value to the motor controller DAC (8155, port A) and latching it (8155, PC0). The platform is allowed twenty seconds to reach the desired speed. The inner loop then begins. At this point, flow rates can be established by sending the appropriate value to the pump controller DAC (8155, port B) and latching it (8155, PC1). The RTC is set for 1 second interrupts to force regular checking for gas entrainment and a steady flow rate. The DO-WHILE loop cycles until either of the above events take place, or until three minutes elapse. The three-minute interval should be enough to form a vortex. If at any point during those three minutes the gas entrainment interrupt is serviced, a picture is taken, one frame of data is recorded, and the pumps are stopped.

If there is no gas entrainment, data acquisition begins. First, a picture is taken by strobing the 8155's PC4 line. Next, twenty frames of data are collected at one second intervals. Data acquired through the MOR-800's ADC employs the optimum conversion procedure described above for the dummy conversion/ADC stabilization. All data frames are

stored in the DS-64's EPROM memory bank.

The procedure used to burn data on EPROMs is also optimized. Location and data to be burned into EPROM are latched into the DS-64. Next, a burn strobe is enabled briefly. A counter keeps track of the number of burn strobes used to burn the datum in question. This sequence is repeated until the datum to be burned is identical to the target location in EPROM. The strobed burn process is then repeated this time for the number of burn strobes it took. Thus, to ensure reliable data retention, a datum is strobe-burned into the target location for twice the amount of time required for retention.

After the data acquisition and the storage phase is complete, pumps are powered-down. The computer waits three minutes for the current vortex to decay. The experiment proceeds to the next flow rate or acceleration level. This cycle is repeated until all twenty-four vortex formation trials have been executed.

Upon completion of all vortex formation trials, both the platform motor and pump controllers are powered down. At this point, FLIGHT has completed execution.

Generic Data Extraction Software: READ.C

READ.C was developed at an early stage when the DS-64 was under test. The only way, at that time, to confirm whether data had indeed been burned into the DS-64 and examine its contents was by using a full-blown EPROM burner like the EP-1. READ was written to allow EPROM data to be dumped directly from the DS-64 to a PC via the CPU-8088's UART serial port.

READ.C is not firmware; it is meant to reside in the MOR-800's scratch-pad RAM

space and execute under Monitor control. It is meant to be executed after GASCAN II returns to WPI. The flight EPROM will be removed and replaced with Onset's Monitor. READ.C will be used to extract EPROM contents into a text file for further analysis. READ.C dumps the address and corresponding datum to a text file. Refer to appendix B for the program listing.

The basic sequence used in READ is as follows: a control structure consisting of two nested loops increments the high and low bytes of the EPROM address to be read. The two control variables are HIBYTE and LOWBYTE. Proceeding through the inner loop, the addresses of the EPROM locations to be read are output to their corresponding ports by using OUTPORTB statements. Next, the datum at that location is read.

Since the datum and its address are in raw hexadecimal, a routine called HEX2ASC to convert hex into ASCII was required. The routine is defined as a C function following the MAIN module. This function is used to convert HIBYTE, LOWBYTE and READ (the datum at the current address) into ASCII characters. Once in ASCII, address and datum are sent to the PC a nibble at a time by placing its ASCII value into the CPU-8088 UART's serial stream. As ASCII characters are received by the PC, the logfile feature of terminal emulators like PROCOMM can be used to capture the data and store it in a text file.

This sequence continues until all locations in the DS-64's 64K EPROM bank are read and relayed to the PC.

Data Examination Software: DATEX.C

DATEX.C considerably extends the capabilities of the generic hex data dump

performed by READ.C and examines data the way it was stored; in terms of frames delimited by start of frame markers. In addition, the data is interpreted to reflect acceleration measurements, temperature, circulation rate, analog voltages issued by the two DACs, time recorded, and errors encountered. DATEX also creates a text file in which all measurements are dumped in decimal so that graphic analysis can be performed by packages such as GRAPHER or Lotus 123. Refer to appendix B for the program listing.

During the year, DATEX was translated from BASIC to C, commented more clearly, and enhanced to include the different devices and report run-time and checksum errors. It provides two forms of reports - a detailed report containing all the data recorded, including whether and when there was gas entrainment, the time the picture was taken, and a summary containing average data and standard deviations.

When the program begins, it asks whether the user wants to record the data to a text file in detailed or brief format. The factors used are adjusted also for real component values as measured by a digital multimeter.

Next the hex data file is opened for scanning. At the same time, another text file is opened to store the extracted data in the decimal form. Now, eleven data bytes, corresponding to one data frame, are read from the hex data file. If frame start and end delimiters are found, the addresses for frame start and end locations are noted. At this stage, the ASCII data can be converted into its decimal representation. This is accomplished by the subroutine *hex2dec*.

Once a data frame has been extracted and its elements processed, the next step is to print. Each frame is written to the output file, in decimal representation. The subroutine

print_frame writes out the frame starting and ending location in EPROM, frame number, acceleration measured by both accelerometers, fluid temperature in three scales, circulation, DAC outputs for motor and pump controllers, time to entrainment, and any relevant status data. This output file can be used for graphical and/or statistical analysis of the data.

The sequence described above is repeated until an end-of-file mark is encountered, at which point DATEX is terminated.

CHAPTER 4 OPERATIONS

This chapter is solely dedicated to provide an explanation of the methods by which the flight hardware is assembled and, once in space, what the order of operations is for each individual component.

Throughout the academic year, one problem surfaced that proved to be more of a practical nature than a critical design flaw. This involved the method for mounting hardware to the platform and, then, to the rest of the GASCAN itself. Due to confined working spaces, and the position of certain equipment, mounting the platform and the components has proven to be both troublesome and very complex. Therefore, it is appropriate to include a section explaining how the assembly can best be done in order to make the mounting of experiments as straight forward as possible.

In addition to providing a step-by-step "instruction manual" on mounting the hardware in its final flight configuration, a second section is provided to explain the sequential operation of the experiment in flight. A copy of the computer timing diagram is included as well.

4.1 MECHANICAL HARDWARE ASSEMBLY

One of the final steps in preparing the experiment for flight is assembly of the rotating platform, and its installation along with other components of the experiment with the shaft of the GASCAN. This experiment differs from the others in that it must rotate on the mounting shaft. In order to rotate the experiment, several of the components must be attached to the shaft separately from the experiment.

The components of the experiment must be mounted to the shaft in a specific order. First, drive gear and belt must be put on the shaft; see figure 4.1. Next, the mounting piece

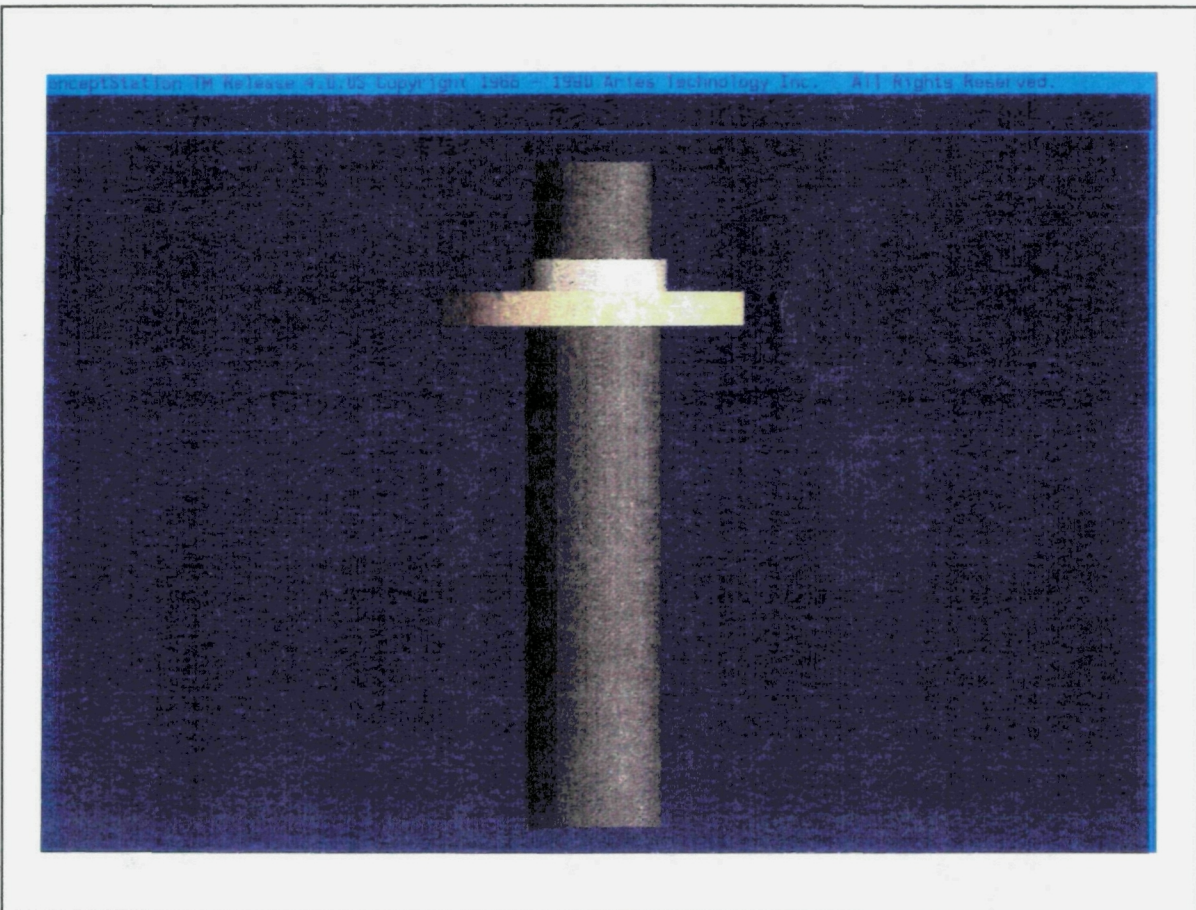


Figure 4.1 Mounting Sequence: drive gear and belt.

that seats the upper bearing must be removed from the upper plate of the platform and put on the shaft; see figure 4.2. Third, the slip-ring components are installed. The slip rings are mounted onto the shaft and their interconnecting wires brought through a small hole in the side of the hollow shaft, run up the length of the shaft, and connected to the GASCAN

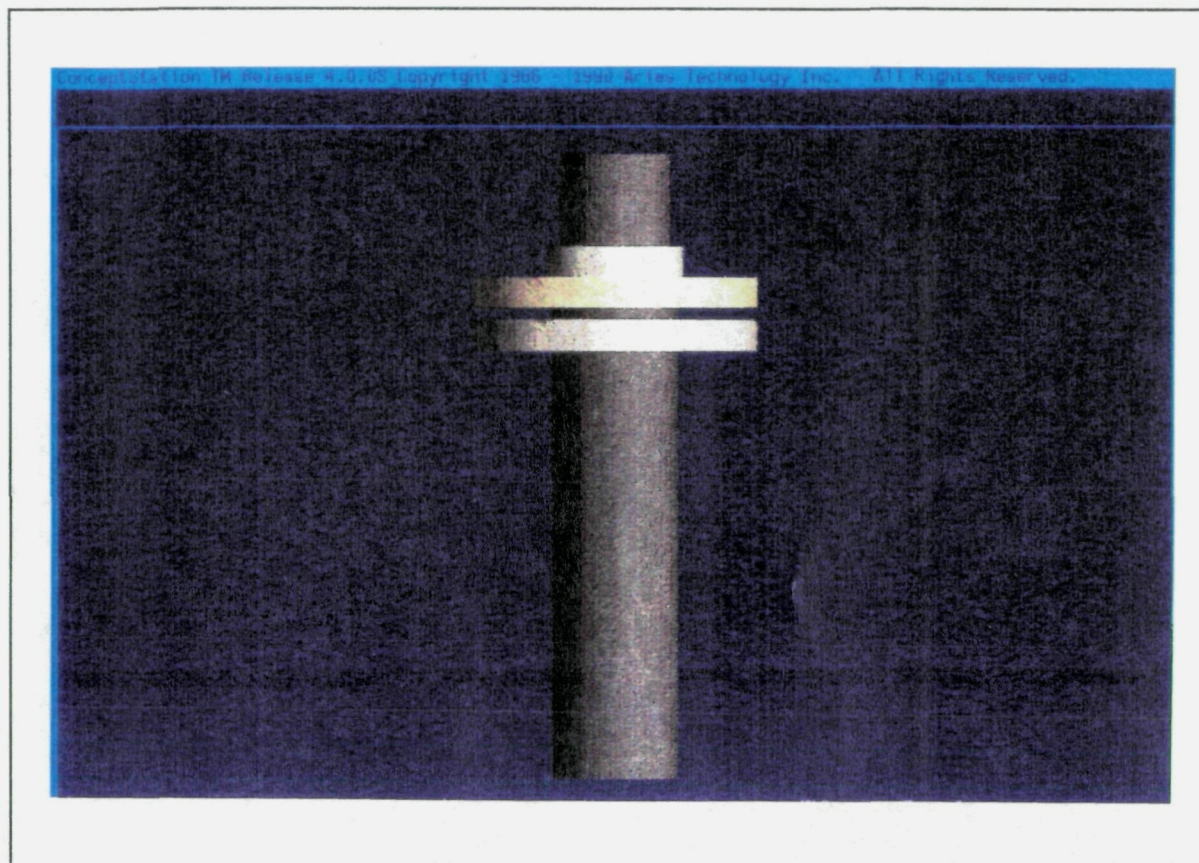


Figure 4.2 Mounting Sequence: upper platform bearing.

battery pack; see figure 4.3. Now, the platform with the experiment mounted on it can be put on the shaft. The platform is placed on the shaft, slipped over the rings, and mounted. The mounting surface device for the upper bearing is then reattached to the upper plate; see figure 4.4. With the platform in place around the slip rings, the brushes that serve to make

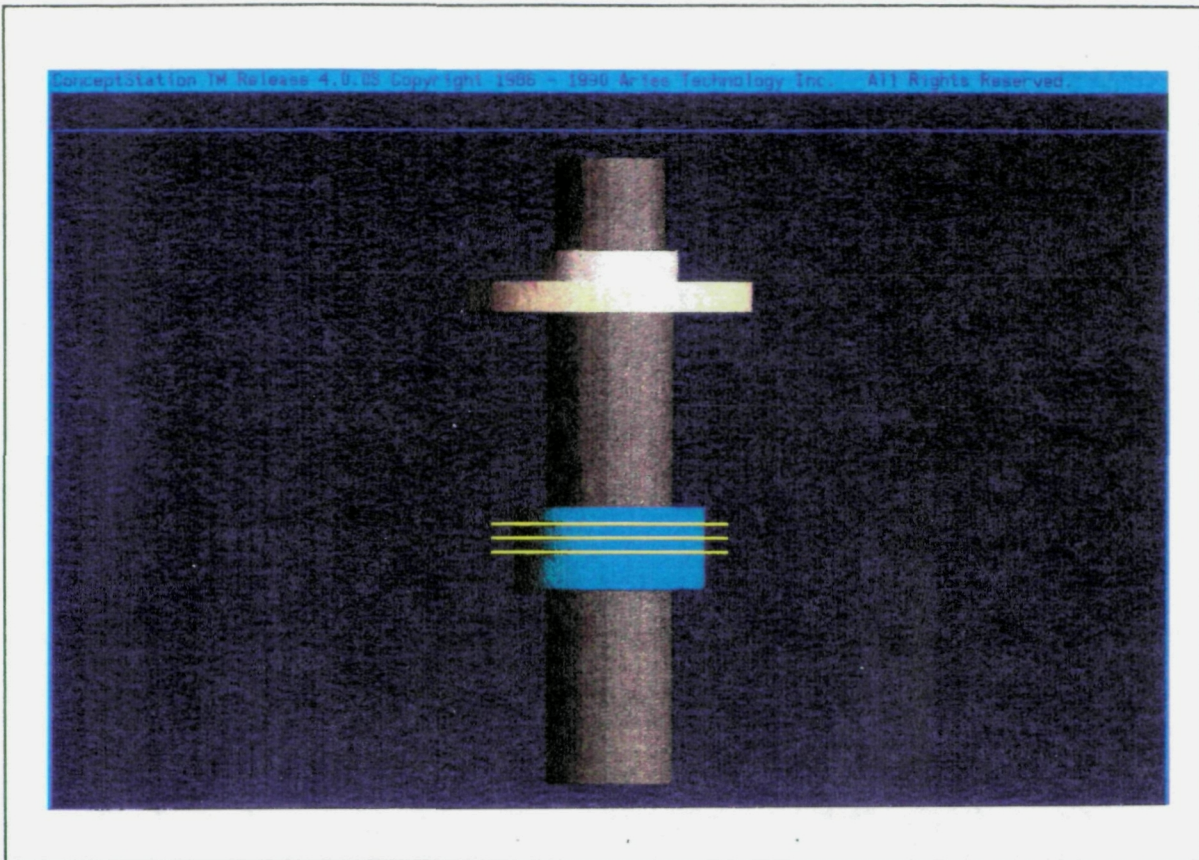


Figure 4.3 Mounting Sequence: slip-ring installation.

electrical connections with to the slip rings are mounted onto the hub of the platform. The final component to be mounted is the drive motor. It is mounted onto the upper plate of the platform and the drive belt is slipped around the gear and motor shaft head; (see figure 4.5). One last operation is to tighten the drive belt. This is accomplished by adjusting the position of the motor on its mounting plate.

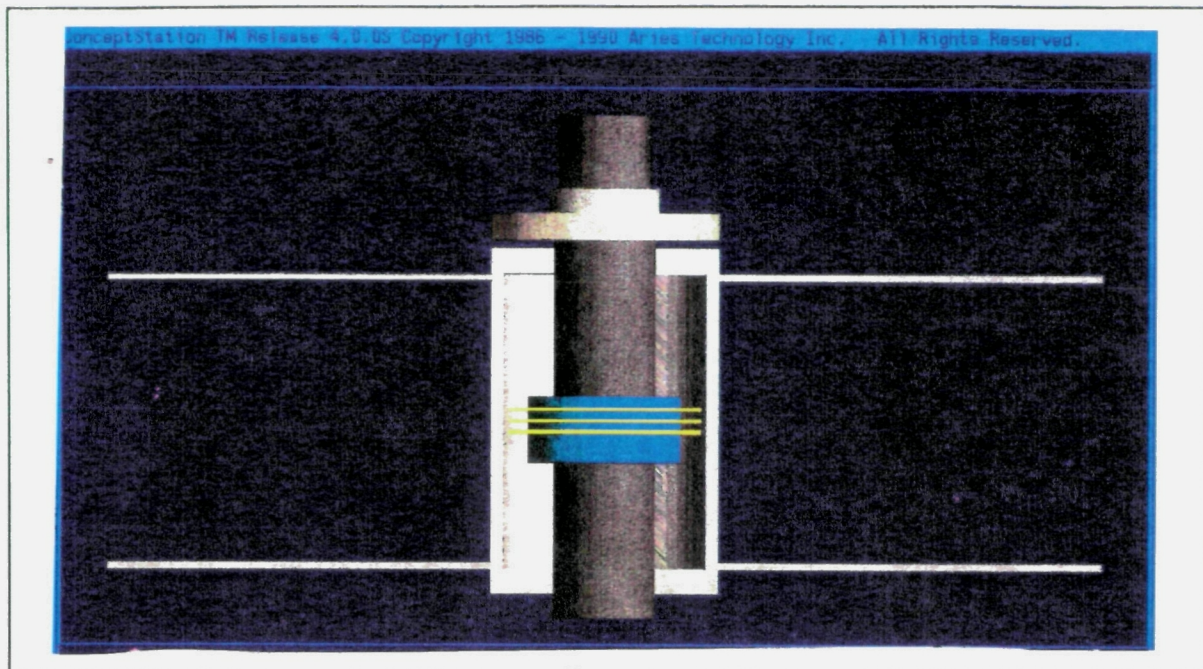


Figure 4.4 Mounting Sequence: platform and experiment installation.

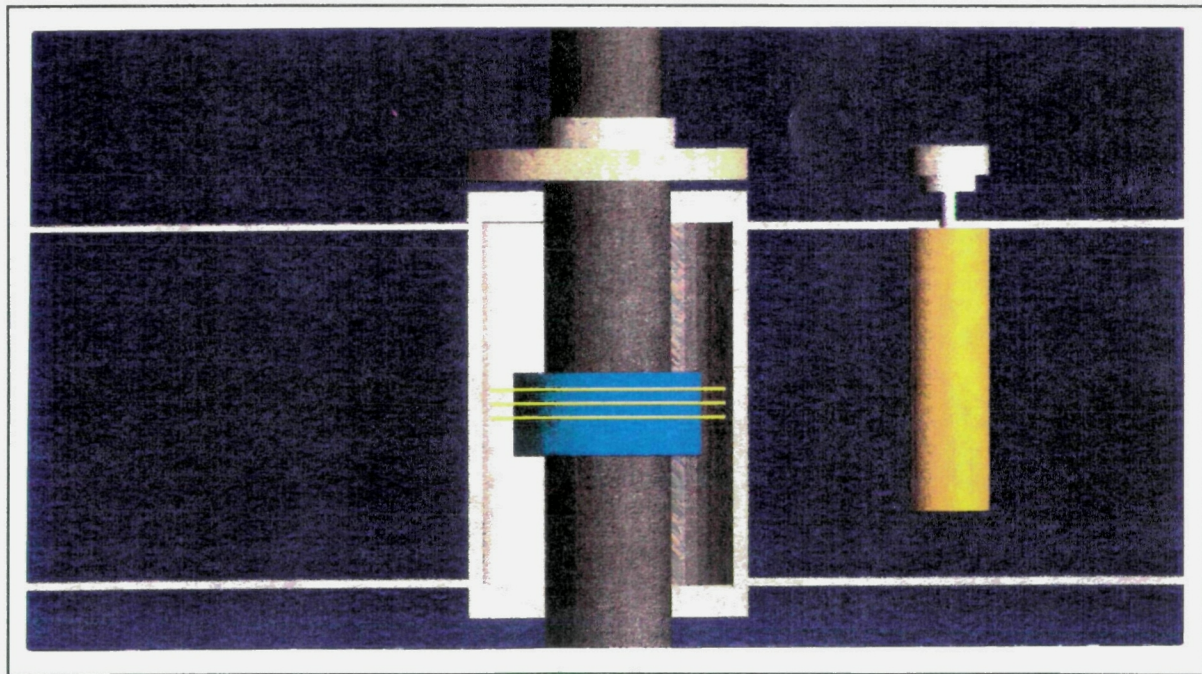


Figure 4.5 Mounting Sequence: drive motor installation.

4.2 FLIGHT OPERATION SEQUENCE

The experiment, which has been tested on earth, will be executed during flight.

There are various tasks that the computer has to perform during flight, which are outlined below in sequence of operation. The timing diagram and explanation for the flight software follow.

The operational scenario proposed by the mechanical engineers aims at examining vortex formation at various acceleration and flow rates. Figure 3.34 (8088 Microprocessor Interfaces) outlines the interface control flow for the vortex experiment. Figure 4.6 (Flow Chart of the Timing Diagram) highlights the operational scenario described below.

After the computer is powered up, it waits a few minutes for the microgravity experiment to complete before initiating the flight sequence.

To perform the vortex formation trials, eight acceleration levels and three flow rates per acceleration level are used. In order to conserve power, the trials are conducted such that the highest acceleration level is used first and the lowest one last. That way, the highest power utilization, as far as the platform is concerned, is the initial power spike to accelerate the platform to the highest rotational speed of interest. Less power is required to sustain a given rotational speed than to step up speed from the lowest level to the highest for each trial.¹

The next step is to establish the acceleration level. A twenty-second delay allows the platform motor to achieve the desired speed.

¹ For further information on the platform motor and motor controller, refer to Michael Sheehan's MQP No. 90D057M.

Once at the specified acceleration level, the pumps are started to induce the required fluid flow rate. A maximum of three minutes are allowed for vortex formation, which previous Mechanical Engineering MQP reports have said is sufficient time for the vortex to develop. However, the computer constantly checks the flow rate, and begins the trial before three minutes are up if a steady flow rate has been achieved. The computer also periodically checks for gas entrainment. If gas entrainment develops, the pumps are stopped, a picture and data readings are taken and recorded, and the operational sequence proceeds to the next vortex formation trial.

When three minutes have elapsed, or if a steady flow rate is reached, the data acquisition phase begins. A picture of the vortex in the containment vessel is taken, after which twenty frames of data are read from the input devices and recorded to EPROMs. A data frame consists of ten data elements in eleven bytes: a frame start marker, a two-byte time value in seconds since the trial began, acceleration readings from the two accelerometers, fluid temperature reading, vortex circulation rate, the current acceleration level issued to the motor controller, the current flow rate issued to the pump controller, a status byte described in figure 3.33b, and a checksum. The status byte contains data such as whether there was an entrainment, whether a picture was taken, and whether all input devices responded correctly. As each frame of data is acquired, it is stored on the flight computer DS-64 EPROM data bank.

After acquiring all twenty frames of data, the vortex formation trial ends. Pumps are powered-down and the vortex is allowed three minutes to decay into a steady-state fluid mass. This operational scenario is then repeated to accommodate the eight acceleration

levels, each with three flow rates, making twenty-four trials in all.

Once the twenty-four vortex formation trials have been conducted, both the motor and pump controllers are powered-down. The complete experiment takes between two and three hours to complete. At this point, the flight computer is ready to relinquish control to the next GASCAN II experiment.

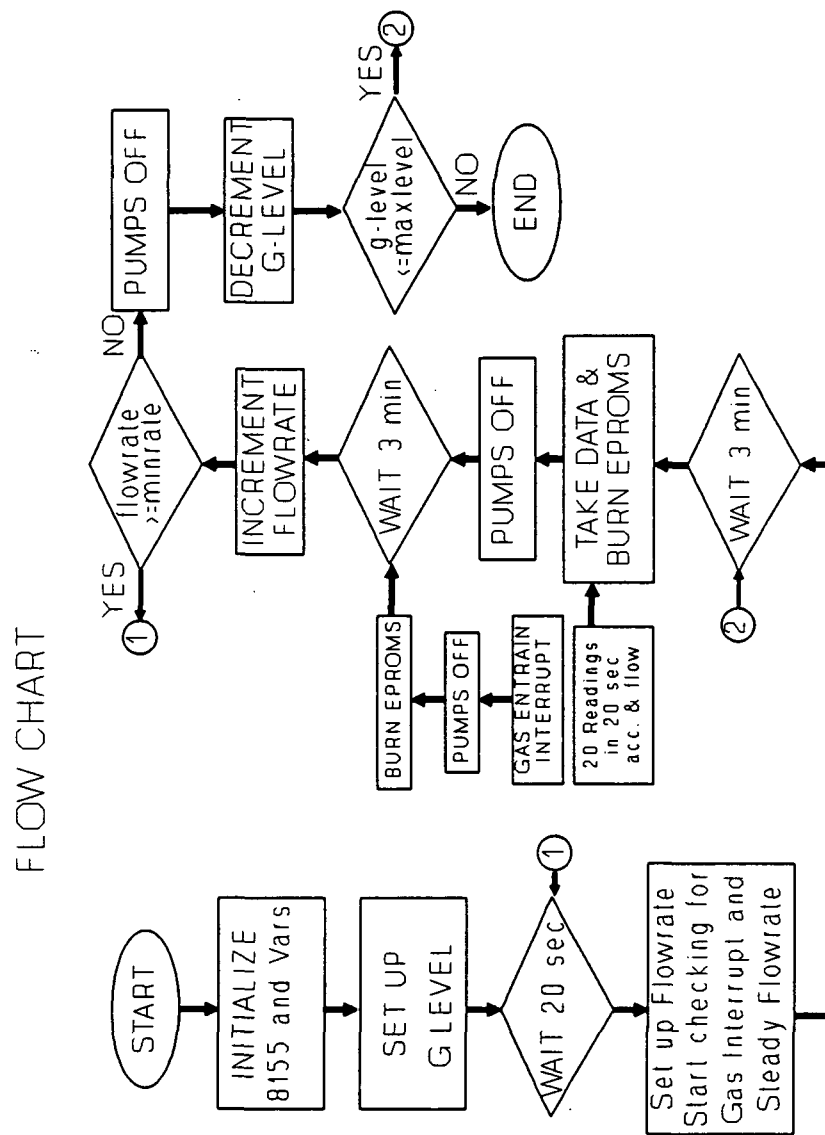


Figure 4.6 Flow Chart of the Timing Diagram.

CHAPTER 5

EARTH-BASED EXPERIMENTS

This chapter describes the results of all the Earth-based testing done throughout the academic year. The chapter is divided into three major sections. The first discusses the goals of the on-Earth experiment. Problems encountered as the fluid within the cylinder was rotated at different rates are described along with the rationale that led to the need to obtain a more powerful pump. The second section describes the testing that was accomplished to locate the camera and flash so that good pictures of the vortex could be obtained during experiment operation. The third and final section describes the testing of electrical circuits used to control the mechanical subsystem of the experiment.

5.1 ON-EARTH EXPERIMENT

After studying the basic mechanics of the microgravity experiment, it was determined that an experiment based in Earth normal gravity would be of significant value. The most persuasive reason for on-Earth experimentation is to check the feasibility of vortex formation even with the unusual forces being placed on the fluid. It was unclear from static tests whether the data gathered by the actual test would be of use, or if a vortex would form at all. The on-Earth system also provides an opportunity to evaluate a variety of cylinder and pump configurations and determine their performance. In addition, if the vortex formed properly, the experiment would be able to provide data for gravitational levels higher than 1G.

5.1.1 Forces Involved

In addition to the desired radial force due to the platform rotation, there is also a coriolis force due to the outward draining of the fluid. This force is the resultant of the angular velocity of the platform and the radial velocity of the fluid; it acts in a direction that it accelerates the fluid in the same direction as the cylinder is rotating on the platform. Also, the force is slightly uneven on the sides of the cylinder since the swirl of the fluid produces a velocity gradient throughout the cylinder. Calculations (see appendix D) show that these added forces produce a tilt of a few degrees in the free surface of the fluid. Static tests prove that tilt could inhibit vortex formation under certain conditions.

5.1.2 Equipment Used

The on-Earth test is a slightly modified and simplified version of the space-based experiment. The most important modification is to suspend the cylinder from the edge of the rotating platform so that it can swing freely to the proper orientation for the speed of rotation. In this way, the resultant force vector is as close as possible to that which would be experienced in space (see figure 5.1).

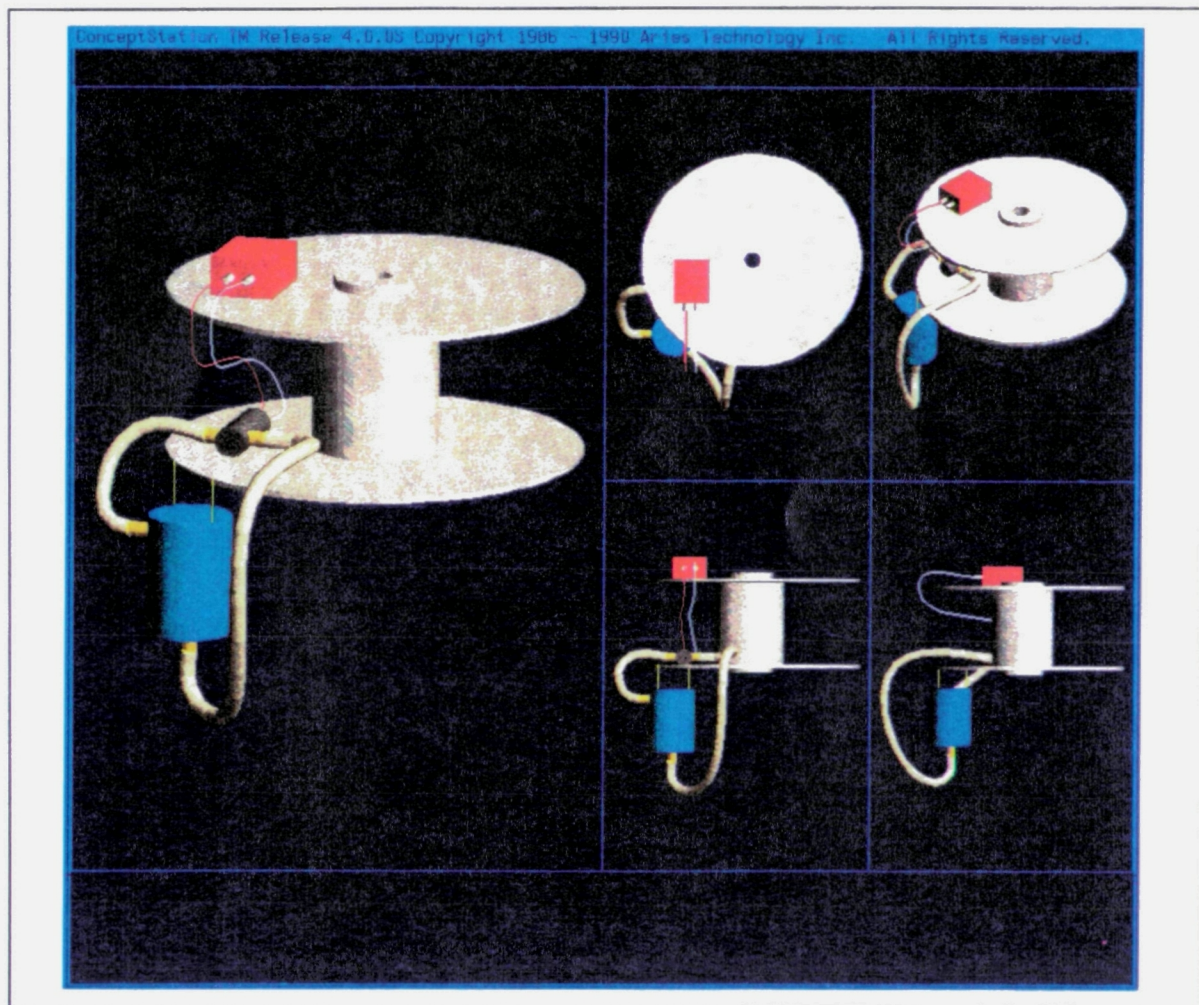


Figure 5.1 On-Earth Experiment. Pump is displayed grey, battery supply is displayed red, and the cylinder is displayed light blue.

5.1.3 Preliminary Design

The first on-Earth experiment was performed using a very simple apparatus. Rotation was provided by a bicycle wheel mounted on a wooden structure. One of the previously manufactured prototype cylinders was suspended from the wheel. The overall performance of this system proved unsatisfactory because of the instability of the support and the age of the wheel bearings. Additional vibrations were created that suppressed the formation of any possible vortices. As a result, a number of modifications were made to the system to assure a smooth operation.

5.1.4 Final Design

The first modification was to strengthen and level the wooden foundation. The actual flight platform was installed on this foundation with the same prototype cylinder dangling freely from it's edge. This resulted in a system as free from superfluous motions as possible.

As the slip rings designated for use on the actual experiment were not yet installed, a simpler system using battery power was devised to run the pump. In addition the motor controlling the speed of the rotation was operated manually rather than by computer since the automation equipment was not available at the time.

5.1.5 Running the Experiment

The experiment was run at a number of rotational rates. Using the known rates and the radial distance to the center of the cylinder, the gravity levels were calculated to be

between 1G and approximately 1.4G. At each of the gravitational levels produced, different flow rates were obtained by altering the voltage supplied to the pump. After the vortex formed and attained steady state, its height relative to that of the overall cylinder was obtained visually.

5.1.6 Problems Encountered

As mentioned previously, while the original structure was not sound, that deficiency was remedied in the final design. The major problem was with the formation of the vortex. The pump chosen for flight was not strong enough to overcome the forces encountered at the higher platform speeds. To combat this difficulty two pumps were connected in tandem to increase the total flow rate. This too proved unsatisfactory and larger pump was obtained to support operation in the flight system

5.1.7 Results

Although vortex formation was slow at slightly in excess of 1G and impossible at higher platform speeds, production of vortices was successful and the validity of the experiment proven. The data acquired (see figure 5.2) proved to be very similar to that of static (non-rotating) vortex tests which were obtained by varying flow rates and fluid viscosities.

d/D vs Froude Number

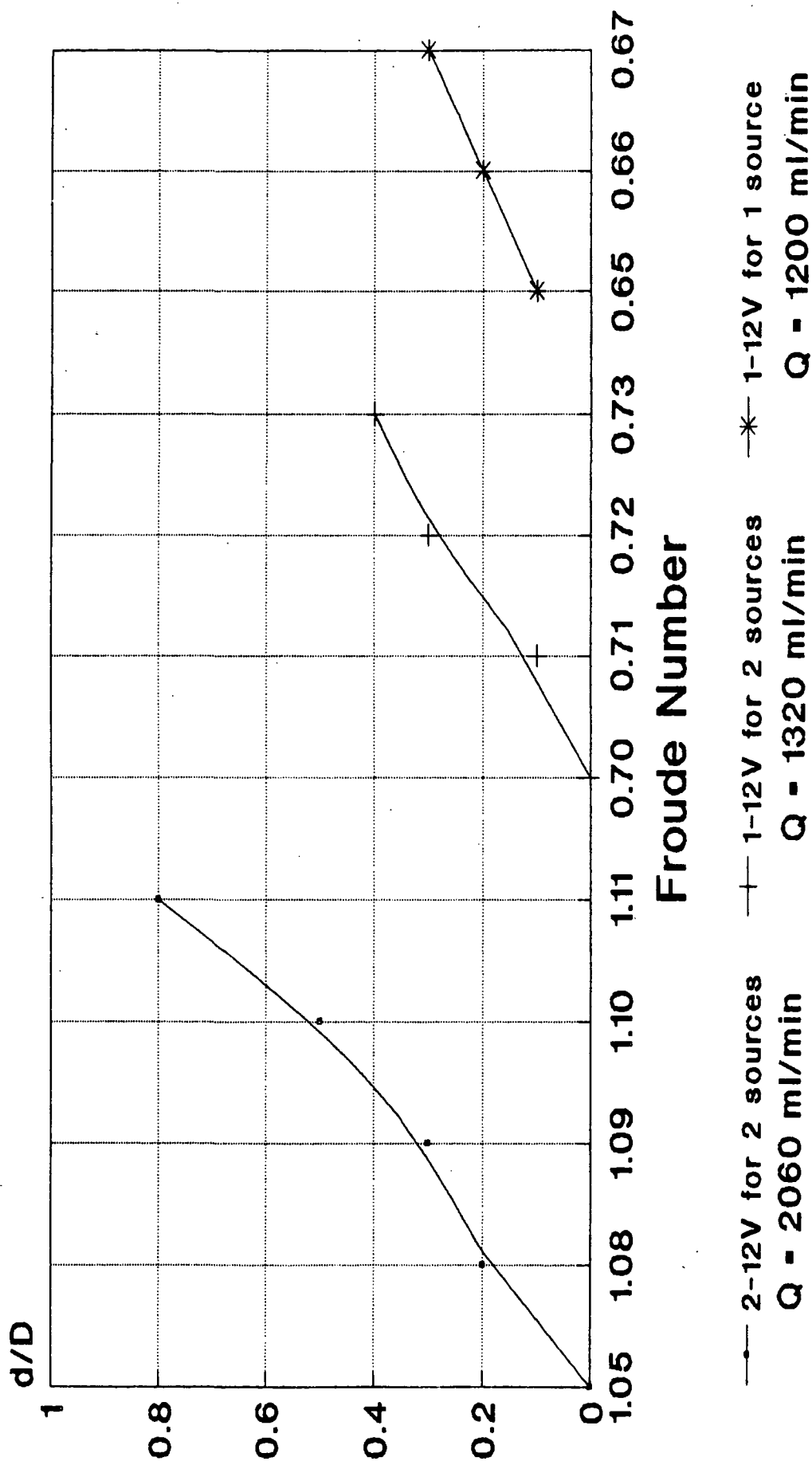


Figure 5.2 Graph of d/D vs Froude Number for different flow rates.

5.2 CAMERA AND FLASH TESTING

Other important testing that was conducted was aimed at finding the best placement for the camera and flash on the platform. Previous groups working on the project had suggested various configurations which had not been tested. These tests are important in making sure that by placing the flash in a certain way there will not be too much glare, or in the opposite sense, not enough lighting when the picture is taken. These tests were conducted so as to simulate as closely as possible the flight configuration. The pictures were taken in a dark room. The cylinder was placed on the plate, which was itself enclosed on all sides, as it would be in the flight canister.

Before discussing the test arrangements used to determine optimum lighting, a brief explanation on the equipment used is appropriate. The flash is a direct-mount unit of the sort commonly used on 35mm cameras. The flash is equipped with a sensor to vary the strength of the light pulse, according to the distance between the object to be photographed and the flash. The diffuser is a plastic covering that diffuses the light emitted by the bulb, scattering the light over a large area. Accordingly, less light illuminates the object and more light illuminates the surroundings. A second diffuser, a common white bed sheet, was placed between the flash and the cylinder. Multiple layers of the sheet were used in order to observe the effect of having such a barrier between the flash and the cylinder. The last piece of equipment is paper. Small rectangle pieces of paper were cut from regular 8x11 in. sheets of white blank paper. These small rectangles were then placed between the flash bulb and the plastic diffuser, reducing even more the strength of the light pulse.

In all, 22 pictures were taken. These were associated with three basic equipment

configurations illustrated and described below. In each configuration, both the flash and the camera were moved to different positions so different lighting options could be evaluated.

In Position A (refer to figure 5.3), the cylinder was placed on a table with the flash aimed directly at it. In this configuration the background behind the cylinder was varied.

In Position B (refer to figure 5.4), the cylinder was placed within the platform, while the camera and the flash were outside of the platform. The flash was placed in different positions; in one, illuminating the cylinder from the same position as the camera and, in another, from behind the cylinder, shooting light toward the camera lens.

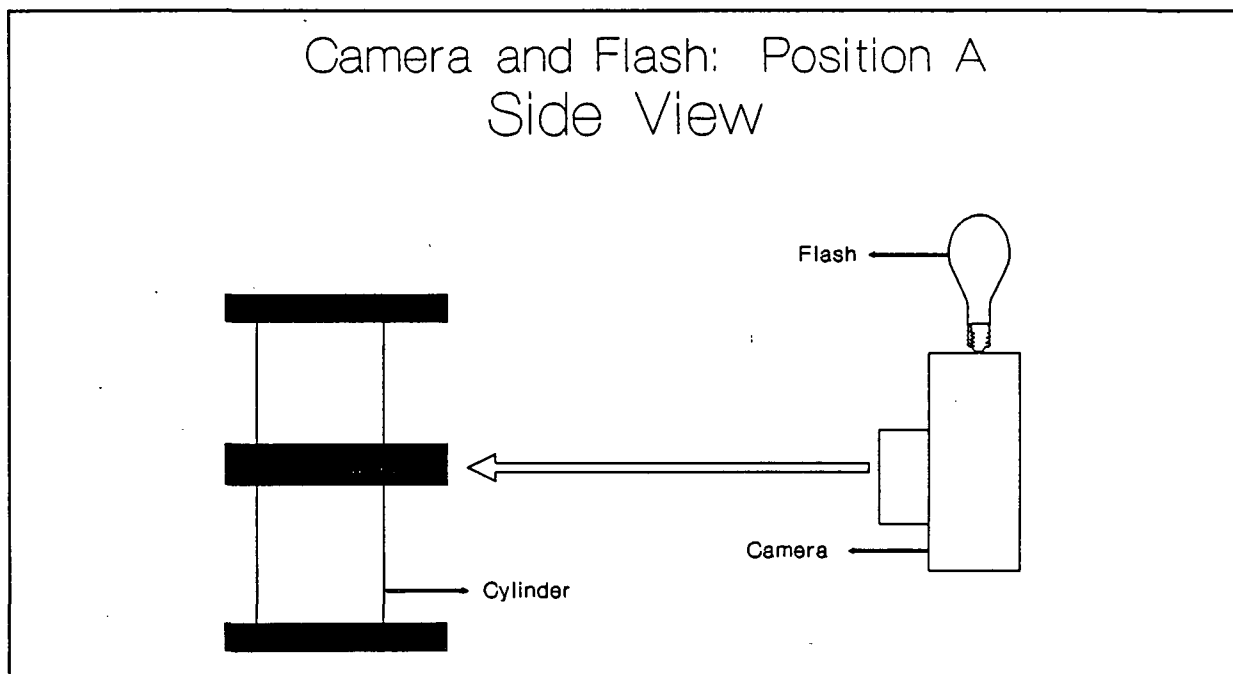


Figure 5.3 Camera and Flash: Position A.

In Position C, both the camera and the flash were placed on the platform. As can be seen from figure 5.5, with the reference being that of the camera, the flash is placed behind the cylinder. In order to better illuminate the cylinder, a mirror was placed in a position to reflect the light generated by the flash in the direction of the camera lens.

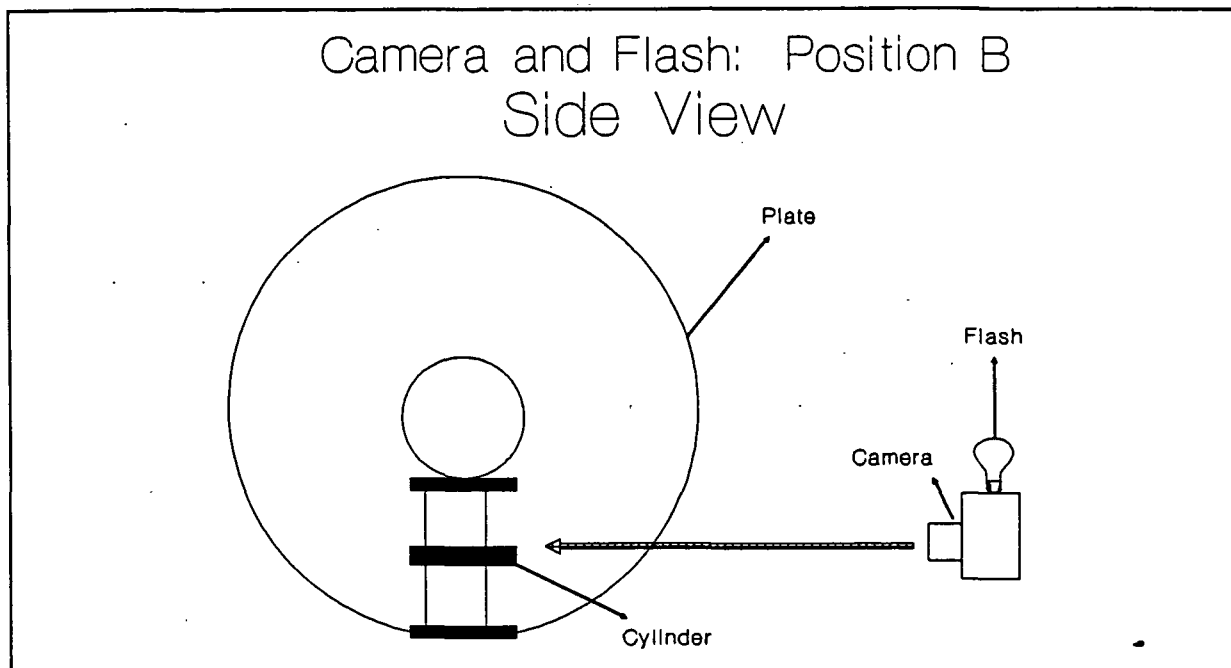


Figure 5.4 Camera and Flash: Position B.

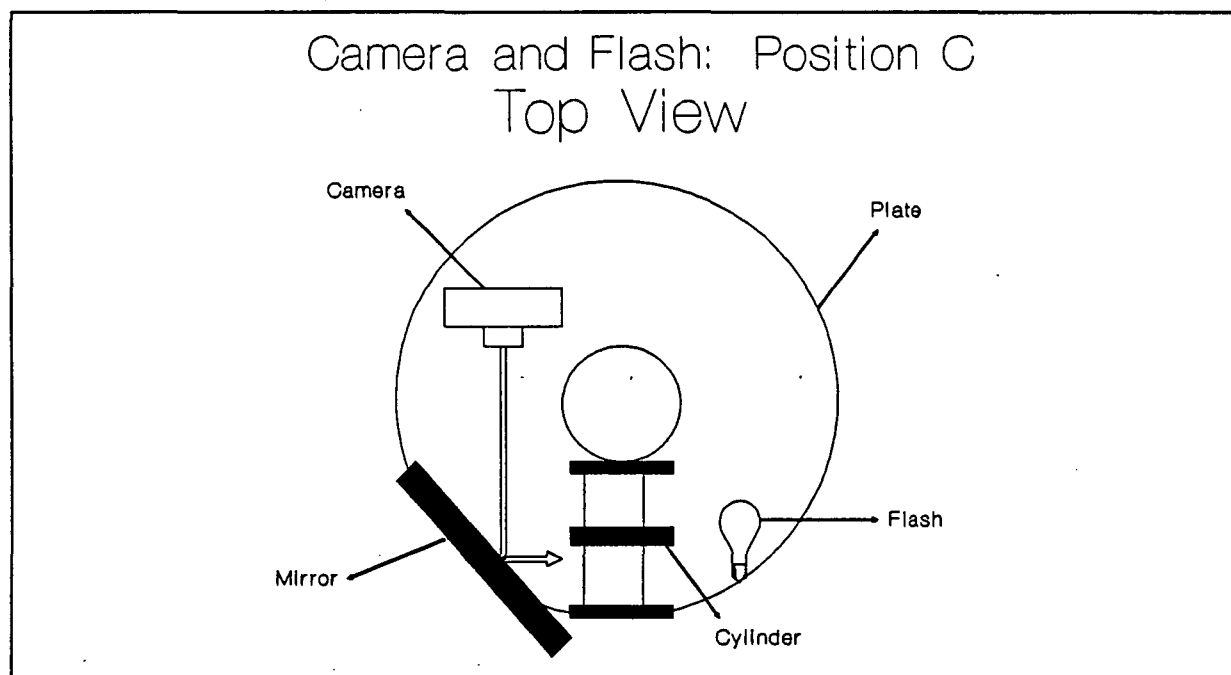


Figure 5.5 Camera and Flash: Position C.

Information pertaining to the three configurations used is summarized in table 5.1. It should be noted that numbers in front of © or P, indicate the layers of cloth or paper used. It

is also noted that the flash was not always pointing directly at the camera, but could have been pointing in a totally different direction.

Below is a list of symbols used to explain the different positions of the camera and flash, as well as the different lighting variations used:

- ⊗ → Diffuser was placed over flash bulb.
- ⊙ → No diffuser was placed over flash bulb.
- ⊙ → Cloth was placed between cylinder and flash.
- P → Paper was placed between flash bulb and diffuser.
- [pm] → Cylinder was placed in platform.
- [cip] → Camera and cylinder were both placed on platform.
- FLSH ↑ → Flash pointed upwards (away from camera lenses).
- FLSH DIR → Flash pointed directly at camera lenses.
- FLSH @ MTL → Flash pointed sideways, bouncing light off aluminum plate. Only in Position C.

Table 5.1

Pict. Number	Diff.	Cloth	Paper	Flash	Position of equip. on platform
1	⊗	1 ⊙		FLSH DIR	Position A
2	⊗	2 ⊙		FLSH DIR	Position A
3	⊗		3 P	FLSH ↑	Position A
4	⊗		1 P	FLSH ↑	Position A
5	○	1 ⊙		FLSH DIR	Position A
6	○	2 ⊙		FLSH DIR	Position A
7	○	3 ⊙		FLSH DIR	Position A
8	⊗	3 ⊙		FLSH DIR	Position A
9	○	4 ⊙		FLSH DIR	Position A
10	⊗	4 ⊙		FLSH DIR	Position A
11	⊗	2 ⊙		FLSH ↑	Position B, [pm]
12	⊗	2 ⊙		FLSH @ MTL	Position B, [pm]
13	⊗		1 P	FLSH ↑ @ ⊙	Position B, [pm]
14	○		1 P	FLSH ↑ @ ⊙	Position B, [pm]
15	⊗	4 ⊙		FLSH ↑ @ ⊙	Position B, [pm]
16	⊗	4 ⊙		FLSH DIR	Position B, [pm]
17	⊗	2 ⊙		FLSH DIR	Position B, [pm]
18	⊗	2 ⊙		FLSH DIR	Position C, [cip]
19	⊗	4 ⊙		FLSH DIR	Position C, [cip]
20	⊗	4 ⊙		FLSH DIR	Position C, [cip]
21	⊗	2 ⊙		FLSH ↑ @ ⊙	Position C, [cip]
22	○	2 ⊙		FLSH ↑ @ ⊙	Position C, [cip]

From comparison of the pictures obtained, it appears that the best results were obtained using Position C (refer to figure 5.5). In this configuration both the camera and the flash were placed in the cylinder. The pictures were taken with the help of a mirror which reflected the beam of light produced by the flash in the direction of the camera lens. Even though the camera did not have a very wide angle lens and was unable to view the whole vortex, the picture clearly shows the vortex with its shape outlined in black over a fairly white background. This is useful since it also displays the ripples in the vortex outline due to the table on which the apparatus was operated.

Figure 5.6 is picture no. 18 and figure 5.7 is picture no. 20 (refer to table 5.1); these are considered the most well defined pictures of the vortex taken to date.

There were of course many problems associated with obtaining the pictures. First, it must be understood that it was almost impossible to achieve the complete darkness that would be found in space inside a sealed GASCAN. Second, when taking the pictures in Positions A and B (refer to figures 5.3 and 5.4), the camera was physically outside of the platform and, thereby, subjected to additional ambient illumination.

The most important factor is the flash. It is obvious that the flash is far too powerful for use in an enclosed area such as that of this experiment. As a result, testing was limited to locating the best placement for the flash with respect to the camera. Future MQP groups must look into lighting options which will give good pictures, such as the ones displayed, but which will not be too powerful for the enclosed area.

There are many options that remain open to solve the illumination problem. One idea is to paint all the exposed metallic surfaces with black paint. As a result, the light pulse of

the flash will not be reflected to the same extent as it would be otherwise. Unfortunately, this causes another problem, especially if the type of film is a black and white. With all the surfaces painted black, the black outline of the vortex (which can be seen in the above picture) would probably not be as visible against a black background.

Other options include using protective devices between the cylinder and the flash, such as those shown in table 5.1. There are however, a number of drawbacks to this option, including the addition equipment to the platform which is not functional.

As was mentioned in section 3.1.3 of chapter 3, one of the best options is to procure a small light bulb that could be installed behind the cylinder, exactly as is shown in figure 5.5 (Position C). Its light output would be selected to be sufficient for illuminating the area around the cylinder. A switch would be required to power the bulb; the switching being activated by the system controller computer prior to initiation of the picture-taking sequence.

The camera does not require any additional major modification, since it has already

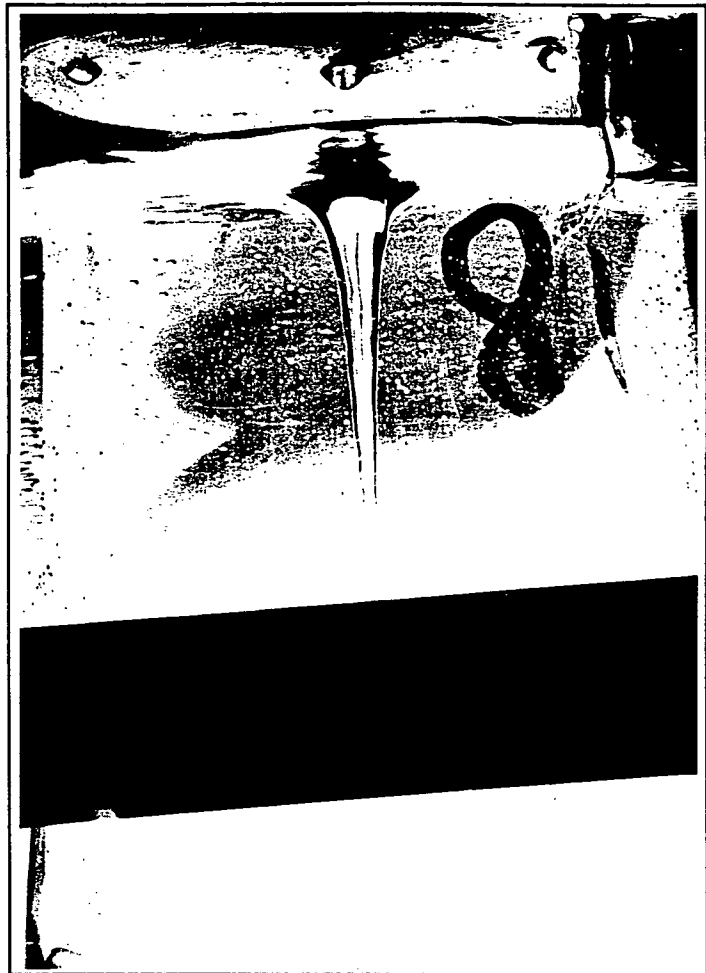


Figure 5.6 Picture no. 18.

been altered accordingly to be electrically triggered.

The currently available lenses are not able to clearly capture the whole cylinder in a single frame. Obtaining a lens that has a shorter focusing distance and a wider angle is advisable since the ability to view the whole cylinder provides the opportunity to obtain full view of vortices as well as those conditions when entrainment occurs. The camera is provided with the ability to use interchangeable lenses. Finding wide angle lenses to meet experimental objectives is essentially unrestrained.

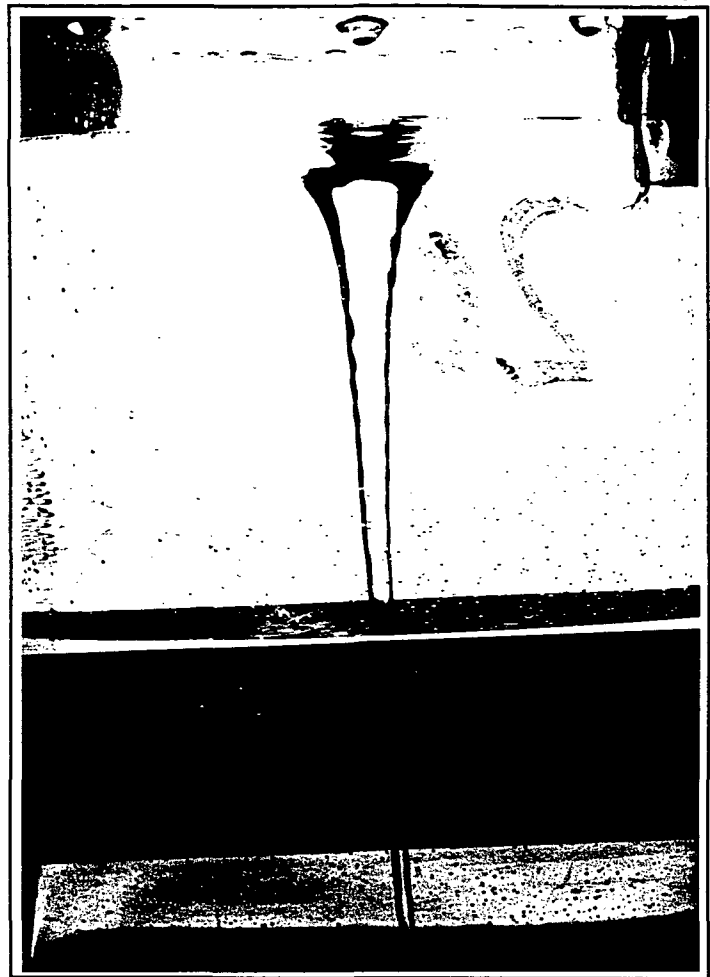


Figure 5.7 Picture no. 20.

Figure 5.8 displays an example of a frame which was subjected to too much light. As can be seen from the photograph, it is nearly impossible to distinguish even the outlines of the cylinder, much less any liquid features that might be contained within it. This photograph is not part of the latest group obtained in early March, but belongs to a set which was taken in early January, prior to the MITRE critical review. It is one of many that proved unusable; the remainder are included at the end of the report. The numbers visible in

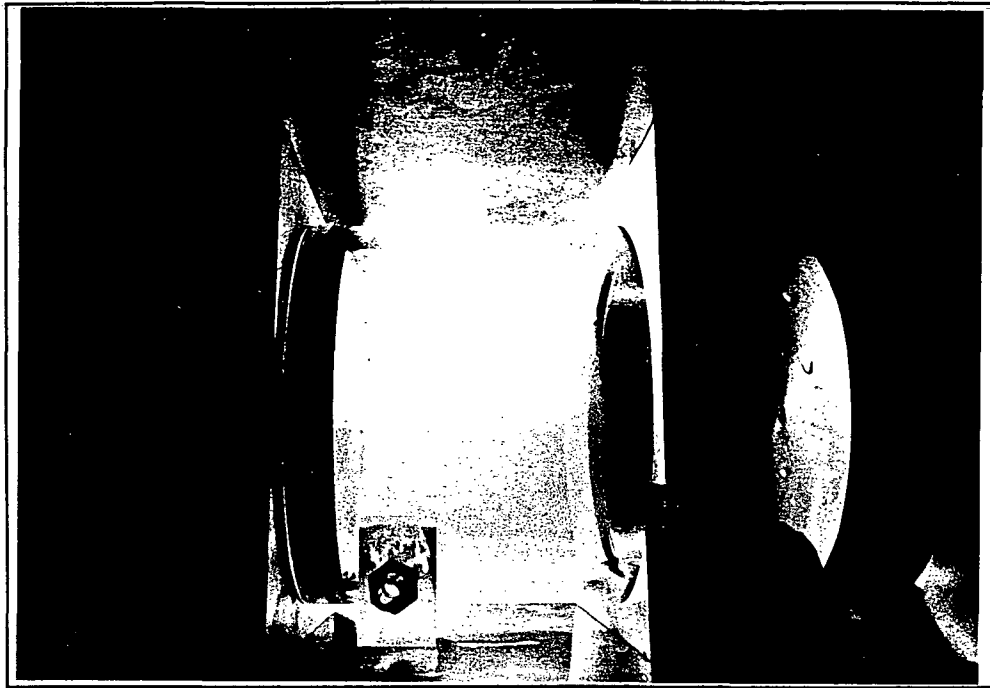


Figure 5.8 Example of too much light from the flash.

the photographs correspond to the numbers included in table 5.1.

Figure 5.9 shows a similarly overpowering effect to that of figure 5.8. A vortex was actually present within the cylinder, but the glare caused by the cylinder's plexiglass parts fully obscures the outline of the vortex.

The photographs displayed, along with those included at the end of the report, suggest that more thought should be given to the final configuration of the camera and the illumination approach that will be used in the flight experiment. Clearly, it should be carefully arranged so that the effects shown in figures 5.8 and 5.9 are avoided and detail shown in figures 5.6 and 5.7 further enhanced if possible.

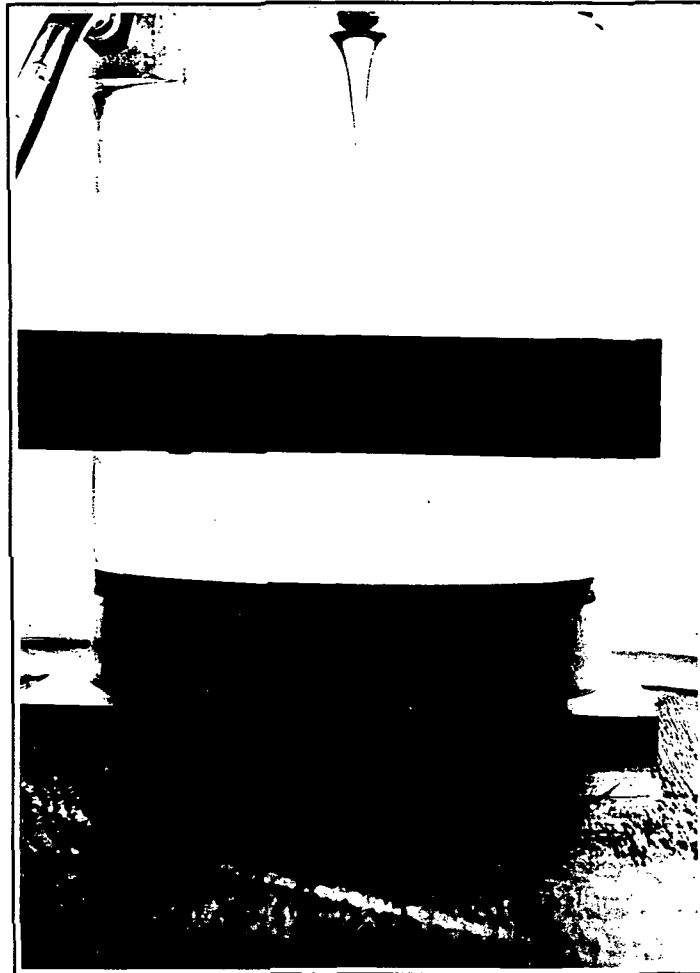


Figure 5.9 Picture no. 8.
Overpowering effect of the flash on
the cylinder containing the vortex.

5.3 ELECTRICAL EQUIPMENT TESTING

During this project year several modifications were made to the existing electrical equipment, and new components were added. All components were fully tested. The results of the testings follows below.

5.3.1 Computer Hardware

The 8088-CPU, DS-64, and MOR-800 boards were completely tested. A program to read data from the different ADC channels on the MOR-800 and send data to the 8155 I/O ports, using the 8155 timer was written. This program, called TEST-MON, was downloaded to the computer using Onset's Monitor software. Its successful execution proved that the 8088-CPU and MOR-800 boards were completely usable. The same program was then recompiled with the additional task of permanently storing, burning, the results obtained on EPROMs. This program, called TEST-RES, was made EPROM-resident and executed without external control. It executed successfully. This proved that the 8088 microprocessor, the 8155 and 8255 chips, the MOR-800 board, and the DS-64 EPROM data bank were all operating properly. It was also found that EPROM-resident programs must be linked using the command

```
ln -c fc00 -d 0060 -o name.exe name.o srom.o c.lib
```

and not with the command described in Michael Sheehan's 1989-90 MQP report. A reasonable amount of time was spent at the beginning of the year identifying this error and

achieving proper operation of all the computer equipment. In this process, it was also found that the hex display devices then used with the system were inoperable; these were replaced.

5.3.2 Hardware Proof-of-Concept Simulator

The interfaces to the peripheral devices comprising the hardware proof-of-concept simulator were replicated on a protoboard. The soldered wires that connected the I/O ports to the computer boards were replaced with ribbon cables. This provided a more reliable platform on which to test experiments than did the breadboard version. In particular, the possibility of errors due to loose connections and short-circuits associated with breadboard-based prototypes was eliminated. Tests were then run to verify the operation of the simulator. The results from these tests follows.

To test the performance of the interfaces to the pump and motor controllers, several digital words were sent to their digital-to-analog converters. The analog voltage generated by the DACs was recorded and compared with theoretical results. The results of this test are as follows:

Controller	Binary Word	Output (V)	Theory (V)	% Error
Motor	01010101	1.7 V	1.7 V	0
Motor	10101010	3.4 V	3.4 V	0
Pump	10101010	3.4 V	3.4 V	0
Pump	01010101	1.7 V	1.7 V	0

The output voltage generated by the interface with the temperature transducer was

measured. This value was compared with the reading displayed by the thermometer in the laboratory. The results of this test:

Output Voltage	Corresponding Temp.	Thermometer Reading
1.8 V	27° C	26° C

The interfaces to the accelerometers were tested by reading the outputs generated as the inclination of the accelerometers with respect to earth was varied. As expected, different inclinations yielded different readings.

5.3.3 Gas Entrainment Detector

Each sub-circuit in the gas entrainment detector was tested for proper operation once the design was completed and built. The following is a description of the tests run and the data obtained.

The current through the IR diode was measured to be 25.75 mA, at the forward voltage drop of 1.2 V. Under this condition, the diode is properly forward-biased and operating far enough from the nonlinear portion of the forward conduction graph for the device. The voltage at the phototransistor's collector when water was present between the IR devices was 2.5 V. When water was replaced by air, this voltage dropped to 0.3 V. This voltage spread is adequate to guarantee the proper operation of the comparator circuit over the complete temperature range expected to be experienced during the actual experiment (-15° C to 30°C). The smallest collector voltage change generated by a bubble going

through the detector sensors was 0.2 mV, a peak large enough to detect all bubbles passing through the detector.

The "2X" amplifier stage doubled the voltage at the phototransistor's collector, as expected. However, this device also amplified the noise present at its inputs. The differentiator responded to this amplified noise by generating signals that were interpreted as bubbles by the Schmitt Trigger. Since the gain of the differentiator proved to be sufficient to generate signals over 0.8 V (the Schmitt Trigger's high trigger level) in response to bubbles going through the detector, the amplifier stage was deleted, and the test was repeated. With this new scheme, the noise problem was eliminated with no significant effect on the sensitivity of the detector.

The inverting Schmitt Trigger was fed with a DC voltage that was steadily increased in order to find the circuit's high trigger level. This voltage was found to be 0.8 V. The DC voltage level was then decreased to find the low trigger level; this value was found to be 0.2 V. These results completely agree with theoretical calculations. When connected to the output of the differentiator, the Schmitt Trigger was able to detect all peaks known to signal the presence of gas bubbles in the liquid.

The comparator circuit provided reliable information about the media (air or water) present between the IR devices. A 12 V output indicated the presence of water, whereas a -12 V output indicated the presence of air.

The precision half-wave rectifiers performed as expected. They generated a 5 V signal in response to a -12 V input signal, and a 0 V signal when a +12 V signal was present at the input.

The D-type flip-flop served its latching purpose as desired, and the input ports were correctly decoded. The demultiplexing circuit for the address/data lines and the data bus transceivers functioned faultlessly. The microprocessor controller encountered no problem when accessing the input ports.

Once proper operation of the gas entrainment detector was verified, the design was ported from the experimental breadboard to a permanent protoboard.

5.3.4 Ultrasonic Circulation Device

The experimental results posted below are the output voltages of the ultrasonic circulation device with phase delays ranging from 0ns to 6ns plus the original 6ns added to the receiver signal. The obtained results resulted by controlling the input delay over the range of 0ns to 6ns at steps of 200 picoseconds.

<u>Phase Delay (nanoseconds)</u>	<u>V_{max} Experimental (volts)</u>
6.0	1.99
6.1	1.98
6.2	1.97
6.3	1.96
6.4	1.95
6.5	1.94
6.6	1.93
6.7	1.92
6.8	1.92
6.9	1.91
7.0	1.90
7.1	1.89
7.2	1.88
7.3	1.87
7.4	1.86
7.5	1.85
7.6	1.85
7.7	1.84
7.8	1.83
7.9	1.82
8.0	1.81
8.1	1.80

<u>Phase Delay (nanoseconds)</u>	<u>V_{max} Experimental (volts)</u>
8.2	1.79
8.3	1.78
8.4	1.78
8.5	1.77
8.6	1.76
8.7	1.75
8.8	1.74
8.9	1.73
9.0	1.72
9.1	1.72
9.2	1.71
9.3	1.70
9.4	1.69
9.5	1.68
9.6	1.68
9.7	1.67
9.8	1.66
9.9	1.65
10.0	1.64
10.1	1.63
10.2	1.62
10.3	1.61
10.4	1.60
10.5	1.59
10.6	1.59
10.7	1.58
10.8	1.57
10.9	1.56
11.0	1.55
11.1	1.54
11.2	1.53
11.3	1.52
11.4	1.51
11.5	1.51
11.6	1.50
11.7	1.49
11.8	1.48
11.9	1.47
12.0	1.45

5.3.5 System Integration

Once all the electrical components were tested and their operation verified, they were interconnected and mounted on a permanent plastic platform. A diagram identifying the

devices on this platform is shown in figure 5.10.

A completely documented software program was developed. This program controls in detail the function and timing requirements of the complete electromechanical system. A listing of this program appears in appendix B.

A final general test was run on the integrated system. The software program was "burnt" into EPROM and executed. Once the experiment was completed, data was extracted from the EPROMs in the DS-64.

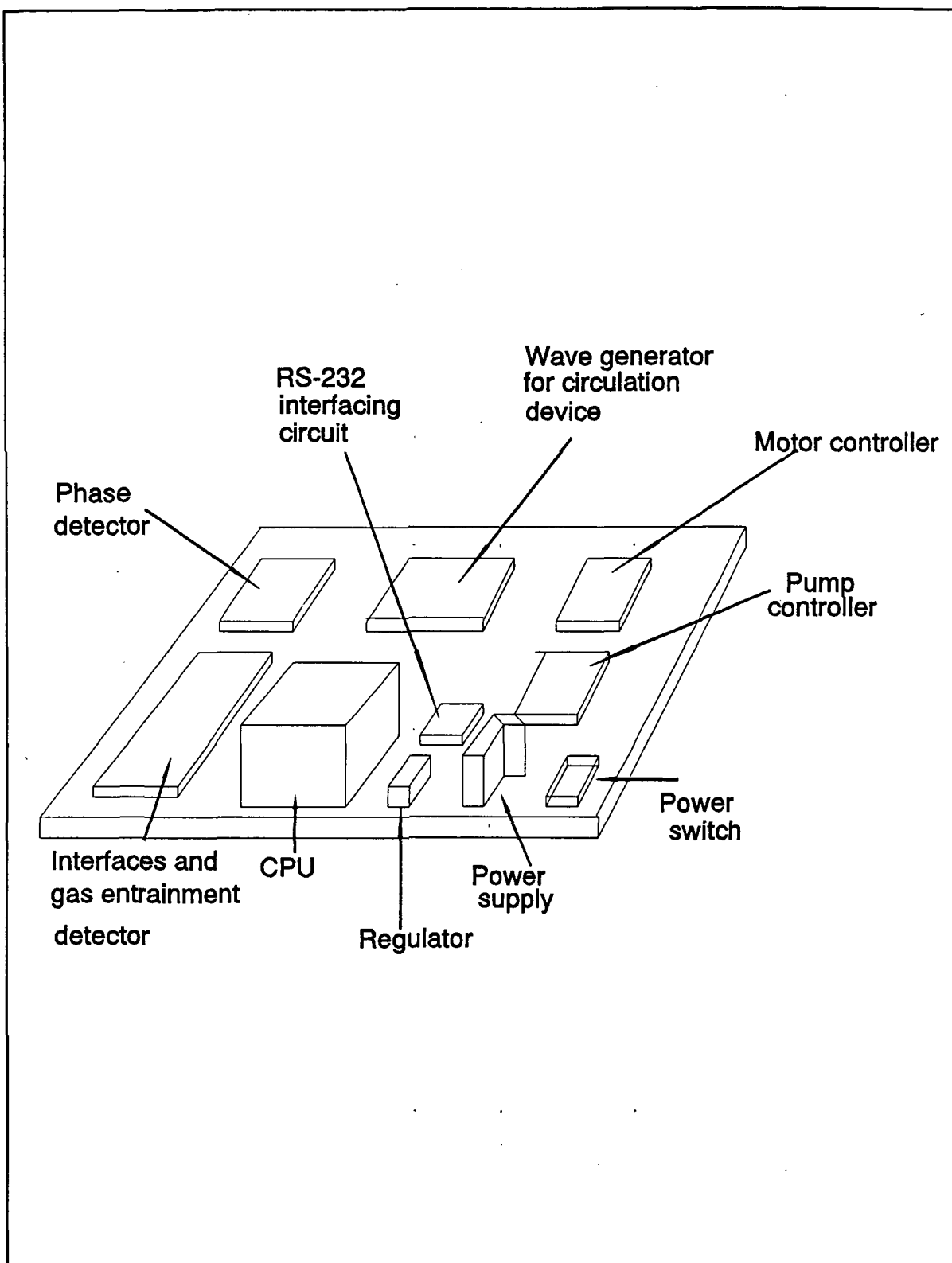


Figure 5.10 Circuit Board.

CHAPTER 6

CONCLUSIONS

Several goals were set at the beginning of this project year. These included verifying that the mechanical equipment developed by previous groups was working according to specifications, deciding on a feasible camera/flash arrangement in order to take pictures of the vortex, revising the computer software for the flight operation sequence, redesigning the ultrasonic circulation device, implementing a gas entrainment detector, integrating the mechanical and the electrical components so they worked as a unit, and documenting all the equipment to allow for future replication of the experiment.

During the year, the above goals were accomplished. Some flaws were found in the original design of the mechanical equipment. The pump chosen by the 1990 MQP team proved to be inadequate to form a vortex under the conditions that the cylinder will experience when rotating at the rates necessary to achieve the G-levels required for the experiment. Testing was conducted to verify fluid transfer requirements and a new pump was purchased; the mechanical equipment now functions properly.

Electrical equipment was upgraded and tested extensively. Computer software was improved and completely documented. The gas entrainment detector was modified to assure the detection of gas bubbles in the vortex and the transfer of that information to the system control processor. The ultrasonic circulation device has been modified as well as is now able to detect reliably time differences as short as 100 picoseconds. After testing, the devices were transferred from the experimental breadboards to permanent protoboards. The hardware proof-of-concept simulator developed last year was enhanced and replicated on a protoboard. These devices, together with the computer hardware and the power supply, were mounted on a plexiglass platform to provide a permanent base to the system.

Unfortunately, the mechanical and the electrical sub-systems could not be fully integrated due to malfunctions with the pump and motor controllers. These controllers were designed during the 1990 project year, but failed to achieve the performance expected of them. As a consequence, the systems required complete redesign during this project.

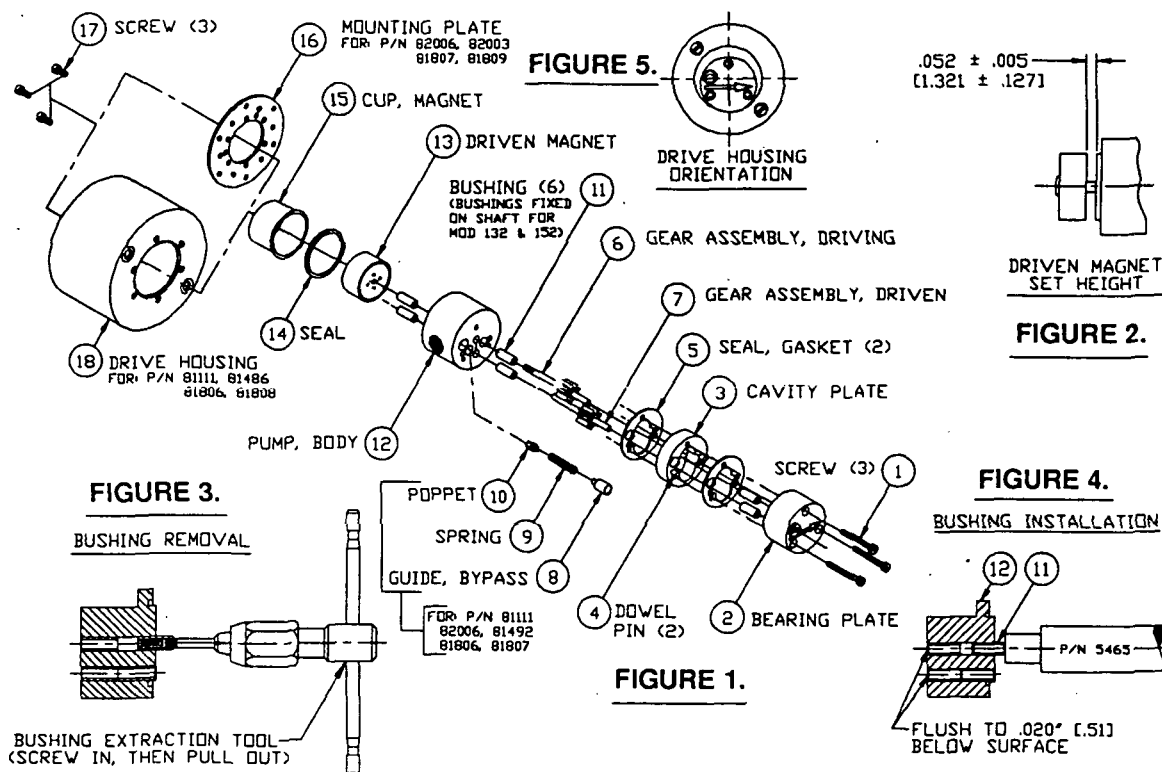
Future projects will be required to complete further testing of the camera and flash arrangement, choose a feasible method of illuminating the cylinder while taking the pictures of the vortex, work closely with future GASCAN Structure teams in order to solve the assembly problem mentioned in chapter 4, do balance testing with the help of the program previously developed, mount all equipment on the platform, complete and construct a final piping layout, and complete vibration and stress testing according to NASA safety specifications. The motor and pump controllers will have to be analyzed and made functional. The signal generator and receiver amplifier of the ultrasonic circulation device will have to be integrated with the phase detector and the chamber in order to assure proper integration. A printed circuit board versions for the electrical circuits must also be implemented, and the complete system fully tested and prepared for flight operation.

APPENDIX A

MECHANICAL EQUIPMENT
DATA SPECIFICATIONS

Service Instructions

FOR MOD. 122, 142, 132, 152



GENERAL:

1. All service work should be performed in a clean area.
2. Care should be taken to avoid scratching any sealing surfaces or allowing metal chips to come in contact with the Driven Magnet Assembly.
3. An even, light coat of high vacuum silicone grease (Dow Corning or equiv.) should be applied to all seals or O-Rings.
4. O-Rings with chamfers should always be installed with the chamfer up, away from the groove.
5. All assembly screws should be tightened evenly and in an alternating pattern.
6. Only Micropump factory authorized replacement parts should be used when servicing any Micropump products.

SPECIFIC:

1. Remove old Bushings(11) with Extraction Tool. The use of a #8 or M4 tap with T-Handle is recommended (See Figure 3.).
2. New Bushing installation is a press fit. Install using P/N 5465 tool. (See Figure 4.)
3. The first two Bushings should be installed into the Pump Body (12) from the gear side. These Bushings should be inserted to .020 inch (.51mm) below seal surface. Then two bushings should be inserted into the Pump Body from the Driven Magnet (13) side. Also, install two Bushings in the Bearing Plate (2).
4. Next install Gears (6) & (7) and Driven Magnet (13). Set Driven Magnet height from Pump Body (12) pilot, as shown in Figure 2, using P/N 6009 Magnet Set Height Tool between Pump Body (12) and Driven Magnet (13), press Driven Magnet (13) down until it touches the Magnet Set Height Tool.
5. Driven Magnet and Gears must rotate freely - tight Bushings may be reamed with a #30 reamer.
6. Install Parts (1) - (5) in order, then complete rest of assembly.

P/N 5838

REVISIONS			
LTR.	DESCRIPTION	DATE	BY
B	REVISED PER ECN-3131.	10/22/90	R.D.H.

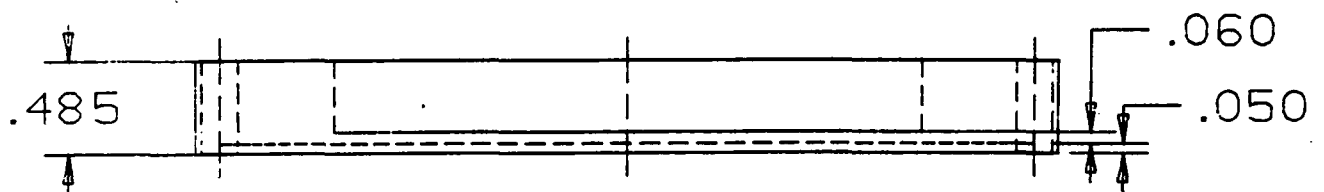
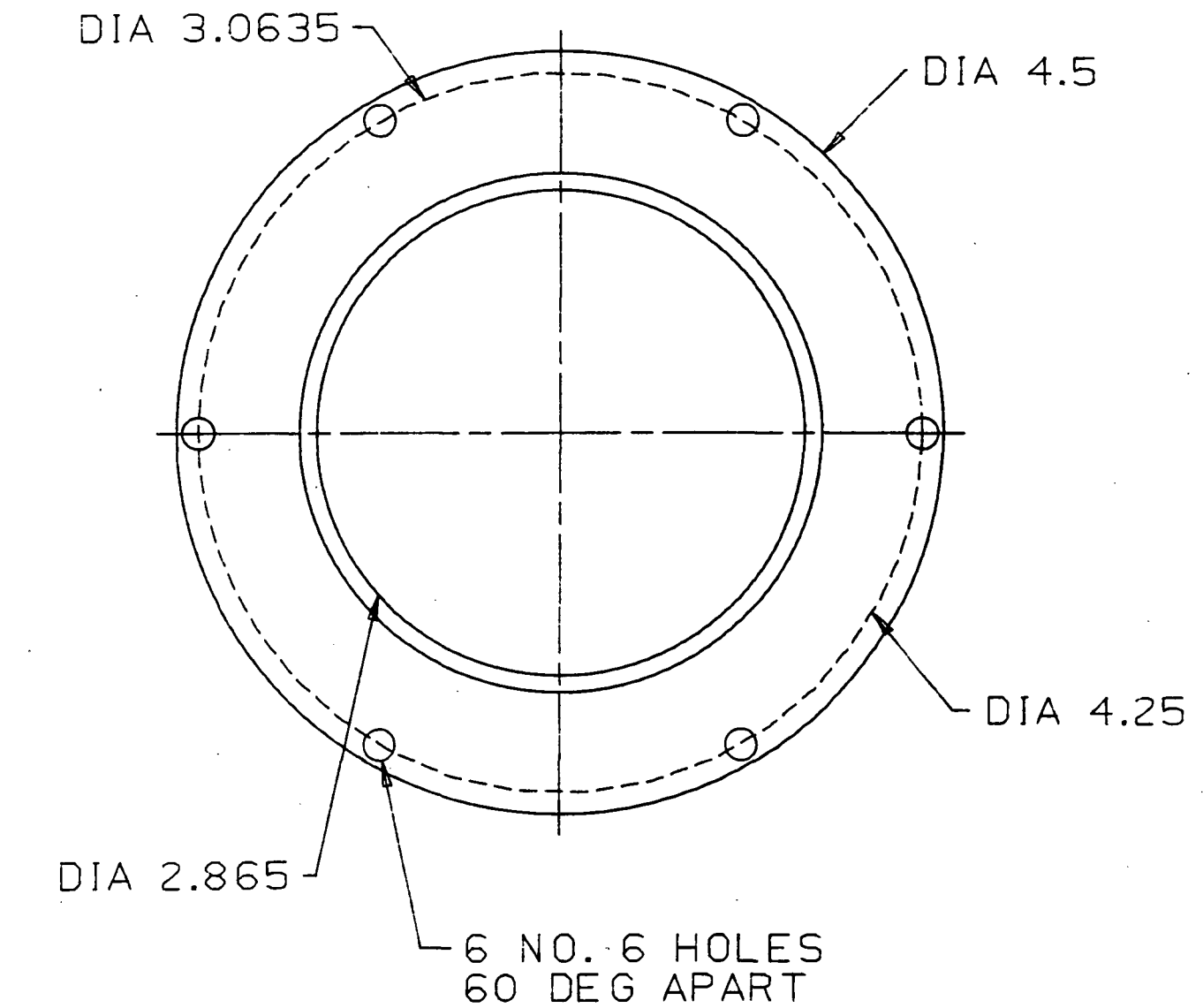
SPARE PARTS LIST
FOR GEAR PUMP MODEL 122, 132, 142, 152
122(81111,82006,81492)
142(81486,82003)
132(81806,81807)

PART NO.	DESCRIPTION	UNITS PER ASS'Y
795	SCREW	3
2301	PLATE, PUMP MOUNTING (82003,82006, 81807,81809)	1
5508	HOUSING (81111,81492,81486,81806,81808 ONLY)	1
3279	CUP, MAGNET	1
2619	SEAL, O-RING	1
80071	MAGNET ASSEMBLY, DRIVING	1
5437	PUMP BODY (81111,82006,81492,81806, 81807 ONLY)	1
5444	PUMP BODY (81486,82003,81808, 81809 ONLY)	1
4513	POPPET (81111,81492,82006,81806,81807 ONLY)	1
4959	GUIDE, BYPASS (81111,82006,81492,81806, 81807 ONLY)	1
4913	* BUSHING (81111,82006,81492,81486,82003 ONLY)	6
5369	* SEAL - GASKET	2
4188	* SEAL GASKET (P/N 81492 ONLY)	2
80491	BEARING PLATE (81111,82006,81492,81806, 81807 ONLY)	1
4971	BEARING PLATE (81486,82003,81808,81809 ONLY)	1
5058	SPRING, BYPASS (81111,82006,81492,81806, 81807 ONLY)	1
80950	* GEAR ASSY, DRIVING (81111,82006,81492, 81486,82003)	1
80951	* GEAR ASSY, DRIVEN (81111,82006,81492, 81486,82003)	1
81608	* GEAR ASSY, DRIVING (81806,81807,81808,81809)	1
81609	* GEAR ASSY, DRIVEN (81806,81807,81808,81809)	1
4355	CAVITY PLATE	1
4226	SCREW	3
4360	DOWEL PIN	2
82131	GEAR SERVICE KIT (81111,82006,81486, 82003 ONLY)	
82141	GEAR SERVICE KIT (81492 ONLY)	
81810	GEAR SERVICE KIT (81806,81807,81808,81809)	
5465	BUSHING INSERTION TOOL (81111,82006, 81492,81486,82003 ONLY)	
6009	MAGNET SET HEIGHT TOOL	
	* Parts available in Gear Service Kit only	

Prices subject to change without notice.

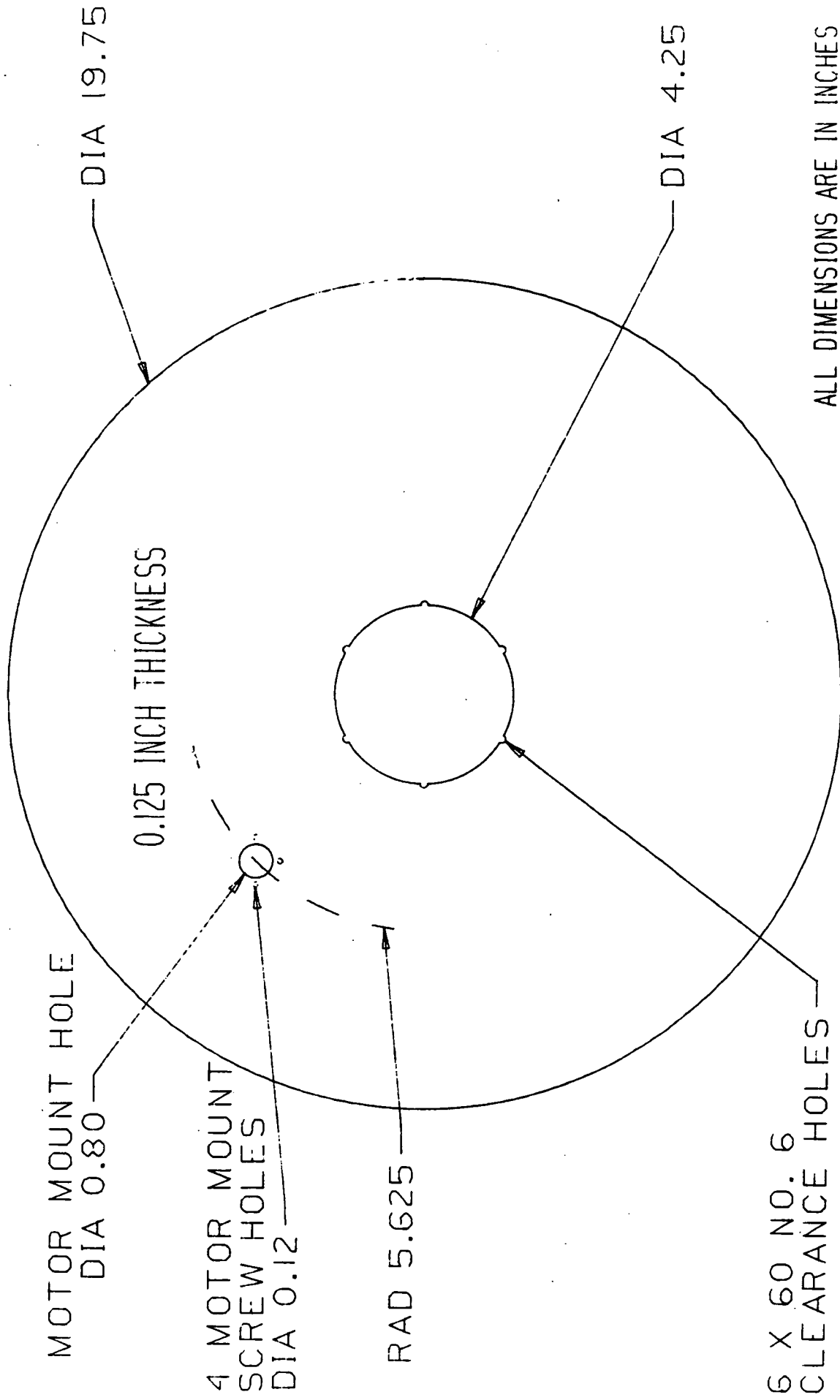
Micropump Corporation

P.O. Box 4001 - Concord, CA 94524 - Phone: (415) 689-6000 - Telex: 753493 - Fax: (415) 680-0754



ALL DIMENSIONS ARE IN INCHES

WPI CAD LAB	TITLE:	PLATFORM CAP
DATE: 4/4/90	DRAWN BY:	ELLIOTT-BARRY
SCALE	NO:	SHEET:



ALL DIMENSIONS ARE IN INCHES

WPI CAD LABORATORY

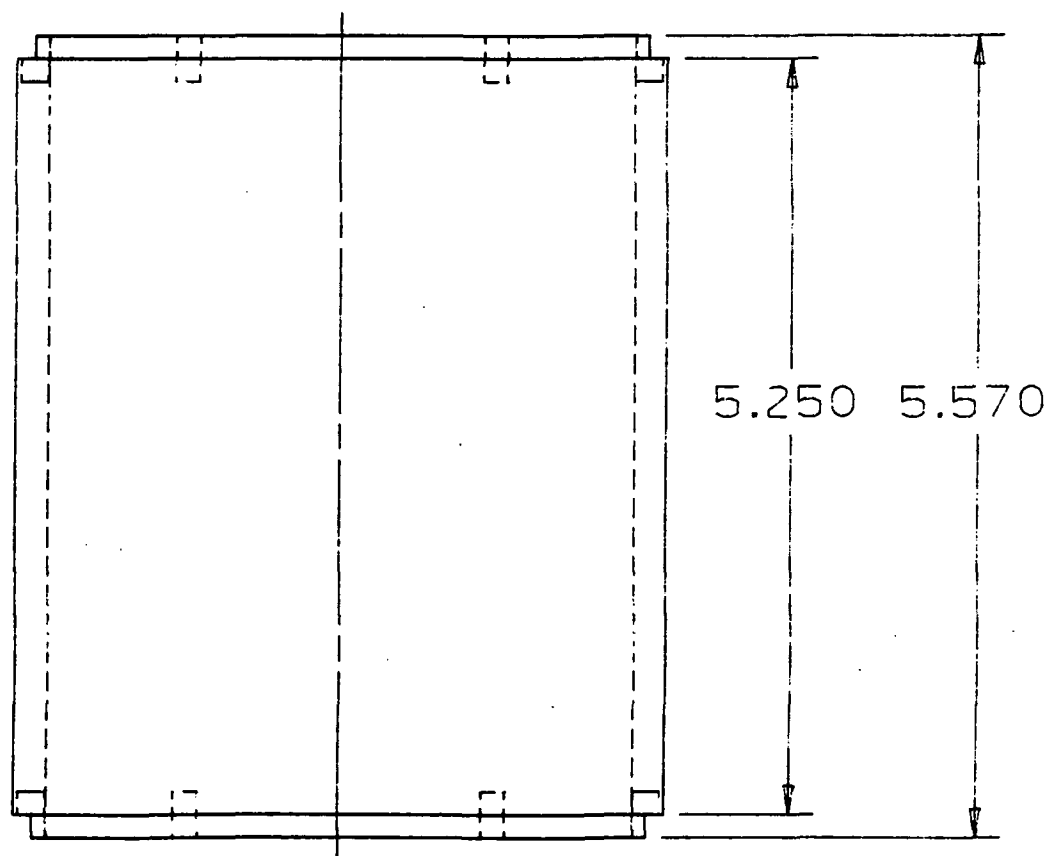
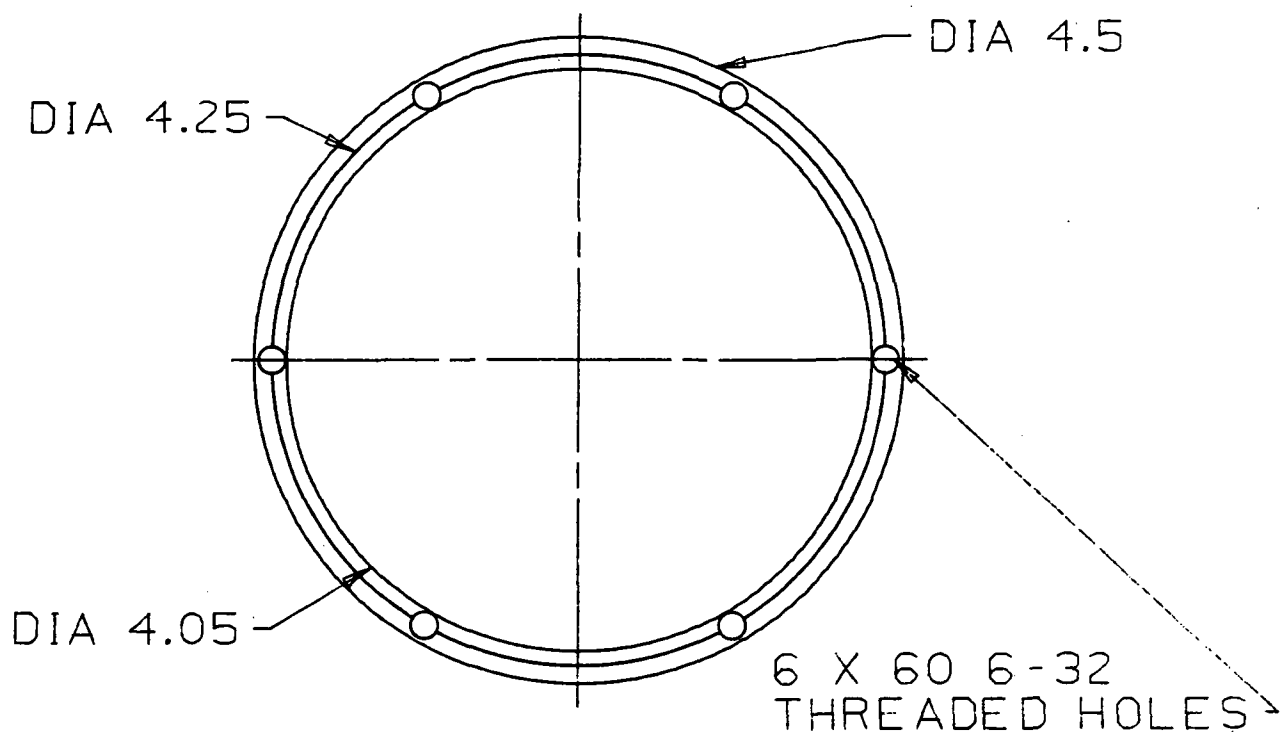
TITLE: UPPER PLATE

NO: 1

SCALE: 0.3 DATE: 4/3/90

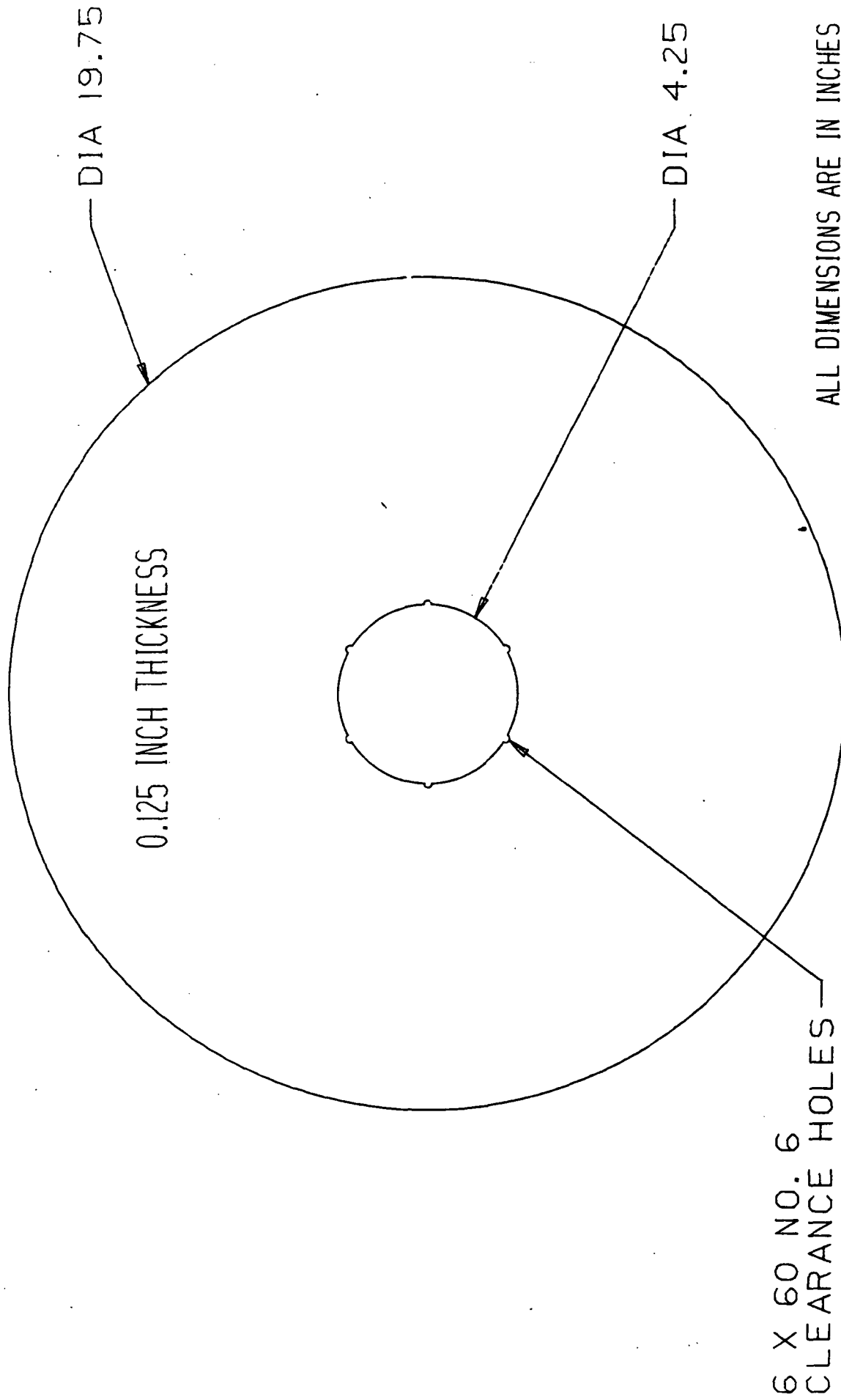
DRAWN BY: ELLIOTT-BARRY

SHEET: 1



ALL DIMENSIONS ARE IN INCHES

PI CAD LAB	TITLE:	PLATFORM HUB
DATE: 4/5/90	DRAWN BY:	ELLIOTT-BARRY
SCALE: 0.75	NO: 1	SHEET: 1



WPI CAD LABORATORY	TITLE:	BOTTOM PLATE	NO: 1
SCALE: 0.3	DATE: 4/3/90	DRAWN BY: ELLIOTT-BARRY	SHEET: 1

APPENDIX B

ELECTRICAL EQUIPMENT
DATA SPECIFICATIONS

Available upon request from

Worcester Polytechnic Institute
Mechanical Engineering Department
Attn: Barbara Rodrique
100 Institute Road
Worcester, MA 01609-2280

Phone: (508) 831-5026
Fax: (508) 831-5680

APPENDIX C
SOFTWARE MANUAL

Software Manual

All flight software is written in Aztec C. DATEX is written in ANSI standard C, and does not compile on Aztec C.

To compile a program, type:

```
cc <name>
```

To link FLIGHT or TEST_RES, and put them in EPROM-resident format, type:

```
ln -c fc00 -d 0020 -o <name>.exe <name>.o srom.o c.lib
```

```
hex86 -s16 <name>.exe
```

To link READ and put it in Monitor format, type:

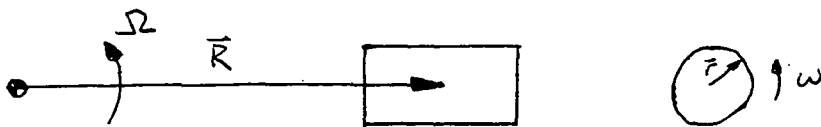
```
ln -c 0020 -d 0060 -o <name>.exe <name>.o srom.o c.lib
```

```
hex86 <name>.exe
```

To link all other programs, type:

```
ln -o <name>.exe <name>.o c.lib m.lib
```


APPENDIX D
FREE-SURFACE VORTEX
CALCULATIONS



- ASSUMPTIONS :
- LARGEST CONTRIBUTION TO SURFACE TILT IS DIFFERENTIAL VELOCITY PROFILE
 - RIGID BODY MOTION OF FLUID (NO BOUNDARY LAYER)
 - $R = 0.17 \text{ m}$
 - $r = 0.05 \text{ m}$
 - $\Omega = 3.4 \text{ rad/s}$ (at minimum g-level of $0.2g$)
 - $\omega = 6.0 \text{ rad/s}$ (at maximum flow rate)

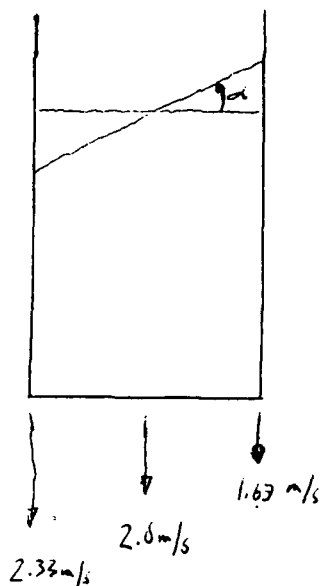
CENTRIPETAL ACCELERATION $A = R\Omega^2$

ACTUAL ACCELERATION $A = R(\Omega \pm r\omega)^2$

$$A_1 = (0.17 \text{ m}) \left[(3.4 \text{ rad/s}) + (0.05 \text{ m})(6.0 \text{ rad/s}) \right]^2 = 2.33 \text{ m/s}^2$$

$$A_2 = (0.17 \text{ m}) \left[(3.4 \text{ rad/s}) - (0.05 \text{ m})(6.0 \text{ rad/s}) \right]^2 = 1.63 \text{ m/s}^2$$

ASSUME ANGLE OF SURFACE TILT IS PROPORTIONAL TO ACCELERATION CHANGE



$$\alpha = \arctan \left(\frac{A_1 - A_2}{A} \right)$$

$$= \arctan \left(\frac{2.33 - 1.63}{2} \right)$$

$$= 19.3^\circ$$